THE DEVELOPMENT OF A REAL-TIME PHOTOGRAMMETRIC SYSTEM FOR PATIENT POSITIONING IN PROTON THERAPY

Graeme van der Vlugt, B.Sc (Survey), Cape Town

October 1991

Submitted to the University of Cape Town
in fulfilment for the degree of
Master of Science in Engineering.

I, Graeme van der Vlugt, submit this thesis in fulfilment of the requirements for the degree of Master of Science in Engineering. I affirm that this this is my original work and that it has not been submitted in this or a similar form for a degree at any University.

ABSTRACT

This thesis concerns the development of a real-time photogrammetric system for the positioning of patients undergoing proton therapy. The positioning of patients involves moving their tumours into a horizontal proton beam. In the past, patients have been mechanically positioned and restrained. However, with the development of this new "StereoPhotoGrammetric" (SPG) system, patients will be positioned using CCD cameras and digital photogrammetric techniques. A specially designed mechanical chair will move the patients at the command of the SPG system.

The tumour is located relative to reference targets on a patient's head using medical imaging. In the treatment room these same targets are imaged and identified by the SPG system. The positions of these reference targets are determined in three-dimensional space and hence the relative position of the tumour can be computed. Using this knowledge, the mechanical chair is automatically sent instructions to move the patient into the desired treatment position. Once the proton beam is switched on, the SPG system monitors the patient in order to detect any movements. The beam is immediately switched off if any substantial movement takes place.

As a basis, some general theory of photogrammetry is covered. The development of reliable and efficient processing routines for the SPG system and the photogrammetric procedures involved in the system, are reported in detail. The routines are composed of a combination of automatic and computer-aided manual processes. The reliability and efficiency of these various routines are evaluated.

The hardware and software were successfully integrated into a functional unit, capable of positioning and monitoring patients. A number of tests of target positioning accuracy were executed with the SPG system and satisfactory results were achieved.

ACKNOWLEDGEMENTS

I am sincerely grateful for all the support and contributions of the following people: my supervisor, Professor Heinz Ruther from the Department of Surveying and Geodetic Engineering at UCT, for all the time he spent with me and for his invaluable guidance; Professor Adams and Anne Tregidga from the Biostereometrics Department for their help with the medical imaging concepts and for the use of their equipment; Mr. Colin Martin from the Department of Surveying and Geodetic Engineering for proofreading this thesis; the staff of the Department of Surveying and Geodetic Engineering; Mr. J. Hesselink from the Department of Electrical and Electronic Engineering for sorting out the synchronisation problems encountered with the CCD cameras, and the staff of the Marine Biology Research Institute for the use of their Apple Macintosh computers and laser printer.

CONTENTS

LIST OF FIGURES

1 INTRODUCTION

1.1 REAL-TIME PHOTOGRAMMETRY

Real-time photogrammetry (RTP) is a relatively new field based on a combination of conventional photogrammetry, image processing and video technology. RTP equipment, such as charge-coupled device (CCD) cameras, analogue-to-digital converters, personal computers and workstations, frame-grabbers and image processors, as well as video monitors, has now become a major part of close-range photogrammetry. The terms "digital photogrammetry", "near-real-time photogrammetry" (NRTP) and "real-time photogrammetry" (RTP) are all used to describe the photogrammetric processing of digital images, which are captured, stored, manipulated and displayed by these hardware components. New techniques and algorithms, unique to RTP systems, have recently been developed and are still emerging.

The main objective of these techniques is to provide automated processing of image data, in order to obtain three-dimensional information of discrete points, surfaces or objects. An RTP system is essentially the integration of various hardware and software components, which together produce a system capable of determining three-dimensional coordinates in real-time. The term "real-time" can be interpreted in a number of ways. Two common definitions of real-time systems can be found in El-Hakim (1986a), and Gruen and Beyer (1987).

El-Hakim gives the following formal definition: a real-time system is "a system that is capable of guaranteeing a response before a fixed time has elapsed, where that fixed time is provided as part of the problem statement." He goes on to explain that "in photogrammetric applications, real-time system can generally be defined as a system without interruptions, or appreciable time lags, between acquiring the image and the final results, ..., the actual speed of the whole operation will vary, depending on the application."

The other definition, given by Gruen and Beyer, is: RTP "is a non-contact three-dimensional measurement technique with a response time of one video cycle."

Neither definition gives an absolute standard for real-time, the former being dependent on the application and the latter being dependent on the video

frame rate. Either definition can be used. However, for the purpose of this thesis, the former is adopted.

Increasing numbers of RTP systems are being developed for research and other applications, and have been described by, among others, El-Hakim (1986a, 1986b, 1989), Gruen and Beyer (1987, 1991), Haggren (1987), Haggren and Leikas (1987), Kratky (1979), Ruther (1989), and Wong and Ho (1986). These RTP systems have been implemented mainly on workstations and are still evolving. However, some successful applications in research projects, industry and medicine, have been reported using digital photogrammetric methods, for example in Beyer, Fassler and Wen (1989), Beyer (1991), Fritsch (1991) and Gruen and Baltsavias (1988).

The positioning accuracies being obtained by these current systems are still far from the accuracies obtainable with conventional camera equipment, such as the extremely high one part in one million proportional accuracy reported by Fraser (1991). Present factors which limit the accuracy of digital systems are the very small imaging area (CCD imaging chips are usually 6 by 4.5 or 8.8 by 6.6 millimetres), limited spatial resolution (compared to traditional film images), and numerous electronic distortions occurring during the transfer of image data from camera to frame-grabber (Gruen, 1988). However, digital systems have many advantages over traditional photogrammetric instruments. One of the most important advantages is their efficiency in data acquisition and processing, thus presenting real-time capabilities. In addition, the improvements expected in hardware design (Real and Fujimoto, 1986 and Gruen, 1989), will no doubt assist RTP systems to reach similar levels of accuracy to those of conventional photogrammetric systems. RTP systems are capable of being utilised for many diverse applications, such as the project described in this thesis, but many areas of research still need to be explored (Wong, 1987) in order for the full potential of RTP systems to be appreciated.

1.2 THE STEREO-PHOTOGRAMMETRIC (SPG) SYSTEM

Parallel to the worldwide growth of RTP systems, has been the development of a low cost PC-based system, PHOENICS (**PHO**togrammetric **EN**gineering and **I**ndustrial digital **C**amera **S**ystem), in the Department of Surveying and Geodetic Engineering at the University of Cape Town (UCT); see Ruther (1989)

and Ruther and Parkyn (1990). PHOENICS has been developed as part of an on-going project, started in 1987, which is aimed at research in aspects of RTP.

One result of this research has been the development of an RTP system designed specifically for positioning patients, undergoing brain tumour treatment, into a proton beam. In the past, mechanical devices have been used to align and restrain patients in position for radiation therapy. The RTP system was chosen to replace these techniques with the objective of improving positioning efficiency and patient comfort.

The decision to use digital photogrammetry originated in December 1988, when a "value engineering workshop" was held in Cape Town to evaluate the "generation of alternatives for a head positioning device to be used in proton therapy" of brain tumours (Adams, 1989). Various alternatives were put forward to the commissioning committee of the National Accelerator Centre (NAC). Motivated by successful applications of PHOENICS, (e.g. Ruther and Wildschek (1989)) an alternative solution using digital photogrammetry was proposed by Adams for the positioning of patients. After visiting the Department of Surveying (which was so named in 1989), where a simple positioning demonstration was given, the NAC commissioning committee decided to use digital photogrammetry as the means of moving a patient so that the tumour lay in a fixed horizontal proton beam. The photogrammetric system which has been developed for this purpose has become known as the SPG (**S**tereo**P**hoto**G**rammetric) system, Figure 1.1.

Closely associated with the SPG system was the development of a patient support chair by the Department of Mechanical Engineering at UCT. The chair was designed to move a patient into the beam line using the information determined by SPG.

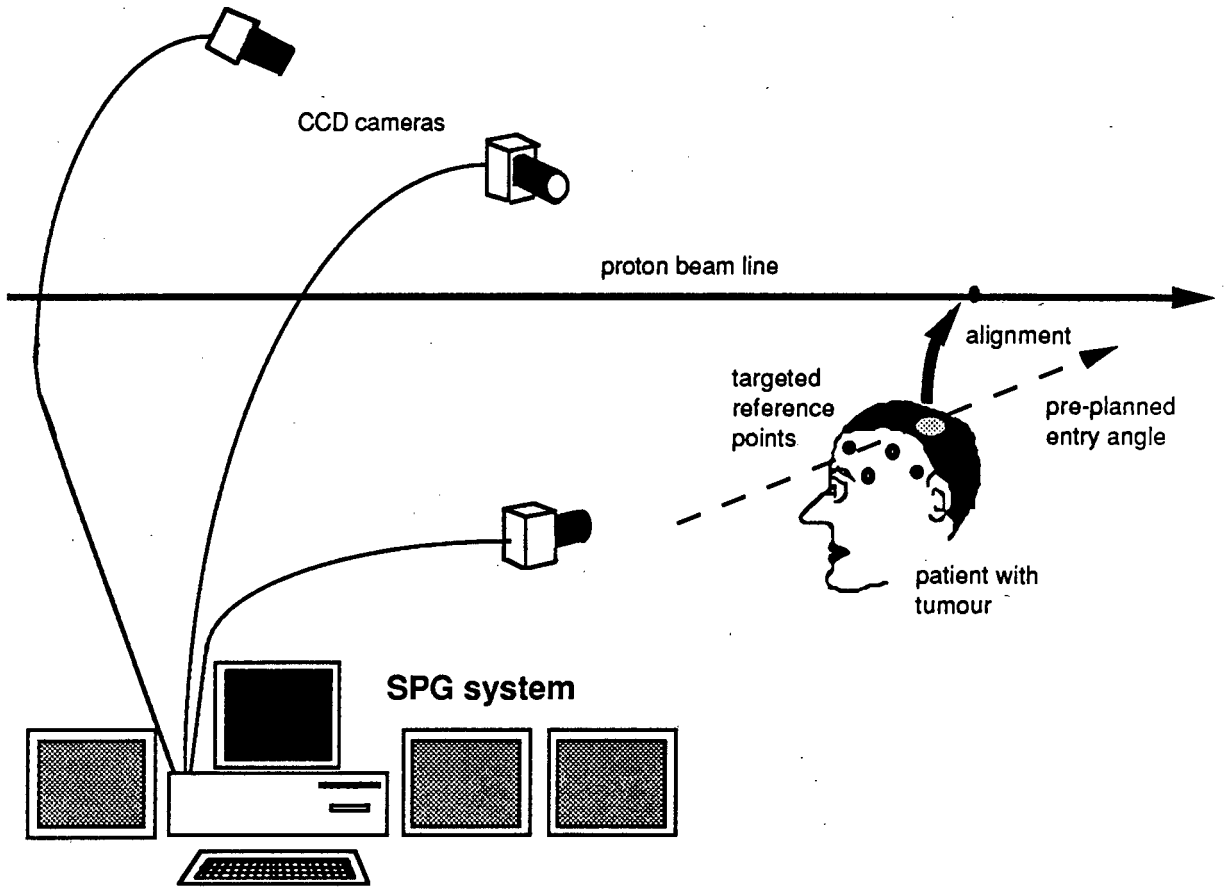

Figure 1.1. The SPG system

This thesis is concerned with the development of SPG. The main objectives of the thesis were to:

(i) integrate the hardware necessary for the functioning of SPG;
(ii) develop reliable and efficient routines, automatic and interactive, required for SPG;
(iii) link the hardware components and software routines into a functional unit;
(iv) carry out preliminary tests with the system;
(v) evaluate the system.

SPG will be installed at the NAC before the end of 1991, and it is expected that the first patients undergoing proton therapy will be treated in mid-1992.

1.3 OVERVIEW

The thesis is divided into twelve chapters:

Chapter 2 covers some basic theory of photogrammetry. A derivation of the collinearity equations is given, and the concepts of the least squares bundle adjustment solution and the partitioning of the associated normal equation matrix are introduced. The idea of additional parameters used to model various distortions is examined.

A second mathematical model, the direct linear transformation (DLT) is also discussed. The reason for including the second model is its advantage over the more rigorous bundle solution in cases where no *a priori* knowledge of the elements of interior orientation are known. This is particularly true for cases where photogrammetric systems are operated by non-photogrammetrists and there is a need for calibration at regular intervals.

Finally, the concept of "aspect ratio" (difference in x and y scales) in digital images is covered.

Chapter 3 describes the hardware components acquired for the development of SPG, which form the basis of a general RTP system.

Chapter 4 describes the image-capturing and processing abilities of the MVP-AT frame-grabber board. The functional sections of the MVP board are discussed and some image processing routines, such as capturing and displaying images, thresholding, and graphic overlaying are discussed. An image search and target centering routine developed specifically for the MVP board is explained. A geometric matching routine was also investigated and is detailed in this chapter.

Chapter 5 reviews the treatment project for which SPG is designed. The basic steps for the solution of the patient positioning problem are outlined, and a flowchart of the process, as seen from a photogrammetric point of view, is presented.

Chapter 6 concerns image creation involving camera / object configuration, control points, targets and lighting. Recommendations given to the NAC

regarding suitable camera / object configurations are detailed. The design and survey of a provisional control frame are described and the concept of the beam coordinate system is introduced. The importance of lighting and targeting is discussed and the reasoning behind the choice of target is explained.

Chapter 7 is concerned with the treatment environment at the NAC and with the other systems involved in the project. Special mention is given to the capabilities of the mechanical chair, as the SPG and chair systems are closely linked in the patient-positioning process.

Chapter 8 describes the various stages and routines involved in SPG, which are:

(i) the calibration stage;
(ii) the system check stage;
(iii) the initial patient-positioning stage;
(iv) the patient-monitoring stage.

Although not part of SPG, the location of the tumour relative to reference targets is mentioned. The various routines within these photogrammetric stages are also discussed in detail.

Chapter 9 is an evaluation of SPG. In particular, the test of target positioning accuracy is detailed and the reliability and efficiency of the system is assessed.

Chapters 10, 11 and 12 complete the thesis, with conclusions, some recommendations regarding SPG, and a few closing remarks.

2 BASIC THEORY

2.1 THEORY OF COLLINEARITY

Most of photogrammetry can be based on a pair of equations known variously as the perspective equations, the imaging equations, the projective equations or the collinearity equations. The latter are used here throughout. The collinearity equations relate the two-dimensional coordinates x and y of image points to the three-dimensional coordinates X, Y and Z of the points in object space. The derivation of these equations and a number of definitions are described below.

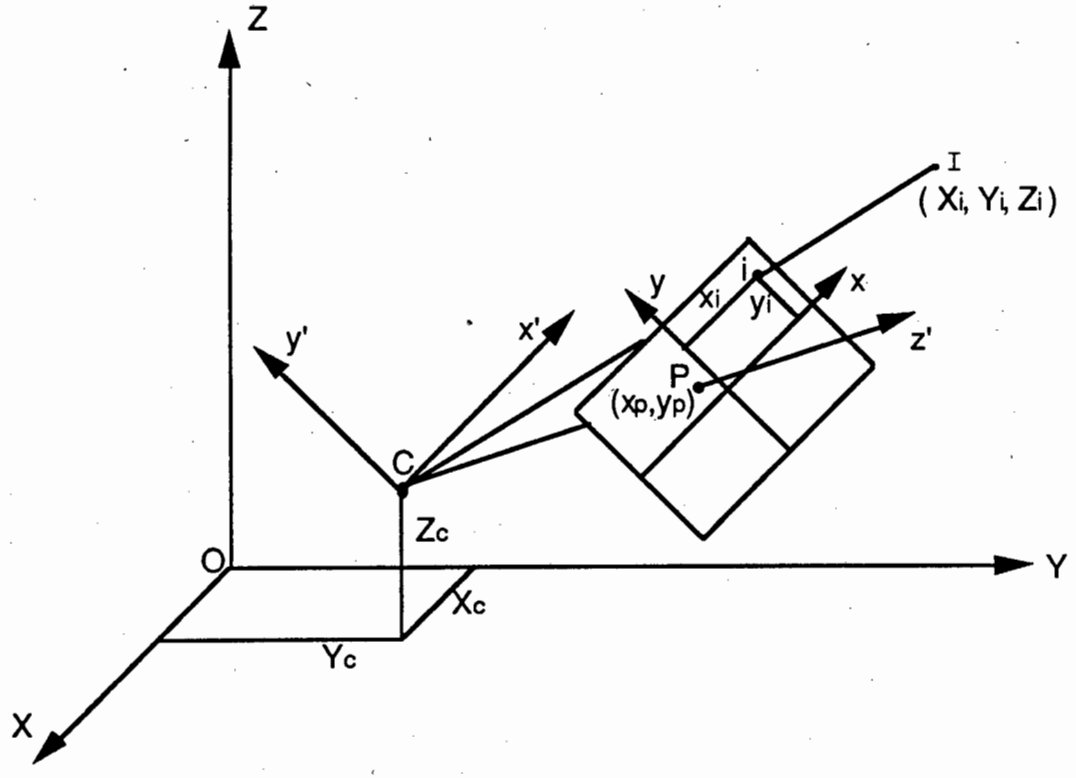

Figure 2.1. The relationship between object space and image space.

In Figure 2.1, the camera is represented by two components, namely the perspective centre of the lens C, and the image plane, shown here as a photographic positive.

Two assumptions about the perspective projection process are made when deriving the collinearity equations:

(i) the image points all lie in one plane (image plane);
(ii) any object point, its image point and the perspective centre C, lie on a straight line (i.e. the collinearity condition).

In practise (i) and (ii) are only approximations, as a number of additional factors such as lens distortions, deviations of the image carrier from a plane, refraction distortions and others, can result in a deviation from these assumptions. Lens distortion is routinely corrected for by adding appropriate parameters to the collinearity equation. This will be discussed in more detail in section 2.2.2.

An image coordinate system x, y of arbitrary origin and orientation is defined in the image plane. An intermediate system x', y', z', is also defined with its origin at the perspective centre C, with the x', y' axes parallel to x, y, and the positive z' axis directed from the perspective centre C, towards the image plane. The z' axis is perpendicular to the image plane. The perpendicular distance between the image plane and perspective centre C, is known as the principal distance or camera constant, and will be denoted here by the lower case letter, c. All image points have z' = c as it is assumed they all lie on the image plane. The point P with image coordinates x_p, y_p, in Figure 2.1, is the principal point and it is defined by the intersection of the z' axis and the image plane.

To obtain the collinearity equations it is necessary to relate the object coordinates of the point i (X_i, Y_i, Z_i) to the intermediate coordinates (x_i', y_i', z_i') through a three-dimensional transformation. The transformation involves three orthogonal rotations, one around each axis, three translations and a scale factor. Mathematically it is represented by:

$$\begin{bmatrix} x'_i \\ y'_i \\ z'_i \end{bmatrix} = \begin{bmatrix} x_i - x_p \\ y_i - y_p \\ c \end{bmatrix} = s\,\underline{R} \begin{bmatrix} X_i - X_c \\ Y_i - Y_c \\ Z_i - Z_c \end{bmatrix} \qquad (2.1)$$

s is the scale factor between the two systems and $\underline{R}$ is an orthogonal rotation matrix whose nine elements are functions of three independent parameters, the angles of rotation around the X, Y and Z, axes, defined here as ω, κ and ϕ, respectively. The rotation matrix $\underline{R}$ is the product of three orthogonal rotation

matrices $\underline{R}_{x\omega}$, $\underline{R}_{y\kappa}$ and $\underline{R}_{z\phi}$, which are matrices describing rotations about the X, Y and Z axes by the angles ω, κ and ϕ, respectively. These can be obtained from first principles and are given by:

$$R_{x\omega} = \begin{bmatrix} 1 & 0 & 0 \\ 0 & \cos\omega & -\sin\omega \\ 0 & \sin\omega & \cos\omega \end{bmatrix} \tag{2.2}$$

$$R_{y\kappa} = \begin{bmatrix} \cos\kappa & 0 & \sin\kappa \\ 0 & 1 & 0 \\ -\sin\kappa & 0 & \cos\kappa \end{bmatrix} \tag{2.3}$$

$$R_{z\phi} = \begin{bmatrix} \cos\phi & -\sin\phi & 0 \\ \sin\phi & \cos\phi & 0 \\ 0 & 0 & 1 \end{bmatrix} \tag{2.4}$$

Note that the symbols used here to describe the angles of rotation differ from the traditional photogrammetric nomenclature.

In analytical photogrammetric solutions it is not necessary to model actual rotations of the camera, so any rotation sequence can be adopted to form the full rotation matrix $\underline{R}$ (Thompson, 1969). The rotation sequence $\underline{R} = \underline{R}_{x\omega}\underline{R}_{y\kappa}\underline{R}_{z\phi}$ is chosen here. This results in:

$$\underline{R} = \begin{bmatrix} r_{11} & r_{12} & r_{13} \\ r_{21} & r_{22} & r_{23} \\ r_{31} & r_{32} & r_{33} \end{bmatrix} \tag{2.5}$$

where
$$\begin{aligned} r_{11} &= \cos\kappa\cos\phi \\ r_{12} &= -\cos\kappa\sin\phi \\ r_{13} &= \sin\kappa \\ r_{21} &= \cos\omega\sin\phi + \sin\omega\sin\kappa\cos\phi \\ r_{22} &= \cos\omega\cos\phi - \sin\omega\sin\kappa\sin\phi \\ r_{23} &= -\sin\omega\cos\kappa \\ r_{31} &= \sin\omega\sin\phi - \cos\omega\sin\kappa\cos\phi \end{aligned} \tag{2.6}$$

$$r_{32} = \sin\omega \cos\phi + \cos\omega \sin\kappa \sin\phi$$
$$r_{33} = \cos\omega \cos\kappa$$

Substituting equation (2.5) into equation (2.1) gives:

$$\begin{bmatrix} x_i - x_p \\ y_i - y_p \\ c \end{bmatrix} = s \begin{bmatrix} r_{11} & r_{12} & r_{13} \\ r_{21} & r_{22} & r_{23} \\ r_{31} & r_{32} & r_{33} \end{bmatrix} \begin{bmatrix} X_i - X_c \\ Y_i - Y_c \\ Z_i - Z_c \end{bmatrix} \tag{2.7}$$

and multiplying out:

$$\begin{bmatrix} x_i - x_p \\ y_i - y_p \\ c \end{bmatrix} = s \begin{bmatrix} r_{11}(X_i - X_c) + r_{12}(Y_i - Y_c) + r_{13}(Z_i - Z_c) \\ r_{21}(X_i - X_c) + r_{22}(Y_i - Y_c) + r_{23}(Z_i - Z_c) \\ r_{31}(X_i - X_c) + r_{32}(Y_i - Y_c) + r_{33}(Z_i - Z_c) \end{bmatrix} \tag{2.8}$$

As the scale factor s, is of no interest in itself, it can be eliminated by dividing the first and second equations of (2.8) by the third equation of (2.8). This results in the two collinearity equations:

$$x_i - x_p = c \frac{r_{11}(X_i - X_c) + r_{12}(Y_i - Y_c) + r_{13}(Z_i - Z_c)}{r_{31}(X_i - X_c) + r_{32}(Y_i - Y_c) + r_{33}(Z_i - Z_c)} \tag{2.9}$$

$$y_i - y_p = c \frac{r_{21}(X_i - X_c) + r_{22}(Y_i - Y_c) + r_{23}(Z_i - Z_c)}{r_{31}(X_i - X_c) + r_{32}(Y_i - Y_c) + r_{33}(Z_i - Z_c)} \tag{2.10}$$

or in a simplified form:

$$x_i - x_p = c \frac{R_1}{R_3} \tag{2.11}$$

$$y_i - y_p = c \frac{R_2}{R_3} \tag{2.12}$$

where,

$$R_1 = r_{11}(X_i - X_c) + r_{12}(Y_i - Y_c) + r_{13}(Z_i - Z_c) \tag{2.13}$$
$$R_2 = r_{21}(X_i - X_c) + r_{22}(Y_i - Y_c) + r_{23}(Z_i - Z_c) \tag{2.14}$$
$$R_3 = r_{31}(X_i - X_c) + r_{32}(Y_i - Y_c) + r_{33}(Z_i - Z_c) \tag{2.15}$$

Equations (2.9) and (2.10) form the basis for the analytical solution of the photogrammetric restitution problem. They give the functional relationship between the image coordinates and object coordinates of a point in an ideal perspective projection, and they contain nine independent camera parameters: x_p, y_p, c, ω, κ, ϕ, X_c, Y_c, Z_c.

2.2 THE BUNDLE ADJUSTMENT

In order to determine the object coordinates of a set of points using photogrammetric techniques, a number of images (photographs) of the points is taken from different positions. Coordinates of all the image points are measured, resulting in a set of equations in the form of equations (2.9) and (2.10). The simultaneous solution of all these equations in a least squares adjustment is known as a bundle adjustment.

As a starting point it is assumed that all nine camera parameters are known for each of n images. The subscript i and the superscript j for the point i appearing on the image j, will be used here. If the image coordinates x_i^j, y_i^j, of a single point i are measured on all n images, then from equations (2.9) and (2.10), 2n equations containing three unknowns, X_i, Y_i, Z_i, can be formulated. Thus, if there are two or more images ($n \geq 2$) then an over-determined solution for the three unknowns exists. If a total of m points are to be coordinated in object space then a set of 2nm equations with 3m unknowns results. Again it can be seen that as long as every point appears on at least two images, the unknown coordinates are determinable.

The method of least squares adjustment is ideally suited for solving redundant equation sets. The least squares approach results in the best linear unbiased estimation (the sum of the squares of the residuals is minimised) as well as providing the covariance matrix of the estimated quantities, which can be directly used to calculate standard deviations for the unknowns.

So far it has been assumed that the 9n camera parameters are all known, but these may also be determined using the collinearity equations. It can be seen that a set of ten equations can be formed if the image coordinates of five points are measured on one image. If the nine camera parameters are unknown but

the five points are all coordinated in object space then this equation set can be solved. Therefore, the camera parameters for a single image can be determined if five or more pre-coordinated points are visible on the image, as long as the points are not co-planar (to avoid a singular normal equation matrix). This principle of using control points (previously coordinated points) for the determination of camera parameters, so that additional point positions can be coordinated, is often used in photogrammetry. Sometimes, numerical problems arising from correlations between the nine unknowns can lead to difficulties in practicle applications.

The next logical step is to solve for both camera parameters and object points in a single least squares adjustment. This is known as the bundle adjustment and was first presented in a general but rigorous solution by Brown (1958). For a solution the following conditions must be satisfied:

(i) every point to be visible on at least two images;
(ii) at least five well-placed points to be visible on each image;
(iii) there must be at least two fully-coordinated points (X, Y and Z) and one partially coordinated point (X, Y, or Z) to define the position and orientation of the network in object space;
(iv) the number of observation equations must be greater than or equal to the number of unknowns.

In order to compensate for random observation errors it is advisable to have a reasonable redundancy in the observation set. An increase in redundancy is achieved by either increasing the number of points or by increasing the number of images. The multi-concept idea, or "repetition and replication, and redundancy in the determination of every unknown variable" (Torlegard, 1981) is a widely accepted method of obtaining high accuracies.

The formulation of the observation equations for the least squares bundle adjustment is as follows. For a point i appearing on an image j, equations (2.9) and (2.10) become:

$$x_i^j - x_p^j = c^j \frac{r_{11}^j (X_i - X_c^j) + r_{12}^j (Y_i - Y_c^j) + r_{13}^j (Z_i - Z_c^j)}{r_{31}^j (X_i - X_c^j) + r_{32}^j (Y_i - Y_c^j) + r_{33}^j (Z_i - Z_c^j)} \qquad (2.16)$$

$$y_i^j - y_p^j = c^j \frac{r_{21}^j (X_i - X_c^j) + r_{22}^j (Y_i - Y_c^j) + r_{23}^j (Z_i - Z_c^j)}{r_{31}^j (X_i - X_c^j) + r_{32}^j (Y_i - Y_c^j) + r_{33}^j (Z_i - Z_c^j)} \tag{2.17}$$

These equations can be rearranged to:

$$F_x = 0 = x_i^j - x_p^j - c^j \frac{r_{11}^j (X_i - X_c^j) + r_{12}^j (Y_i - Y_c^j) + r_{13}^j (Z_i - Z_c^j)}{r_{31}^j (X_i - X_c^j) + r_{32}^j (Y_i - Y_c^j) + r_{33}^j (Z_i - Z_c^j)} \tag{2.18}$$

$$F_y = 0 = y_i^j - y_p^j - c^j \frac{r_{21}^j (X_i - X_c^j) + r_{22}^j (Y_i - Y_c^j) + r_{23}^j (Z_i - Z_c^j)}{r_{31}^j (X_i - X_c^j) + r_{32}^j (Y_i - Y_c^j) + r_{33}^j (Z_i - Z_c^j)} \tag{2.19}$$

For a least squares solution, the functions F_x and F_y must be linearized using a Taylor series expansion. It must be remembered that the rotation elements ($r_{11},...,r_{33}$) are themselves a function of the three rotation angles ω, κ and ϕ. So, linearizing gives:

$$F_x = (F_x)_0 + \frac{\partial F_x}{\partial x_i^j} dx_i^j + \frac{\partial F_x}{\partial x_p^j} dx_p^j + \frac{\partial F_x}{\partial c^j} dc^j + \frac{\partial F_x}{\partial \omega^j} d\omega^j + \frac{\partial F_x}{\partial \kappa^j} d\kappa^j + \frac{\partial F_x}{\partial \phi^j} d\phi^j + \\ + \frac{\partial F_x}{\partial X_c^j} dX_c^j + \frac{\partial F_x}{\partial Y_c^j} dY_c^j + \frac{\partial F_x}{\partial Z_c^j} dZ_c^j + \frac{\partial F_x}{\partial X_i} dX_i + \frac{\partial F_x}{\partial Y_i} dY_i + \frac{\partial F_x}{\partial Z_i} dZ_i + ... \tag{2.20}$$

$$F_y = (F_y)_0 + \frac{\partial F_y}{\partial y_i^j} dy_i^j + \frac{\partial F_y}{\partial y_p^j} dy_p^j + \frac{\partial F_y}{\partial c^j} dc^j + \frac{\partial F_y}{\partial \omega^j} d\omega^j + \frac{\partial F_y}{\partial \kappa^j} d\kappa^j + \frac{\partial F_y}{\partial \phi^j} d\phi^j + \\ + \frac{\partial F_y}{\partial X_c^j} dX_c^j + \frac{\partial F_y}{\partial Y_c^j} dY_c^j + \frac{\partial F_y}{\partial Z_c^j} dZ_c^j + \frac{\partial F_y}{\partial X_i} dX_i + \frac{\partial F_y}{\partial Y_i} dY_i + \frac{\partial F_y}{\partial Z_i} dZ_i + ... \tag{2.21}$$

From (2.18) and (2.19) it is obvious that,

$$\frac{\partial F_x}{\partial x_i^j} = 1 \quad \text{and} \quad \frac{\partial F_y}{\partial y_i^j} = 1$$

The quantities dx_i^j and dy_i^j are the corrections (residuals) associated with the observations x_i^j and y_i^j, so that, in least squares nomenclature, they can be

written as Vx_i^j and Vy_i^j. Rearranging equations (2.20) and (2.21) and with $F_x = F_y = 0$ one obtains:

$$Vx_i^j = -(F_x)_0 - \frac{\partial F_x}{\partial x_p^j} dx_p^j - \ldots\ldots - \frac{\partial F_x}{\partial Z_c^j} dZ_c^j - \frac{\partial F_x}{\partial X_i} dX_i - \frac{\partial F_x}{\partial Y_i} dY_i - \frac{\partial F_x}{\partial Z_i} dZ_i \qquad (2.22)$$

$$Vy_i^j = -(F_y)_0 - \frac{\partial F_y}{\partial y_p^j} dy_p^j - \ldots\ldots - \frac{\partial F_y}{\partial Z_c^j} dZ_c^j - \frac{\partial F_y}{\partial X_i} dX_i - \frac{\partial F_y}{\partial Y_i} dY_i - \frac{\partial F_y}{\partial Z_i} dZ_i \qquad (2.23)$$

For every point measured on an image, a pair of equations such as (2.22) and (2.23) can be formulated. The entire set of equations can then be represented by the matrix equation:

$$\underline{v} = \underline{A}\,\underline{x} - \underline{l}\ , \qquad (2.24)$$

which is the classical notation for the observation equations, with the vector $\underline{x}$ containing all the unknown corrections to the parameters (the parameters need to have provisional values), the design matrix $\underline{A}$ containing all the coefficients to the unknowns, the vector $\underline{l}$ containing the "free terms" (all the $(F_x)_0$ and $(F_y)_0$ terms) and the vector $\underline{v}$ containing all the residuals relating to the observations. The $(F_x)_0$ and $(F_y)_0$ terms are equal to the evaluation of F_x and F_y in equations (2.18) and (2.19) respectively, using the provisional starting values for all the unknown parameters.

Equation (2.24) leads to the unbiased minimum variance estimators shown in (2.25), (2.27) and (2.28) below:

$$\hat{\underline{x}} = (\underline{A}^T \underline{P}\, \underline{A})^{-1} (\underline{A}^T \underline{P}\, \underline{l}) \qquad (2.25)$$

or simplified,

$$\hat{\underline{x}} = \underline{N}^{-1} \underline{c}\ , \quad \text{with } \underline{N} = \underline{A}^T \underline{P}\, \underline{A} \text{ and } \underline{c} = \underline{A}^T \underline{P}\, \underline{l} \qquad (2.26)$$

$$\hat{\sigma}_0^2 = \frac{\underline{v}^T \underline{P}\, \underline{v}}{f} \qquad (2.27)$$

$N x = C$

$$\underline{v} = \underline{A}\,\hat{\underline{x}} - \underline{l} \qquad (2.28)$$

where the following symbols are used:

f ... degrees of freedom = no. of observations - no. of unknowns;
$\underline{P}$ ... *a priori* weight matrix of the observations;
$\hat{\sigma}_0$ ... *a posteriori* standard deviation of unit weight;
^ ... indicating a least squares estimator.

If 100 points are coordinated in object space using five images and ten control points, and if all points were visible on all images, there would be 110x5x2=1100 observation equations in the form of (2.24) and there would be 5x9+100x3=345 unknowns to calculate. This means that the design matrix $\underline{A}$, has dimensions 1100 by 345 and the normal equation matrix $\underline{N}$, has dimensions 345 by 345. If a direct solution on a computer was attempted, problems would be encountered with space (to store all the large matrices) and time (inversion of the big normal equation matrix $\underline{N}$). It is possible to reduce the amount of space by forming $\underline{N}$ directly and hence not needing to allocate storage space for $\underline{A}$, as well as by only storing the upper or lower triangular portion of $\underline{N}$ ($\underline{N}$ is always real symmetric and positive-definite provided there is no rank deficiency). However, the computer may still not have the capacity to store all the necessary elements of $\underline{N}$ and it must also be remembered that much larger systems are often encountered.

From the above discussion it is obvious that the direct solution of the normal equations is not practicable for larger systems, but on closer inspection of the structure of the normal equation matrix $\underline{N}$, it can be seen that the bundle adjustment is suited to a solution by partitioning. This is discussed in section 2.2.1.

The bundle adjustment method can also be adapted for solving triangulation networks observed with theodolites, (see section 6.2).

2.2.1 Partitioning

For a detailed description of the partitioning mentioned below, the reader is also referred to Brown (1958). The normal equation matrix $\underline{N}$, described in the last

section, takes the form shown in Figure 2.2 if the following partitioning is adopted in equation (2.26):

$$\underline{N} = \begin{bmatrix} \dot{\underline{N}} & \overline{\underline{N}} \\ \overline{\underline{N}}^T & \ddot{\underline{N}} \end{bmatrix} \quad , \quad \hat{\underline{x}} = \begin{bmatrix} \dot{\underline{x}} \\ \ddot{\underline{x}} \end{bmatrix} \quad \text{and} \quad \underline{c} = \begin{bmatrix} \dot{\underline{c}} \\ \ddot{\underline{c}} \end{bmatrix} \tag{2.29}$$

in which the single dot refers to the elements related to the camera parameters, the double dot refers to the elements related to the object point coordinates and the overbar refers to the "mixed" elements. Equation (2.26) becomes:

$$\begin{bmatrix} \dot{\underline{x}} \\ \ddot{\underline{x}} \end{bmatrix} = \begin{bmatrix} \dot{\underline{N}} & \overline{\underline{N}} \\ \overline{\underline{N}}^T & \ddot{\underline{N}} \end{bmatrix}^{-1} \begin{bmatrix} \dot{\underline{c}} \\ \ddot{\underline{c}} \end{bmatrix} \tag{2.30}$$

m = no. of object pts.
n = no. of cameras.

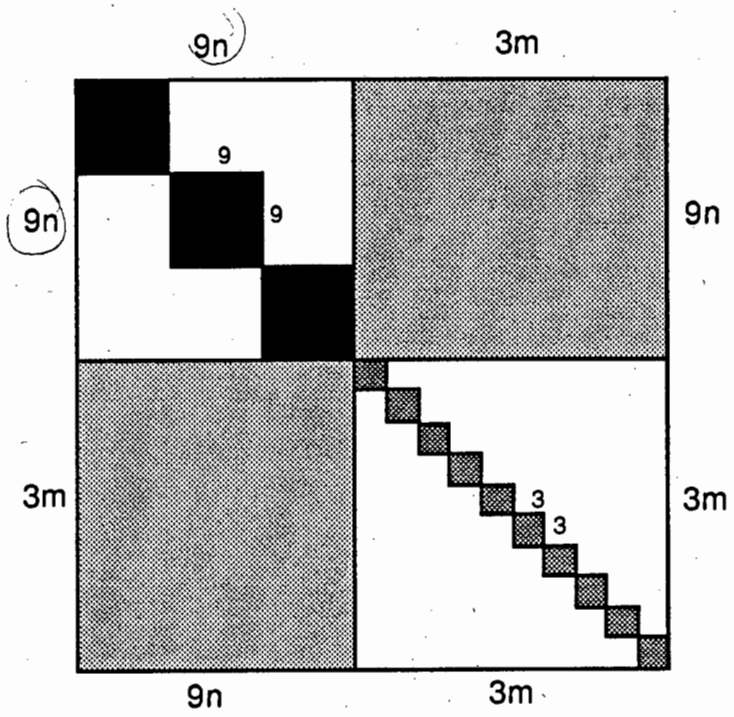

Figure 2.2. The structure of the normal equation matrix $\underline{N}$

The inversion of $\underline{N}$ can be achieved through this partitioning. Assume

$$\underline{N}^{-1} = \begin{bmatrix} \dot{\underline{N}} & \overline{\underline{N}} \\ \overline{\underline{N}}^T & \ddot{\underline{N}} \end{bmatrix}^{-1} = \begin{bmatrix} \dot{\underline{M}} & \overline{\underline{M}} \\ \overline{\underline{M}}^T & \ddot{\underline{M}} \end{bmatrix} \tag{2.31}$$

Substituting (2.31) into (2.30) gives:

$$\begin{bmatrix} \dot{\underline{x}} \\ \ddot{\underline{x}} \end{bmatrix} = \begin{bmatrix} \dot{\underline{M}} & \overline{\underline{M}} \\ \overline{\underline{M}}^T & \ddot{\underline{M}} \end{bmatrix} \begin{bmatrix} \dot{\underline{c}} \\ \ddot{\underline{c}} \end{bmatrix} \tag{2.32}$$

and multiplying out results in:

$$\dot{\underline{x}} = \dot{\underline{M}}\,\dot{\underline{c}} + \overline{\underline{M}}\,\ddot{\underline{c}} \quad \text{and} \tag{2.33}$$

$$\ddot{\underline{x}} = \overline{\underline{M}}^T\,\dot{\underline{c}} + \ddot{\underline{M}}\,\ddot{\underline{c}} \tag{2.34}$$

From the definition of inversion,

$$\begin{bmatrix} \dot{\underline{N}} & \overline{\underline{N}} \\ \overline{\underline{N}}^T & \ddot{\underline{N}} \end{bmatrix} \begin{bmatrix} \dot{\underline{M}} & \overline{\underline{M}} \\ \overline{\underline{M}}^T & \ddot{\underline{M}} \end{bmatrix} = \begin{bmatrix} \underline{I} & \underline{0} \\ \underline{0} & \underline{I} \end{bmatrix} \tag{2.35}$$

which, when multiplied out gives four simultaneous equations:

(i) $\dot{\underline{N}}\,\dot{\underline{M}} + \overline{\underline{N}}\,\overline{\underline{M}}^T = \underline{I}$

(ii) $\dot{\underline{N}}\,\overline{\underline{M}} + \overline{\underline{N}}\,\ddot{\underline{M}} = \underline{0}$

(iii) $\overline{\underline{N}}^T\,\dot{\underline{M}} + \ddot{\underline{N}}\,\overline{\underline{M}}^T = \underline{0}$

(iv) $\overline{\underline{N}}^T\,\overline{\underline{M}} + \ddot{\underline{N}}\,\ddot{\underline{M}} = \underline{I}$ (2.36)

Solving for $\bar{\underline{M}}^T$ in (iii) of (2.36) gives:

$$\bar{\underline{M}}^T = -\dot{\underline{N}}^{-1}\bar{\underline{N}}^T\dot{\underline{M}} \qquad (2.37)$$

Substituting (2.37) into (i) and (iv) yields:

$$\dot{\underline{N}}\dot{\underline{M}} - \bar{\underline{N}}\dot{\underline{N}}^{-1}\bar{\underline{N}}^T\dot{\underline{M}} = \underline{I} \quad \text{and} \qquad (2.38)$$

$$-\bar{\underline{N}}^T\dot{\underline{M}}\bar{\underline{N}}\dot{\underline{N}}^{-1} + \ddot{\underline{N}}\ddot{\underline{M}} = \underline{I} \qquad (2.39)$$

The solutions of $\dot{\underline{M}}$ and $\ddot{\underline{M}}$ come directly from (2.38) and (2.39) respectively:

$$\dot{\underline{M}} = (\dot{\underline{N}} - \bar{\underline{N}}\dot{\underline{N}}^{-1}\bar{\underline{N}}^T)^{-1} \quad \text{and} \qquad (2.40)$$

$$\ddot{\underline{M}} = \ddot{\underline{N}}^{-1} + \ddot{\underline{N}}^{-1}\bar{\underline{N}}^T\dot{\underline{M}}\bar{\underline{N}}\dot{\underline{N}}^{-1} \qquad (2.41)$$

Therefore, once $\dot{\underline{M}}$ has been evaluated from equation (2.40), $\bar{\underline{M}}$ and $\ddot{\underline{M}}$ are evaluated from equations (2.37) and (2.41) respectively. Equations (2.33) and (2.34) can now be solved for the unknowns.

With the partitioning introduced, the main computational problem becomes the inversion of the matrix in equation (2.40) which has dimensions equal to the total number of unknown camera parameters. The inversion of $\ddot{\underline{N}}$ does not pose any problem as it consists of m diagonally placed matrices of order 3x3.

Certain other properties of the normal equation matrix $\underline{N}$, can be used to further increase the efficiency of this solution. It is possible to determine suitable provisional values for the object points, so that the vector $\ddot{\underline{c}}$ reduces to zero. This is achieved through a preliminary iterative procedure. Equations (2.33) and (2.34) would then become:

$$\dot{\underline{x}} = \dot{\underline{M}}\dot{\underline{c}} \quad \text{and} \qquad (2.42)$$

$$\ddot{\underline{x}} = \bar{\underline{M}}^T\dot{\underline{c}} \qquad (2.43)$$

In addition, using equations (2.37), (2.42) and (2.43), $\ddot{\underline{x}}$ can be formulated in terms of $\dot{\underline{x}}$ by:

$$\ddot{\underline{x}} = -\dot{\underline{N}}^{-1}\underline{\dot{N}}^{T}\dot{\underline{x}} \qquad (2.44)$$

An assumption has been made throughout section 2.2.1 that all the camera parameters and all the object coordinates are unknown. However, this is not necessary for the partitioning to be valid, and the appropriate row and column of the normal equation matrix $\underline{N}$, can be eliminated if a certain parameter is to be treated as fixed or known. This is easily incorporated into the partitioning described above.

2.2.2 Additional Parameters

As mentioned in section 2.1, two assumptions were made about the perspective projection process when deriving the collinearity equations. These were that the image points all lie in one plane and that any object point, its image point and the perspective centre, lie on a straight line. It is often possible to improve the mathematical model by including additional parameters. These additional parameters could be corrections for: lens distortions, departures of the image from a plane, refraction, differences in x and y scale on the image (especially in the case of video images) or other systematic errors.

Distortions of the lens are a major source of error, particularly when non-metric cameras are employed. In principal, every camera lens system suffers from aberrations which cause deviations from the collinearity condition. In some cases these distortions are so small that they need not be modelled, while in others the effects need to be compensated for. The two main types of lens aberration which affect the location of the image and which cannot be eliminated by physical means, are radial distortion and decentering distortion.

Radial distortion results in the radially symmetric displacement of an image from its true position. This distortion may be negative (barrel distortion) or positive (pin-cushion distortion) depending on the lens system. Fryer (1989) states that, "Radial distortion may be slightly asymmetric, but it is conventionally shown as symmetric about a 'principal point of best symmetry'." This point can be considered as coincident with the principal point for the "accuracies and methods of non-topographic photogrammetry."

Decentering distortion occurs due to physical defects in the lens system. In a perfect lens system the centres of curvatures of all of the optical surfaces are strictly collinear. Deviations from linearity result in decentering distortion.

Lens distortions can be formulated as corrections to the observed image coordinates of points. A number of different expressions for these corrections have been devised. Brown (1980) uses the following well-established lens distortion model:

$$\Delta x = \bar{x}\,(k_1 r^2 + k_2 r^4 + \dots) + \left[P_1 (r^2 + 2\bar{x}^2) + 2P_2 \bar{x}\,\bar{y} \right] \left[1 + P_3 r^2 + \dots \right] \quad \text{and}$$

$$\Delta y = \bar{y}\,(k_1 r^2 + k_2 r^4 + \dots) + \left[2P_1 \bar{x}\,\bar{y} + P_2 (r^2 + 2\bar{y}^2) \right] \left[1 + P_3 r^2 + \dots \right] \qquad (2.45)$$

where,

$$\bar{x} = x - x_p, \quad \bar{y} = y - y_p, \quad r = \sqrt{\bar{x}^2 + \bar{y}^2} \qquad (2.46)$$

(k_1, k_2, ...) are the coefficients of radial distortion and (P_1, P_2, ...) are the coefficients for decentering distortion.

El-Hakim (1986a) proposed a new model for the correction of systematic errors occurring in images obtained from CCD cameras. The additional parameters in this model were chosen to correct for:

(i) lens distortions;
(ii) scale variation in x and y image axes;
(iii) non-perpendicularity of the x and y axes;
(iv) non-perpendicularity of the optical axis with the image plane.

The corrections are given by:

$$\Delta x = \bar{x}(a_4 r^2 + a_5 r \cos 2\lambda + a_6 r \sin 2\lambda) + a_7 \bar{y} \quad \text{and}$$

$$\Delta y = \bar{y}(a_1 + a_2 \cos\lambda + a_3 \sin\lambda + a_4 r^2 + a_5 r \cos 2\lambda + a_6 r \sin 2\lambda) \qquad (2.47)$$

where $\bar{x}, \bar{y}$ and r are the same as in (2.46) and λ is the angle whose tangent is $\bar{y}/\bar{x}$. In this model there is only one parameter, a_4, to compensate for radial lens distortion, while a_1 and a_7 are included for affine film deformation and non-perpendicularity of the image axis. The other parameters are part of a harmonic function to model other systematic errors. El-Hakim has shown that the application of these functions (in CCD images) resulted in a 30 percent increase in accuracy for his test objects.

The coefficients (of the corrections Δx and Δy) for both models can be determined by including these coefficients as additional parameters within the bundle adjustment. The incorporation of these additional parameters results in a corrected photogrammetric model (from equations (2.11) and (2.12)), given by:

$$x_i - x_p + \Delta x_i = c\frac{R_1}{R_3} \tag{2.48}$$

$$y_i - y_p + \Delta y_i = c\frac{R_2}{R_3} \tag{2.49}$$

The expressions for the corrections Δx_i and Δy_i, must be linearized when executing a bundle adjustment or least squares direct linear transformation (see section 2.3).

For a particular photogrammetric measuring process, a particular error model will be best suited. Often, some of the additional parameters cannot be reliably determined as they may be highly correlated within themselves or with the other collinearity parameters. These should be eliminated from the solution. Any distortions which are equivalent in magnitude to the precision of observations required for a certain task, should be corrected for by the addition of suitable parameters. In the case of CCD cameras, different causes of errors, among others sensor distortion and horizontal line jitter (Lenz and Fritsch, 1990), are also encountered.

2.3 THE DIRECT LINEAR TRANSFORMATION (DLT)

"An alternative formulation of the analytical orientation problem is the Direct Linear Transform, or DLT, ... The main advantages of the method are that it does not require a calibrated camera, or one with fiducial marks, and can be solved without supplying initial approximations for the parameters", (McGlone 1989). The DLT, or "projective transformation" as referred to by Adams (1981) and Adams et al (1983), is given by equations (2.50) and (2.51):

$$x_i + \Delta x_i = \frac{b_{11} X_i + b_{12} Y_i + b_{13} Z_i + b_{14}}{b_{31} X_i + b_{32} Y_i + b_{33} Z_i + 1} \qquad (2.50)$$

$$y_i + \Delta y_i = \frac{b_{21} X_i + b_{22} Y_i + b_{23} Z_i + b_{24}}{b_{31} X_i + b_{32} Y_i + b_{33} Z_i + 1} \qquad (2.51)$$

Where x_i, y_i, are the image coordinates of point i, Δx_i, Δy_i, are the systematic errors of the image coordinates of point i (caused by lens distortion, etc.), X_i, Y_i, Z_i, are the object coordinates of point i and the b terms are the unknown transformation parameters from which the elements of interior and exterior orientation can be calculated. This linearly dependent equation set involves eleven transformation parameters instead of the nine linearly independent camera parameters of the collinearity equations. An approximation lies in ignoring the linear dependence between parameters. However, the DLT solution does have some advantages in that it converges quickly even for poor provisional values and it appears to converge in spite of the high correlations which would affect a bundle solution.

Karara and Abdel-Aziz (1973) point out that "the linear components of lens distortion and film deformation are taken into account by the eleven transformation coefficients" and go on to show that for all the cameras that were tested, the k_1 coefficient (equivalent to k_1 in equation (2.45)) is the most significant when representing lens distortion.

If any of the nine physical parameters of the camera(s) are needed, they can be approximately (i.e. non-uniquely) calculated once the eleven DLT transformation parameters are known. The DLT also offers a quickly converging method for determining provisional values for a bundle adjustment.

2.4 ASPECT RATIO IN DIGITAL IMAGES

The location of each pixel (PICture ELement) in a digital image is given by its row and column number. A typical digital image has 512 rows by 512 columns. These pixel coordinates must be transformed into units of millimetres on the image plane, which in the case of CCD video cameras is an imaging chip. Imaging chips come in a variety of sizes and with a variety of sensor (pixel) array dimensions. For example, the Philips cameras used in SPG have an imaging chip of 6.0 by 4.5 millimetres. The distinction between chip pixels and image pixels must be noted. As can be seen, the 512 by 512 digital image contains a scale difference in the horizontal and vertical directions. This is known as the aspect ratio.

The pixel coordinate system of the digital image, and the traditional image coordinate system are depicted in Figure 2.3.

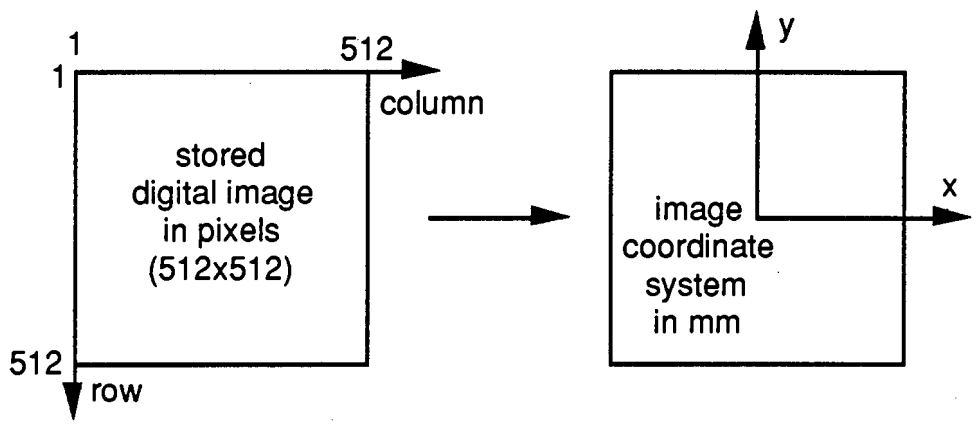

Figure 2.3. Transforming pixel coordinates into image coordinates

The transformation between the two systems can be seen as a translation to move the origin into the approximate centre of the image, a reflection to change the direction of the positive vertical axis, and a horizontal and vertical scale to change image pixels into millimetres. The transformation is given by equations (2.52) and (2.53):

$$x_{mm} = (\text{column} - \frac{h}{2})\, s_h \quad \text{and} \tag{2.52}$$

$$y_{mm} = (\frac{v}{2} - row)\, s_h \qquad (2.53)$$

where h is the total number of image pixels in a row, v is the total number of image pixels in a column and s_h and s_v are the horizontal and vertical scale between pixel coordinates on the digital image and image coordinates in millimetres, respectively.

The ratio between s_h and s_v is the aspect ratio. An approximation to determine s_h is to divide the length of the image chip (6 millimetres) by the number of horizontal image pixels (512). Similarly, to determine s_v, one could divide the width of the chip (4.5 millimetres) by the number of vertical image pixels (512). Often, for a certain make of camera, a number of edge pixels on the chip are inactive, resulting in the active chip area being less than expected. This results in the values for s_h and s_v being smaller. More reliable values for the scales s_h and s_v can be determined by a camera calibration. The aspect ratio (s_h/s_v) determined for the Philips cameras, used in SPG, is 0.01096 / 0.0076.

3 HARDWARE OF THE SPG SYSTEM

As was mentioned in section 1.2, SPG was based on earlier work (Ruther and Parkyn, 1990) for the development of PHOENICS. A number of hardware improvements exist in the present SPG system, these being:

(i) a faster and bigger personal computer;
(ii) a more powerful and flexible video framegrabber;
(iii) three CCD video cameras instead of two.

The hardware components of SPG (Figure 3.1) have been chosen with the treatment of brain tumours specifically in mind. The system comprises:

(i) three Philips CCD video cameras, three power supply units (PSU) and a signal processor interface (SPI);
(ii) a Matrox MVP-AT frame-grabber and image processor;
(iii) a Unisys 386 PC (with an 8087 maths co-processor);
(iv) three external Philips video monitors.

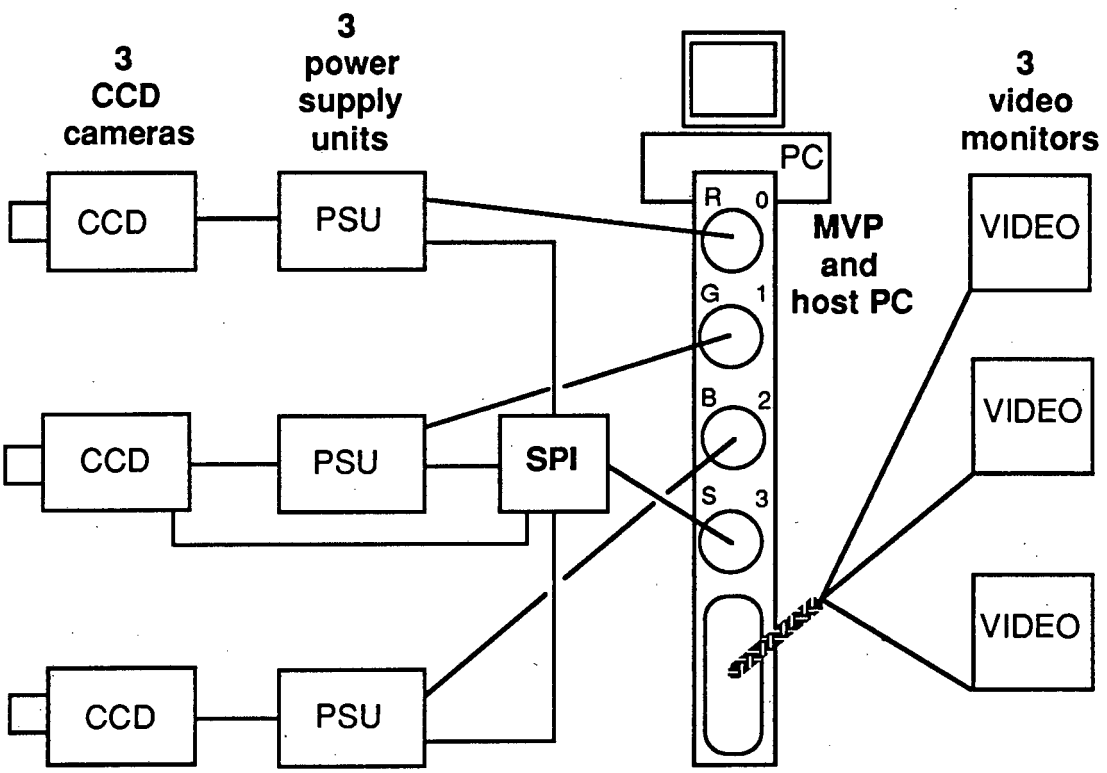

Figure 3.1. Hardware components of the digital camera system

Channels 0 - 2 on the MVP receive the video signals from the three black and white CCD cameras. Channel 3 is used for the synchronisation (sync) input. The power supply units (PSU) provide power for the cameras as well as providing "sync" signals. The MVP frame-grabbing and image processing board is situated in the host computer, which can address the board through a software library (written and compiled in Microsoft C) provided by the manufacturers. The MVP outputs the three video signals to the three video monitors. A more detailed description of the various components is now given.

3.1 CCD CAMERAS

The three system cameras are 12 V DC CCIR Philips LDH 0600/00 indoor cameras. The image sensors inside the cameras are frame transfer imaging devices with a 6.0 by 4.5 millimetres imaging area and a pixel array of 604 (horizontal) by 576 (vertical) elements. Telephoto zoom lenses (12.5 to 75 millimetres) are being used with the CCD cameras. Figure 3.2 shows one of the CCD cameras.

Figure 3.2. CCD camera with telephoto zoom lens

Each camera is operated from a mains driven 12 V PSU. The PSU also provides the necessary "sync" signals. The SPI acts as a distribution amplifier bringing the "sync" and video signals up to the required amplitude and waveshape, and isolating the input from the output. Double terminations are thus avoided and perfect matching (i.e. 75 ohms) is obtained. (Private communication Mr J Hesselink, Department of Electrical and Electronic Engineering, UCT).

3.2 MVP-AT FRAME-GRABBING AND IMAGE PROCESSING BOARD

In general, frame-grabbing boards such as the MVP provide:

(i) analogue-to-digital conversion on an incoming video signal;
(ii) the ability to capture, store and display a digital image;
(iii) a certain amount of image processing capabilities.

The MVP occupies 64 Kbytes of memory locations and thirty-two eight-bit I/O locations in the host computer address space. The front end of the MVP consists of a row of four RCA-type connectors for video input and a nine-pin female D-type connector for video monitor output (MATROX, 1989).

The video input connectors are used to connect video sources (cameras, etc.) to the MVP input channels. Up to four sources can be connected at a time (for sequential use), and each channel is selectable by software. Any one of channels 0 to 3 can be used for black and white (B/W) input. For colour input or simultaneous B/W input from three sources, channels 0 to 2 are used for the three inputs (red, green and blue (RGB) in the case of colour). Figure 3.3 shows the relationship between RGB colour and the input channels.

Channel	RGB Colour
0	red
1	green
2	blue
3	*

* Channel 3 can be selected as a video input channel or as an input for an external synchronisation source.

Figure 3.3. Video channels on the MVP-AT

In the case of three B/W cameras, the video signal entering channel 0 is treated as the red signal, the signal entering channel 1 as green and the signal entering channel 2 as blue.

The monitor output connector supplies video to the external monitors. The MVP display resolution can be configured in several possible ways. For SPG the display is set as:

(i) 10 MHz pixel clock frequency (giving a 4 to 3 aspect ratio);
(ii) interlaced scanning method;
(iii) European television standard.

The MVP is capable of capturing 30 frames per second in interlaced mode. However, the MVP supports a number of video standards, including the CCIR standard (50Hz) of the SPG cameras (i.e. 25 frames per second).

The MVP can also use three different synchronisation types. These are:

(i) internal "sync";
(ii) external composite "sync";
(iii) separate external "sync".

The choice of internal and external "sync" can be selected through the MVP software. External composite "sync" is used in SPG.

A precision phase-locked loop (PLL) provides a drift-free genlock ("sync" lock) which locks the board to the incoming signal. The manufacturers best estimate is that lock is achieved in about five lines from the beginning of the frame. Once locked the generated pixel clock becomes extremely stable; pixel jitter (i.e. the tendency of a pixel position to drift) is reduced to under 10 nanoseconds (which is the best estimate) or about 1/10th of the size of the pixel.

In SPG, three images need to be captured and displayed simultaneously, therefore it was necessary to obtain a frame-grabber which could meet this requirement. The MVP can simultaneously grab from three separate input sources three entirely separate input images. The MVP digitises these incoming images into 256 discrete intensity levels (i.e. grey values), equivalent to eight bits. By defining the memory (see section 4.1) as 512 by 512 by 24-bits (colour), three B/W 512 by 512 by 8-bit images can be simultaneously captured and stored. These three images can then be output at the same time, each through a separate output look-up table. In addition the above configuration can have one four-bit overlay for graphics and text. This overlay can be used on any or all of the three output images.

3.3 SUITABLE PC AND EXTERNAL MONITORS

A personal computer must satisfy two important conditions if it is to be utilised in an RTP system.

(i) It must be compatible with the frame-grabber board;
(ii) its processing speed must be fast enough to complete any necessary calculations in the required time period (this depends on the process being measured).

The computer used for SPG is a 25 MHz Unisys 386 with an 8087 maths co-processor installed. Three external monitors are needed to display each of the video channels. Those used are the Philips RGBCM 8833. Figure 3.4 shows the PC and the three external monitors.

Figure 3.4. PC and external monitors

4 IMAGE PROCESSING WITH THE MVP-AT

The MVP-AT is a sophisticated card capable of many image processing routines of which only a handful are used in SPG. This chapter gives a brief overview of the card, its software capability and some of the extra software routines developed with the MVP.

4.1 MVP-AT SYSTEM OVERVIEW

The MVP comprises a number of functional sections (see Figure 4.1):

(i) the input section;
(ii) the memory section;
(iii) the statistical section;
(iv) the graphics section;
(v) the display section;
(vi) the arithmetic section.

The input section is configured through software to match the devices connected to the front of the MVP. It is made up of look-up tables, logic to adjust the gain and offset, and analogue-to-digital convertors. The input look-up table (ILUT) can be programmed to change the image in a predictable way before it is stored in memory. Incoming pixel intensity values are used as addresses to the look-up table. The data stored at these addresses are used as new pixel intensity values.

The memory section consists of 1 Mbyte of video memory used for storing the digital images. This memory can be divided into different frame buffer configurations depending on which parameter values are used in the various software commands. One large (1024 by 1024 by 8-bit) frame buffer, two medium-sized (512 by 512 by 16-bit) frame buffers or four small (512 by 512 by 8-bit) frame buffers can be chosen. In SPG, the four small frame buffers are chosen, three for storing the three separate images and the fourth one for overlaying or for using as an intermediate buffer in certain calculations (see section 4.3.1).

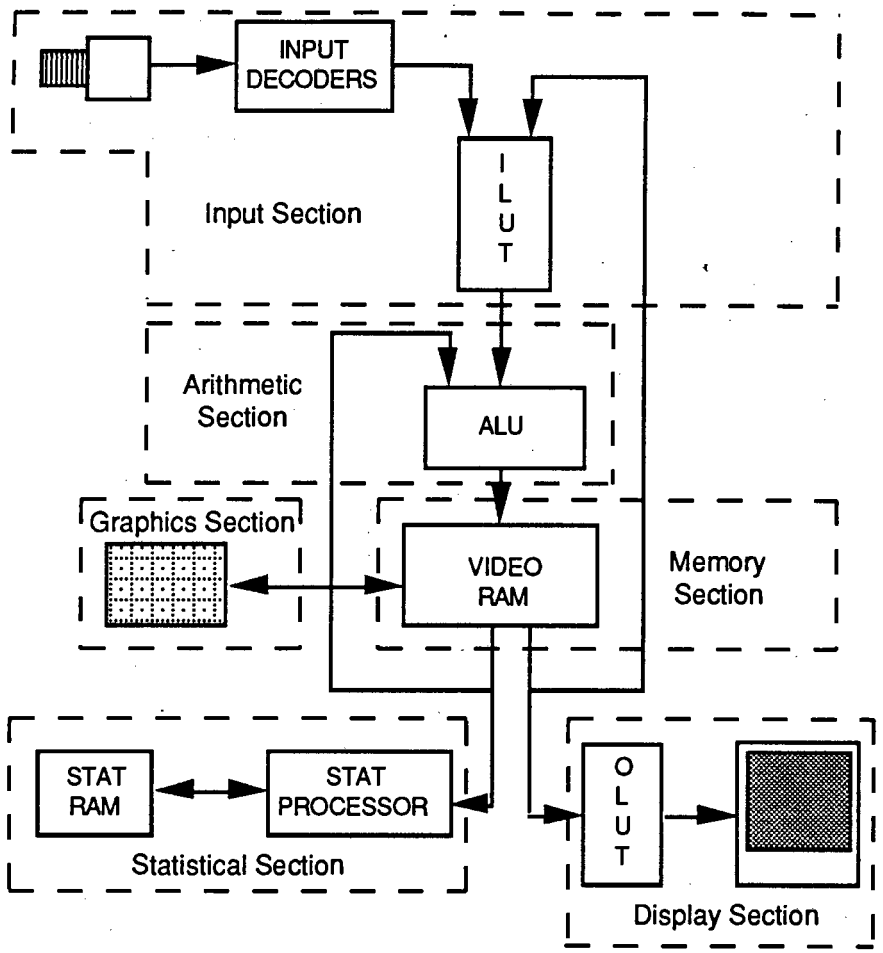

Figure 4.1. Functional sections of the MVP-AT

The statistical section is a hardware section that performs intensity histograms and profiles.

The graphics section allows the user to perform drawing routines.

The display section extracts information from memory, converts it to video and sends it to the display. Display features include overlays, windows and keying (i.e. mixing memory contents with an input signal) which are all user-selectable. This section also has an output look-up table (OLUT) that can be addressed by the user.

The arithmetic section, also described as the arithmetic logic unit (ALU), performs all arithmetic and logical routines either on one frame buffer, between one frame buffer and a constant, or between two frame buffers. These routines

operate in real-time with a camera input. Neighbourhood and shape-determining operations are also possible with this section.

4.2 BASIC IMAGE PROCESSING ROUTINES USING THE MVP-AT

The following sub-sections describe a number of software-based routines that are all utilised in SPG. Library files, containing routines to address the MVP are provided by the manufacturers. These are written in Microsoft C and can be linked directly with a user-program written in C, or invoked indirectly through an interpreter which allows interactive access to all of the MVP commands.

4.2.1 Initialising the Board

The board is initialised by calling two library routines: **selboard** and **init**. The former selects which board in a multi-board system will be accessed, while the latter initialises this board to default values. As not all the default values are suitable for SPG, extra commands are necessary to correctly set up the board. These are:

(i) **disformat 0 1 0** (which sets the display format to: 10MHz pixel clock frequency; interlaced monitor and a European television standard);
(ii) **iowin 0 0 512 512** (this sets the I/O window to the stated pixel coordinates);
(iii) **procwin 0 0 512 512** (which sets the processing window to the stated pixel coordinates);
(iv) **inmode 2** (which selects the current input source as RGB);
(v) **sync 1 1** (which selects the "sync" source as external and coming from channel 3);
(vi) **video 1 0** (this activates the display from the camera connected to the current channel (which is channel 0 after a call to **init**)).

At this stage the board is properly initialised for a live display from the camera connected to channel 0. The board is now in processing mode, which is one of four board modes:

(i) input/output mode (selected by **opmode 0 n**);
(ii) graphics mode (**opmode 1 n**);
(iii) processing mode (**opmode 2 n**);
(iv) continuous grabbing mode (**opmode 3 n**).

The parameter **n** refers to the current frame buffer. The correct board mode must be chosen for each library command, otherwise unpredictable results may occur.

4.2.2 Capturing, Displaying and Transferring Images

Before explaining the image capture and display procedures it is necessary to discuss the component frame buffers. As mentioned in section 4.1 the configuration chosen comprises the four small frame buffers. These are defined as being 0, 1, 2 and 3. Frame buffer 2 is used as a possible overlay while 0, 1 and 3 are the basic frame buffers which make up a combined frame buffer defined as 6.

Images can be displayed directly from the video sources (i.e. cameras) or indirectly through the frame buffers. To view a live image from a camera, the **video 1 0** command is used as in section 4.2.1. To view images stored in the frame buffers, the **video 1 1** command is used. The displayed frame buffer is selected using the **outpath** command.

If three images are to be captured and displayed simultaneously, then the combined frame buffer (6) must be selected for storing these images. For one image, any of the basic frame buffers (0, 1 or 3) can be used. To capture an image in a frame buffer, the **snapshot** command (in processing mode) or the **cgrab** command (in continuous grabbing mode) can be used. The former only allows one frame to be captured, whereas the latter can either grab a set amount of frames or continually grab frames until a further command halts the process. However, it must be noted that only the current frame is resident in memory. Continuous grabbing into frame buffer 6 is used when "live" images from the three cameras need to be displayed.

Images can be stored on disk by copying the contents of any of the frame buffers. Likewise an image can be retrieved from disk into a specified frame buffer. The input/output mode must be used when writing to or reading from disks.

4.2.3 Thresholding

The concept of a thresholded image is central to the target search routine described in section 4.3.1. Thresholding an image entails setting all the pixel intensity values above a selected threshold value to 255 (white) and all below to 0 (black). Thus a black and white "binary" image is obtained which highlights contrasts. In SPG, suitable threshold values are used to separate the photogrammetric targets from the background.

The most efficient way of thresholding an image is via the input look-up table (ILUT). The ILUT is programmed so that all its addresses (input values) less than the threshold value contain 255, and all above contain 0 as an output value to the frame buffer (Figure 4.2). This inversion is necessary as the ILUT maps in reverse order when digitising and in forward order when using feedback.

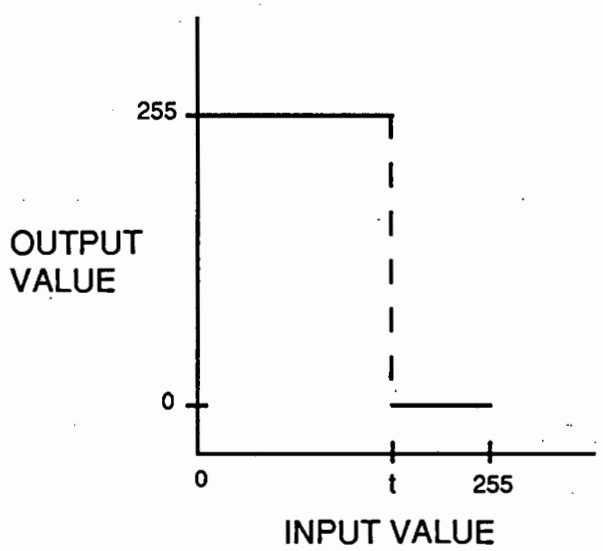

Figure 4.2. Thresholding of input

A software routine was written which lets the user change the threshold value, t, and thus the ILUT, so changing the display. Thus, within seconds the user can find by inspection a suitable threshold value for the image.

4.2.4 Graphic Overlays

An overlay is useful when information needs to be displayed over a stored image without actually changing the contents of the image. As mentioned before, frame buffer 2 is used as the overlay buffer. This overlay can be used on any one, or on all three output images. The overlay is closely linked with the output look-up tables (OLUT). Pertinent symbols and/or text are written into frame buffer 2, such as a circle to indicate a target and text to identify the name of the target. The overlay is "enabled" using the **olutlay**, **slut** and **outpath** commands. The user then views the contents of frame buffer 2 overlayed on the image buffer. Any changes in either frame buffer does not affect the other.

4.3 FURTHER IMAGE ROUTINES

4.3.1 Image Search and Target Centering

The search routine developed for SPG is composed of three stages:

(i) searching for targets on a thresholded (binary) image;
(ii) detecting the edge of the targets using the thresholded image;
(iii) determining the centre of the target using the weighted centre of gravity method.

The routine has been optimised for use with the MVP-AT, but could easily be altered for use with another frame-grabber with similar library routines.

The search component of the routine is carried out on a thresholded image. A suitable threshold value is chosen via an interactive routine with the ILUT (as described in section 4.2.3). Once this threshold value is found, the grey image is captured in one of the basic frame buffers (0, 1 or 3). The ILUT is then programmed for a threshold mapping, to change the grey image into a thresholded image. The thresholded image is stored in frame buffer 2. This mapping is performed using the **inmap** command.

Now that the thresholded image is accessible, the target search routine can be executed. The search proceeds row by row. A row (512 pixels) is read into a buffer (array of characters) and the first occurrence, if any, of 255 (white pixel) is found. If no white pixel is found then the next row is searched. Once a white pixel is found (indicating the top left target pixel) the next stage of detecting the edge of the target begins. This is accomplished by chain-coding as discussed, among others, in Rosenfeld (1984) and Gonzales and Wintz (1977). The edge of a target can be found and mapped using a chain-code (Figures 4.3 and 4.4).

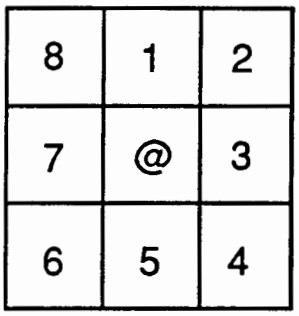

Figure 4.3. Chain-coding. The current pixel is denoted by @ and the directions to the neighbouring pixels are coded from 1 to 8

The current pixel (or last detected pixel) is represented by @ in Figure 4.3. Each neighbouring pixel value can be directly read from frame buffer 2, which contains the thresholded image. The direction to the next edge pixel can be coded using the eight directions shown. For example, the edge of the binary target in Figure 4.4, can be represented by the code 344566788122, if the starting pixel is the pixel marked '1' in the figure.

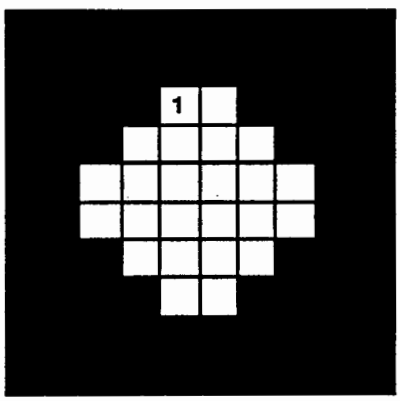

Figure 4.4. A target on the binary image. The pixel marked '1' is the first target pixel detected

There are eight possible directions in which to begin the search for the next edge pixel. An obvious but inefficient method would be to always start looking in the next direction (in a clockwise sense) to that of the previous edge pixel. If an edge pixel is not found then the following directions are sequentially searched. For example, if the previous edge pixel is at 7 the search will start from direction 8. If no edge pixel is found then the following directions are searched until one is found. This pixel becomes the new current pixel. This method, although theoretically sound, is inefficient because as the example shows, there should be no need to search in directions 8 or 1 as these pixels should have been checked from the last current pixel.

The direction in which to start searching for the next edge pixel can be derived from the direction in which the current pixel was found. If the last successful direction was towards 1 or 2 then the current search must start from direction 8. Likewise 3 or 4 gives 2, 5 or 6 gives 4 and 7 or 8 gives 6 as the new starting direction. Thus, the starting search directions for each of the edge pixels in Figure 4.4 beginning with pixel '1', are 2, 2, 2, 2, 4, 4, 4, 6, 6, 6, 8 and 8 respectively. Note that the reason for starting the very first search towards direction 2 and not towards direction 3, is that the routine has four possible starting directions: 2, 4, 6 and 8.

Each time a new edge pixel is found it alters the detected target size and position. If this new current pixel is found to be the same as the starting pixel, the detection of the target edge is complete. Otherwise the routine continues.

Once the entire target is found it is erased from the thresholded image so that it is not re-detected. This is accomplished by writing a rectangular block of zeros (black) onto the thresholded image, in place of the detected target. In addition, if the target extent is smaller or larger than preset values then it is discarded as a non-target.

Target centering, unlike the search, is carried out on the original grey image to ensure that all available information is used. At this stage the extent and position of the target are known from the search of the thresholded image, so the corresponding intensity values on the grey image (in the source frame buffer) can be read into a two-dimensional array with dimensions the same as

the binary target. The threshold value is subtracted from all the intensity values in this array. Due to the fact that the array is rectangular and the target edge elliptical, there will be a few elements in the corners of the array which were not part of the binary target. These elements will have a negative intensity value after the subtraction of the threshold value. All these resulting negative values are set to zero. A weighted centre of gravity routine, using the new intensity values as weights, is then employed to determine the centre of the target in x, y image coordinates. The "non-target elements" will therefore be zero-weighted.

Once the centre is determined the image coordinates can be written to disk. The next targets are then searched for, until no more are found. The calculated target positions can then be indicated on the original grey image by drawing circles (in the frame buffer) centred at these positions.

Various other approaches along similar lines could be undertaken for the automatic search and centering of targets. El-Hakim (1986b) describes a method of creating a binary image by adopting different threshold values for different windows in the image. This is carried out by dedicated hardware. The remaining white spots on the binary image are classified into targets and non-targets by comparing the characteristics of the observed spots with characteristics of an ideal target.

Although not as sophisticated (only one threshold value for the whole image is used), the routine developed for SPG has been found to be reliable (see section 9.5) for all the completed tests.

4.3.2 Target Matching

Sophisticated least squares correlation routines, such as has been developed by Gruen (1985), exist for matching an object on one image with its appearance on another image. These routines are generally time-consuming, so for SPG a geometric solution has been investigated. The solution assumes that the camera parameters are known and that the targets have already been located. This matching process is not directly related to the MVP; however it does involve image processing, so it has been included under chapter 4.

The approach that is used, is for all targets on the first image to be matched, if possible, to targets on the second and third image. Basically, a comprehensive combination of intersections is performed using all the targets.

The first target on the first image is intersected with every target on the second image, and all intersections with an *a posteriori* standard deviation, $\hat{\sigma}_0$, less than 0.010 (say) are kept as possible matches. Similarly every target on the third image is intersected with this first target on the first image. All combinations of these possible matches are now used in intersections from all three images and the combination with the smallest $\hat{\sigma}_0$ (less than 0.010) is chosen as the correct one. If none is smaller than 0.010 then the smallest combination from two images only is taken. It is possible for the first target on the first image to have one of the following:

(i) no matches on the other two images;
(ii) a match on one of the other two images;
(iii) matches on both of the other images.

Once the correct combination is found, these targets (on the second and third images) are not reconsidered. The routine then moves onto the next target on the first image and the process is repeated until all targets on the first image have been processed. Remaining targets on the second image are then considered one by one with any remaining targets on the third image. The routine ends when all targets are matched or discarded.

It is possible for a target to be incorrectly matched when it only appears on two images. This may occur when another target appearing on the second image lies in the same plane (defined by the first target and the two perspective centres) as the first target. If a third ray from another image exists then the ambiguity would fall away (unless the two targets were virtually in the same position in object space).

The routine described above is effective for targets appearing on more than two images. Targets appearing on two images only might cause ambiguity problems. Another method, that of using epi-polar planes in a geometrical solution, was also investigated; however, it proved less reliable than the first method.

It was decided that no target matching routine would be used for SPG, as some of the targets would often appear on only two cameras. Instead, a combination of automatic and computer-aided manual routines have been employed to identify targets on each of the images (see chapter 8).

5 THE PROTON THERAPY TREATMENT PROJECT

Patients suffering from brain tumours are to be treated by exposing the tumour to a proton beam. The proton beam is situated in a specially designed room at the National Accelerator Centre (NAC) at Faure outside Cape Town. The development of a system for treating these patients and the placing and alignment of these patients in the beam-line has involved a number of scientific disciplines.

As mentioned in section 1.2, mechanical devices have been used to position and restrain patients undergoing this form of treatment in the past. A new positioning method, using digital photogrammetry, has been developed in the Department of Surveying and Geodetic Engineering at the University of Cape Town (UCT), with the objective of improving patient comfort, convenience of use and positioning speed. In conjunction with this new method, the Department of Mechanical Engineering at UCT has developed a special computer-controlled chair for seating and moving the patient into position.

Figure 5.1 shows the sequence of the various stages involved with the photogrammetric positioning of the patient. The stages are:

(i) Preliminary stages. The cameras must be calibrated before any positioning takes place. The chair is also initialised at this stage and the two systems are subsequently checked relative to each other. If this check fails then the cameras are re-calibrated and the chair is re-initialised.

Using medical imaging, the position of the tumour inside the patient's head is determined relative to special reference targets on the outside of the head. The tumour and reference targets are imaged on a CT (Computer Tomography) scan or MRI (Magnetic Resonance Imaging) scan. At present, small ball bearings are used as reference targets to be visible in the CT scan, whereas for the MRI scan small plastic capsules filled with fish oil are used. These scans have the capability of allowing three-dimensional coordinates of the tumour and reference targets to be determined.

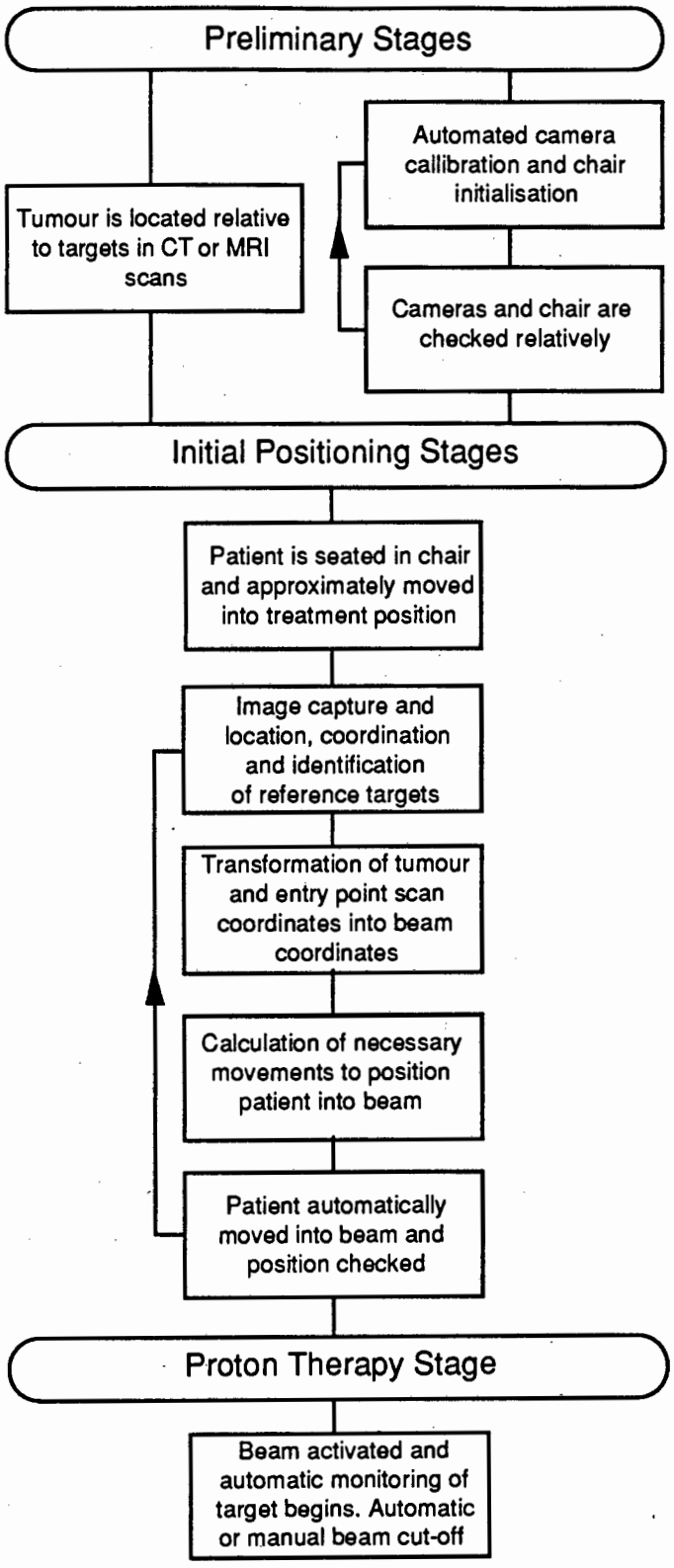

Figure 5.1. Sequence of procedures

Once the tumour is located, medical specialists decide on a suitable beam entry point on the head, in a position which ensures that no sensitive areas of anatomy (e.g. eyes, spinal chord) will be passed through by the beam. The vector between beam entry point and tumour must be positioned in the beam line before therapy can begin.

(ii) Initial positioning stages. The patient is first seated in the computer controlled chair which is manually moved into the provisional treatment position. Then, using digital photogrammetry with three cameras, the reference targets (now special reflective targets) are coordinated. The scan coordinates of the tumour and entry point are transformed into the beam system using the reference targets for determining the transformation parameters. Translations and rotations, relative to the beam system, are then worked out for aligning the tumour and entry point into the beam. The chair's computer changes these into mechanical movements and commands the chair to move. After the movements are completed, the reference targets are again coordinated to check that the patient is in the correct position. If the patient is not in position, the stages as indicated in Figure 5.1 must be repeated. If the patient is in position, the proton therapy stage begins

(iii) Proton therapy stage. The beam is switched on and the patient is closely monitored by the cameras for any movements. This continues until the treatment is complete and the beam is switched off. If the patient moves too much, this is detected during the monitoring and the beam will be automatically switched off.

Each patient will have numerous treatment positions (i.e. entry points) so that the tumour accumulates all the radiation, while the healthy brain tissue suffers minimal damage. The photogrammetric procedures are discussed in full detail in chapter 8.

6 IMAGE CREATION

The term "image creation" describes the preparation of external factors which affect the characteristics of the end product of the imaging process, i.e. the image. It involves a number of parameters such as the light source, the object(s) reflecting the light, the camera / object configuration and camera settings such as aperture, zoom and focus. These factors, as they apply to SPG, are discussed in detail in the following chapter.

6.1 CAMERA / OBJECT CONFIGURATION

In the project, the configuration of the cameras relative to the treatment room and the control frame (see section 6.2) depended on a number of factors. These were

(i) the physical constraints of the treatment room;
(ii) the possible positions of the reference targets on the patients' heads;
(iii) some geometrical considerations for positioning accuracy.

As mentioned, three cameras will be used simultaneously during the operation of SPG. The third camera provides a degree of redundancy, so increasing the reliability of the solution.

At the beginning of the SPG project, a decision had to be made regarding the position of the cameras, so that camera mounts (stations) could be designed as part of the treatment room. At that time:

(i) the shape of the treatment room (Figure 6.1) at the NAC was known;
(ii) it was understood that equipment related to the proton beam would surround the beam line up to approximately 1.5 metres from the chair;
(iii) it was not known whether a patient mask was to be used, i.e. it wasn't then clear if reference targets could be placed anywhere on the head;
(iv) the only restrictions on the beam entry point on the head were imposed by the mechanical movements of the chair (see section 7.3) and by certain sensitive areas of anatomy; thus a patient could

be sitting upright, at an angle, or lying down, and at the same time facing the front, side or back of the room.

In light of the two uncertainties, a decision was made to have coverage of the head area from many angles around the room. Bearing geometry in mind as well, possible camera positions were proposed to the NAC. These recommendations are shown in Figures 6.1 and 6.2.

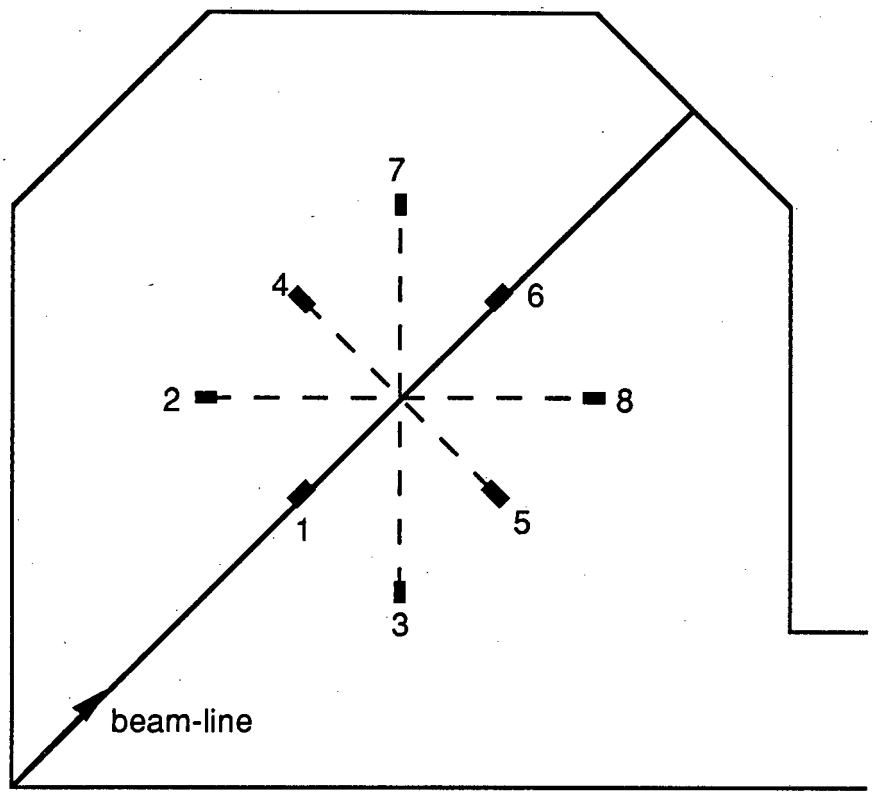

Figure 6.1. Plan view of proposed camera positions

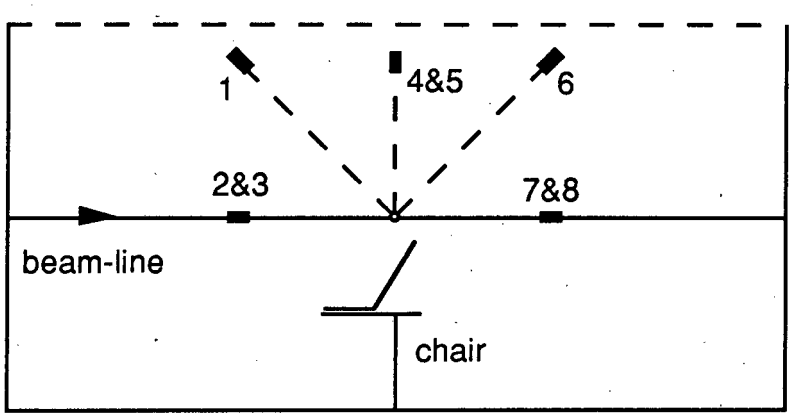

Figure 6.2. Vertical section along beam line

Four camera stations (2, 3, 7 and 8) will be at the level of the beam-line, while the other four (1, 4, 5 and 6) will be approximately at a forty-five degree angle above the horizontal. The camera stations will be 2.5 to 3.0 metres from the tumour point (intersection of the vertical chair axis with the beam line). The camera axes will all converge at the tumour point.

6.2 CONTROL TARGETS

The CCD cameras are to be regularly calibrated in the beam coordinate system, using control targets of known position. The control targets are attached to a metal frame, which is stable but movable. Permanent mounts are being designed in the treatment room, so that the frame can be replaced in exactly the same position before each camera calibration. When the frame is in position, the centre of the frame will be approximately coincident with the tumour point.

Twelve to fourteen control targets, visible from each camera station, was considered optimal for SPG, the reasons being:

(i) less targets would be too unreliable and
(ii) twelve to fourteen targets would provide enough control for a suitable determination of the DLT transformation parameters, as long as the control targets were surveyed to a high precision and reasonably well configured.

Consequently, to ensure suitable calibrations from all eight camera stations, a test control frame consisting of forty suitably placed circular targets was built. These targets were positioned in such a way, that a camera at any one of the stipulated stations would have at least twelve or more targets visible. This control frame, which was used for the development of the SPG routines, is shown in Figure 6.3. The frame is in the form of a cube with 60 centimetre sides.

Figure 6.3. Test control frame with targets

The control targets were coordinated using theodolite observations from six concrete pillars in the instrument laboratory (see Figure 6.4) in the Department of Surveying and Geodetic Engineering, UCT. The theodolite used was the Wild T1000, a single second (resolution) electronic theodolite. Horizontal angles were measured between the pillars, and both horizontal and vertical angles were observed to all the control targets on the frame. Instrument height differences between the theodolite stations were obtained by sighting a levelling staff from each pillar. Targets were observed at top, bottom, left and right, the mean giving the centre. One distance was measured between pillars 3 and 1, using a subtense bar, to provide a scale for the horizontal net.

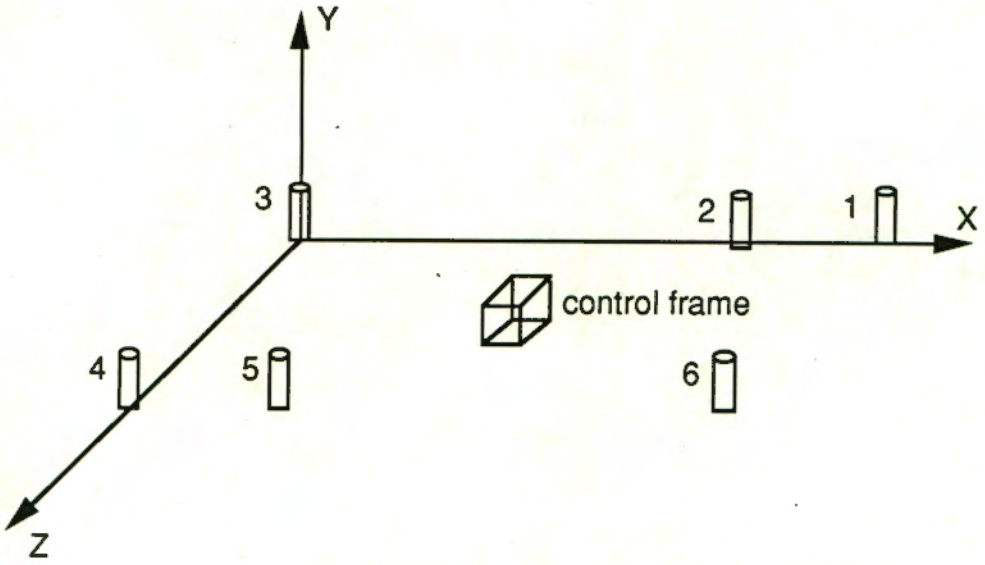

Figure 6.4. The pillars used as stations, for fixing the control frame targets

This three-dimensional network was solved using a bundle adjustment algorithm with fictitious images (Brown, 1985), derived from the observed theodolite angles. Computations were executed in four steps:

(i) Three-dimensional coordinates were determined for each of the theodolite stations. A network adjustment was used to calculate the horizontal positions (X and Z) of the instruments. Y-coordinates of the instruments were directly observed, to the nearest millimetre, from observations to an arbitrarily positioned levelling staff (the vertical angle was set to 90 and 270 degrees).

(ii) Fictitious image coordinates at each station were calculated from the observed horizontal and vertical angles to the targets.

(iii) A bundle adjustment program, written by the author, was then used to determine a final set of coordinates for the frame targets (see Appendix A). The solution treated the perspective centres and the parameters of interior orientation (of the fictitious images) of all six stations as fixed quantities. The rotation angles were treated as unknown quantities. All observations were given equal weight in the adjustment. Standard deviations (1σ level) in the order of 0.1 millimetre in X, Y and Z were achieved for the frame targets. Because a principle distance of 206.265 millimetres was fixed for each fictitious image, one second of arc was approximately 1 micron on the fictitious image.

The computed *a posteriori* standard deviation of unit weight $\hat{\sigma}_0$, was 0.0027 which thus corresponds to approximately 2.7 seconds of arc.

These results were accepted as sufficient for the development phase of SPG. When the system is finally implemented, a new control frame will be built, to be more aesthetically appealing. It will also be necessary to transform these local control target coordinates into the beam coordinate system. The beam coordinate system is defined as having:

(i) its origin at the beam tumour point;
(ii) the positive Y axis vertical;
(iii) the positive Z axis along the beam towards the beam delivery system;
(iv) the positive X axis directed so as to make the coordinate system orthogonal and right-handed.

The survey of the control targets and mechanical chair in the beam coordinate system, is outside the scope of this thesis project, therefore only a brief description will be given.

The beam line and hence the direction of the Z axis will be calculated by coordinating two (or more) points on the beam. The axis of the vertical rotation of the chair will also be determined. The intersection of the beam line with this chair axis defines the beam tumour point and hence the origin of the system. In addition, the orientation of the chair relative to the beam line, will be surveyed. Finally, the control frame will be placed in its calibration position, and a number of its control targets coordinated in the beam system. These targets will then act as common points to transform all the local control target coordinates into the beam coordinate system.

6.3 TARGETS AND LIGHTING

The practical success of an automatic or semi-automatic system such as SPG, depends largely on the ability of the software to identify targets correctly. The targets must be sufficiently different to the background scene in order to be recognised as targets. The target detection approach that has been adopted (section 4.3.1), is to discern targets on the image by their intensity values (through thresholding), rather than by their shape. This leaves two obvious

alternatives: having the targets brighter or darker than the background. Constructing a truly black target is not easy, because most materials reflect light to some degree (for example, blackboards can be highly reflective in some light). Ruther and Parkyn (1990) describe a method of using a "black hole" as a target. This target consists of a hollow cylinder painted black on the inside, which is closed at one end and partially covered except for a circular hole on the other end. The outside is then painted white to contrast with the black hole. This black hole provides almost an ideal target for thresholding techniques, however it is not easily attached to the relevant object, such as on a person's face in this treatment application. As a control target it would be suitable, so long as no other dark patches (maybe due to insufficient light) appeared on the image. As it was preferable to have both control and object targets with similar intensities, it was decided to work towards bright white (highly reflective) targets.

White targets, in general, will not stand out sufficiently from a normal surround to enable automatic detection using thresholding. This is because other surfaces and objects, although not white, might be reflecting equal or more light than the targets. A highly reflective material with which to construct targets is needed. Such a material is the self-adhesive retroreflective tape manufactured by the Scotchlite division of the 3M company. "When illumination is provided by a compact ring strobe centered about the camera lens, the return of light from a target of retroreflective material can be from several hundred to over one thousand times brighter than that of a diffuse white target of equal size," (Brown,1982). For this project similar retroreflective tape was used. For the development stage of SPG, lighting was provided by three standard study lamps, with 100 watt bulbs. These were positioned slightly above the CCD cameras and were manually directed towards the targets. The lights provided enough illumination to make the targets much brighter than the general surround, although a few odd surfaces gave occasional problems in certain light conditions. To reduce the amount of reflected light coming back from other reflective surfaces, the apertures of the lenses can be stopped down, so that only the targets remain bright. Camera lighting is very critical when retroreflective tape is used in combination with a thresholding target detection technique. Figures 6.5 and 6.6 show the reflective property of retroreflective tape. Figure 6.7 shows the effect of aperture. In the final implementation of the project, suitable lights centred around the camera lenses will have to be installed (see recommendations in chapter 11).

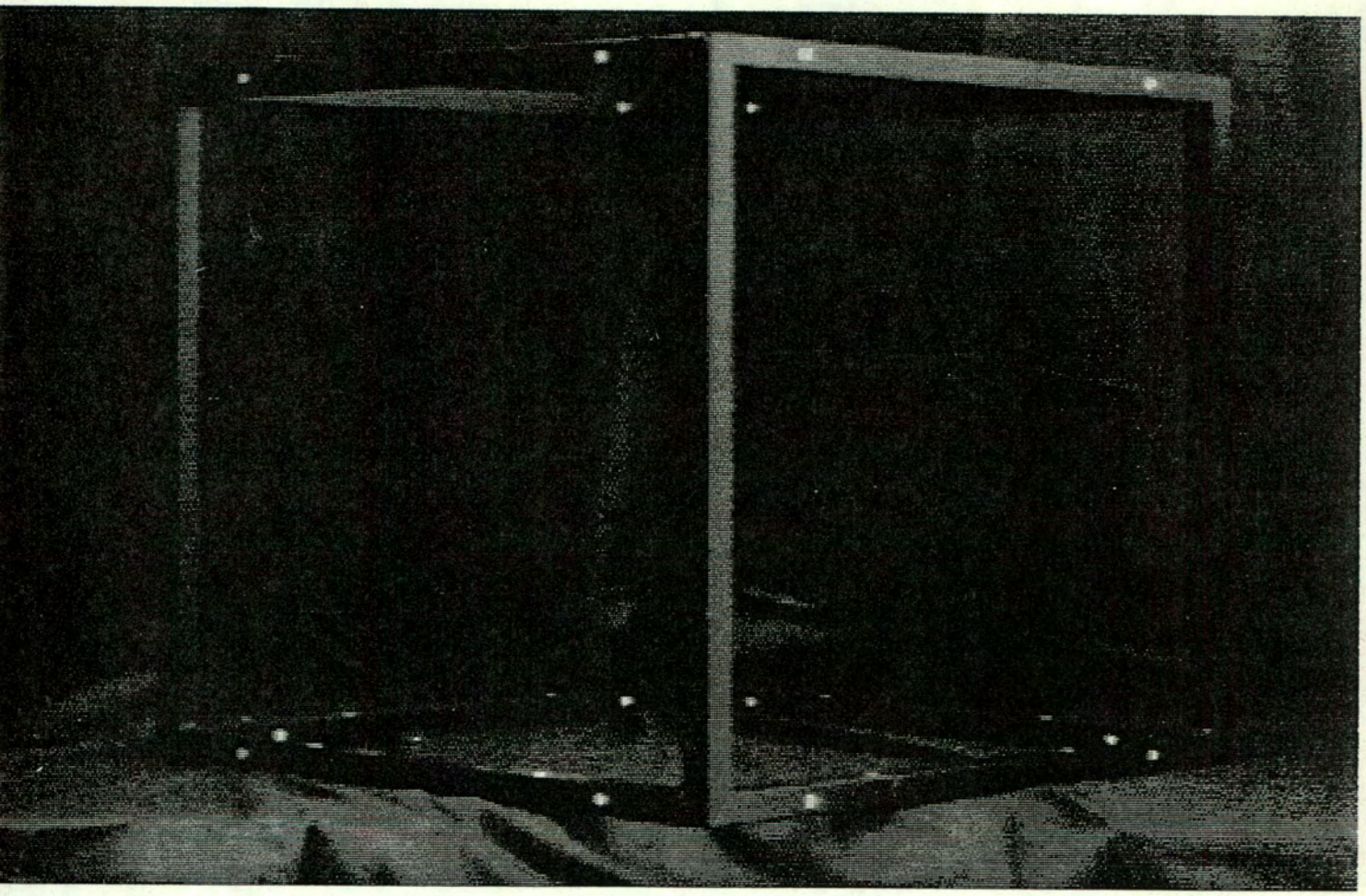

Figure 6.5. Video image showing the control frame under normal room lighting (with wide aperture)

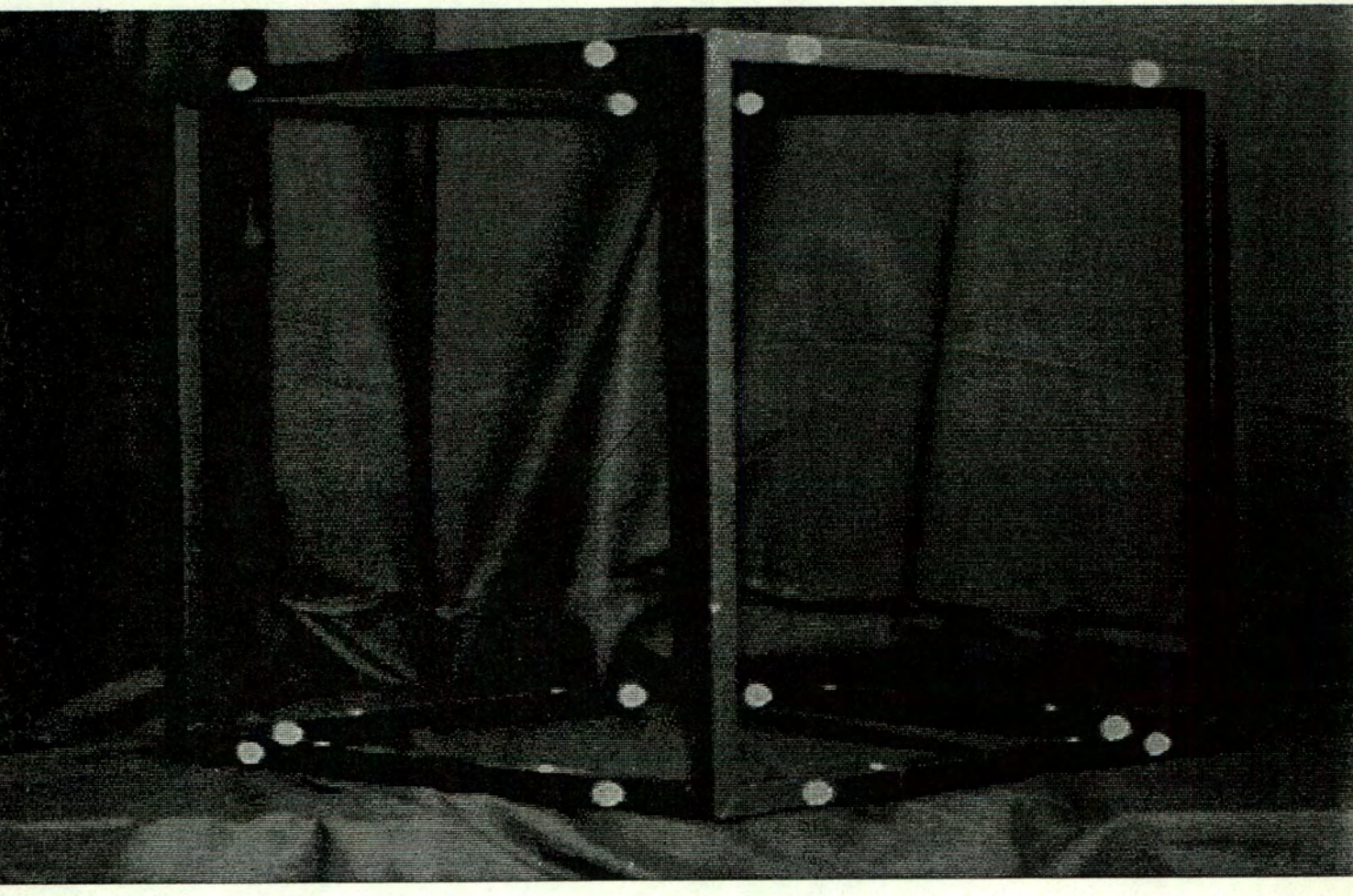

Figure 6.6. Video image showing the control frame under directional lighting (with wide aperture)

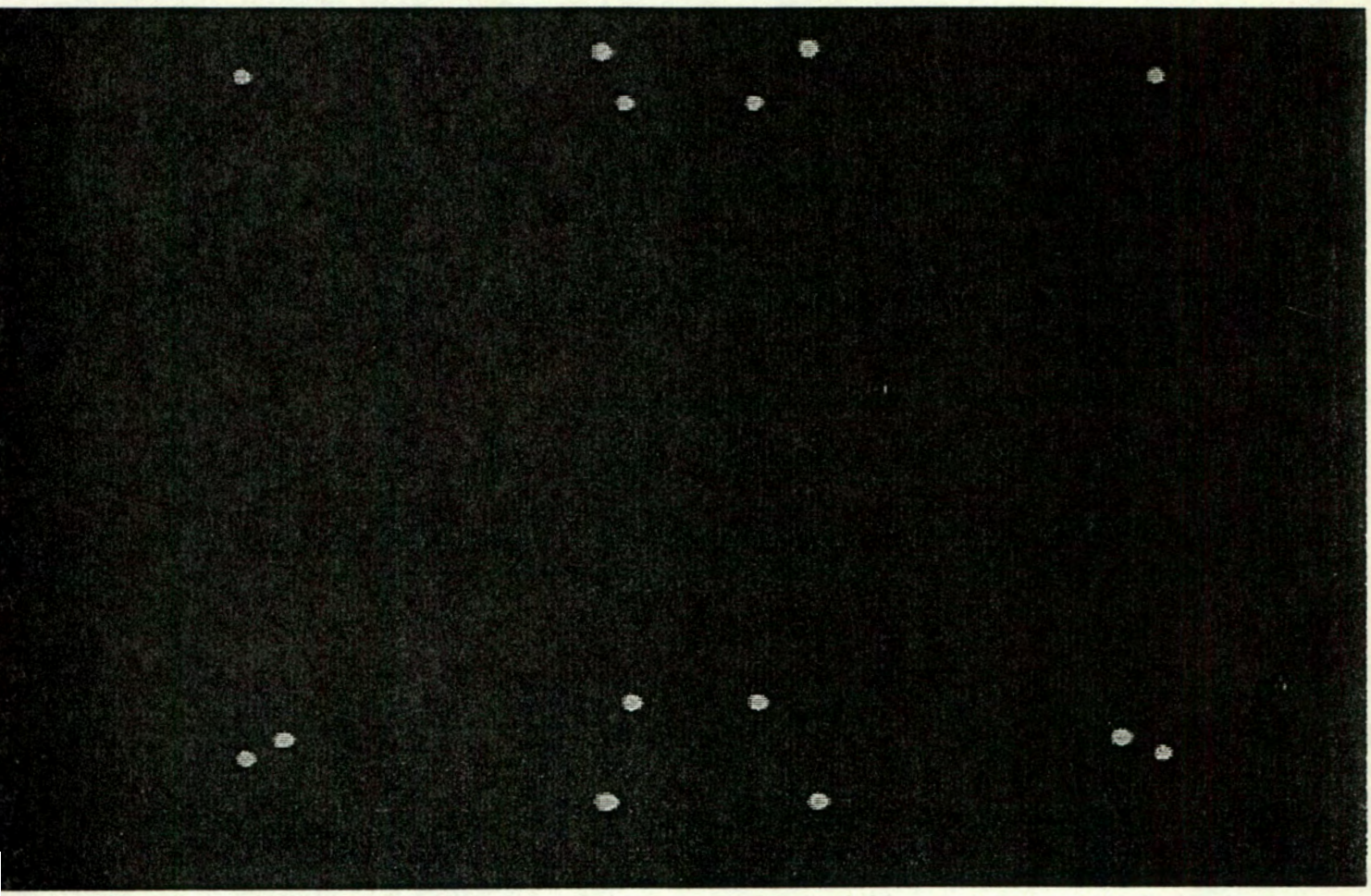

Figure 6.7. Video image showing the control frame under directional lighting (with the aperture stopped down)

Although shape is not used here to detect a target, it is important for finding the centre of the target for position determination. A symmetrical target is ideally suited to centre determination using the weighted centre of gravity routine, which is utilised for SPG. Circular retroreflective targets of eight millimetre

diameter (sufficiently large to be easily visible on the image) were therefore used for control targets. A sample is given in Figure 6.8.

Figure 6.8. A sample of a retroreflective control target

The targets were made with an eight millimetre punch and were directly attached to the control frame, using their own self-adhesiveness. The control frame was painted black to provide a good contrast. Similar sized targets will be used on the patients' heads once the project becomes operational.

7 THE TREATMENT ENVIRONMENT

7.1 THE SYSTEMS INVOLVED

SPG is affected by the operation of the other patient support systems, designed for the proton therapy, (Figure 7.1). Of special importance is the relationship between SPG and the mechanical chair and interlock systems.

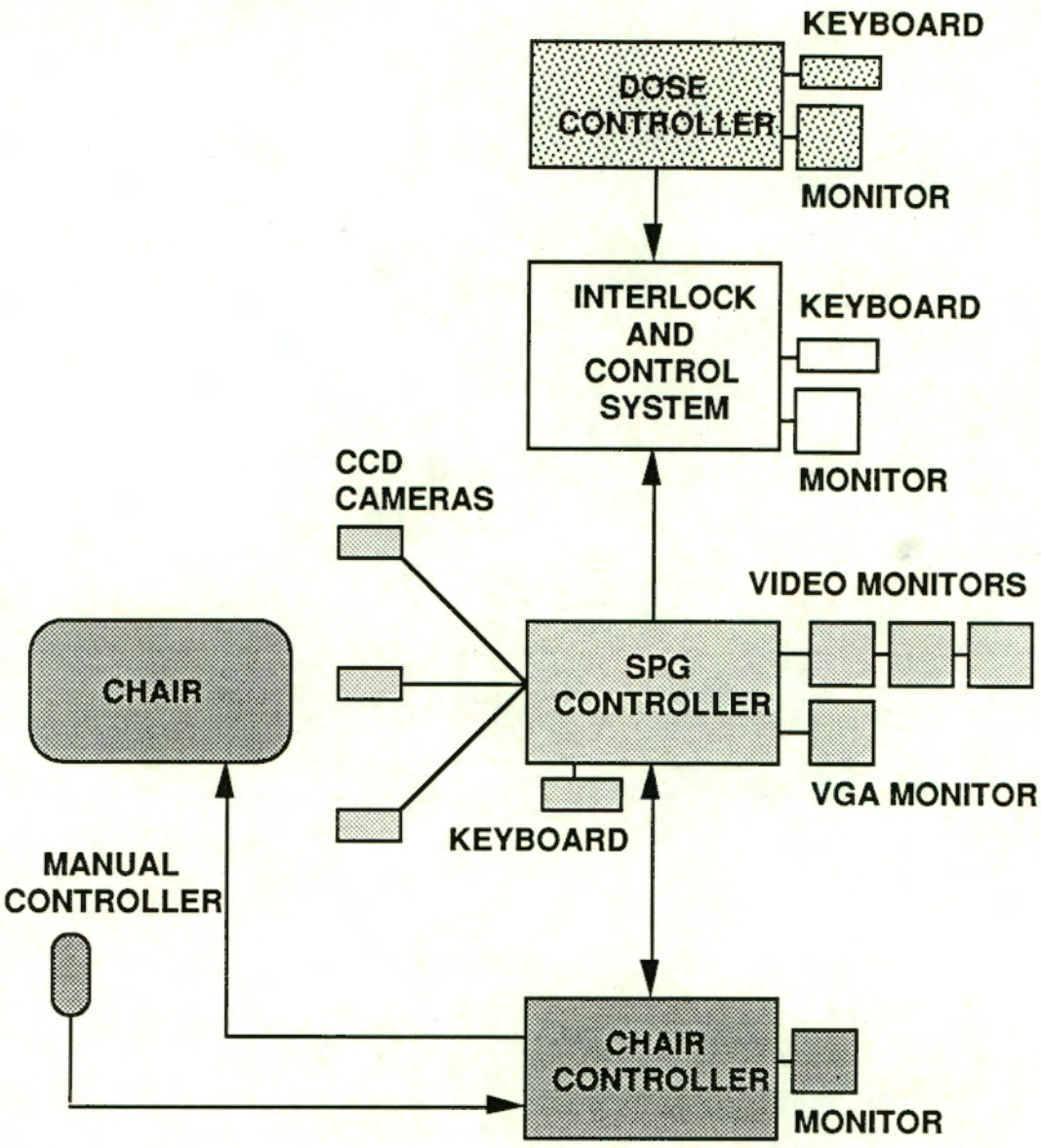

Figure 7.1. A simplified diagram of the operating systems

The SPG controller (computer) is connected to the chair controller through its communication port, and to the interlock and control system through a relay. The chair system is described in more detail in section 7.4. The interlock system is a safety device which ensures that all the necessary procedures have been completed, before the treatment can begin. These include activating various switches, passing check points, closing safety gates and various other precautionary measures. These procedures must be strictly adhered to by the operators in the interests of patient and staff. The interlock controls the activation and deactivation of the proton beam. The control system also has a keyboard and monitor for various operator inputs. The dose controller is a separate system connected to the interlock and control system.

7.2 TREATMENT ROOM

The treatment room is being constructed in a concrete vault in the NAC at Faure. The shape of the room has been shown earlier in Figure 6.1, the distance between opposite walls being ten metres. The walls are very thick, with the narrowest portion being about two and a half metres wide. Due to the height of the vault and the fact that the beam line comes out of a corner a few metres above the bottom of the vault, a raised floor consisting of steel and wood is being built approximately 1.25 metres below the beam line. The section of the vault below the floor is likely to be used for storing the chair controller. Figure 7.2 shows where the beam enters the room while Figure 7.3 shows the floor under construction.

Figure 7.2. This photograph shows where the beam enters the treatment room. The precise level is being used to set out the floor.

Figure 7.3. The raised floor under construction

A stable steel support (Figure 7.4) for the chair has been constructed from the bottom of the vault, as it is an important requirement that the whole chair structure is stable and free of any substantial distortions or deformations.

Figure 7.4. The steel support for the chair

7.3 PROTON BEAM

According to Adams and Ruther (1989), the NAC's cyclotron was "designed as a multidisciplinary facility to produce high energy particles for nuclear physics research, isotope production and radiation therapy with neutrons or protons." "A solid pole light ion injector cyclotron produces protons with a maximum energy of 8 MeV and a maximum current of 100 microamps. This in turn feeds a variable energy separated sector cyclotron which can accelerate protons to a maximum energy of 200 MeV with a maximum current of 10 microamps." The treatment vault "will contain a switching magnet to deflect a 200 MeV proton beam between a horizontal beam delivery system." The proton beam will be directed horizontally across the treatment room and will come to a stop in the concrete wall. The beam itself is fairly wide, so a collimator will be placed in the

beam line, reducing the beam to a parallel ray with the shape and size of the tumour (see section 8.2.3).

7.4 MECHANICAL CHAIR

The mechanical chair (Figure 7.5) is capable of being controlled automatically by SPG (through the chair's computer) or by a hand-held manual controller which will be directly utilised by the operators.

Figure 7.5. The mechanical chair developed by the Department of Mechanical Engineering, UCT

The chair computer keeps track of the position and orientation of the chair, so that the rotations given in the beam coordinate system, by the SPG software, can be transformed into meaningful (equivalent) mechanical rotations. The chair is capable of two rotations and three translations as seen in Figure 7.6. One rotation is around the vertical axis (which defines the tumour position on the beam line) and the other is a backrest rotation about a horizontal axis displaced from the vertical axis.

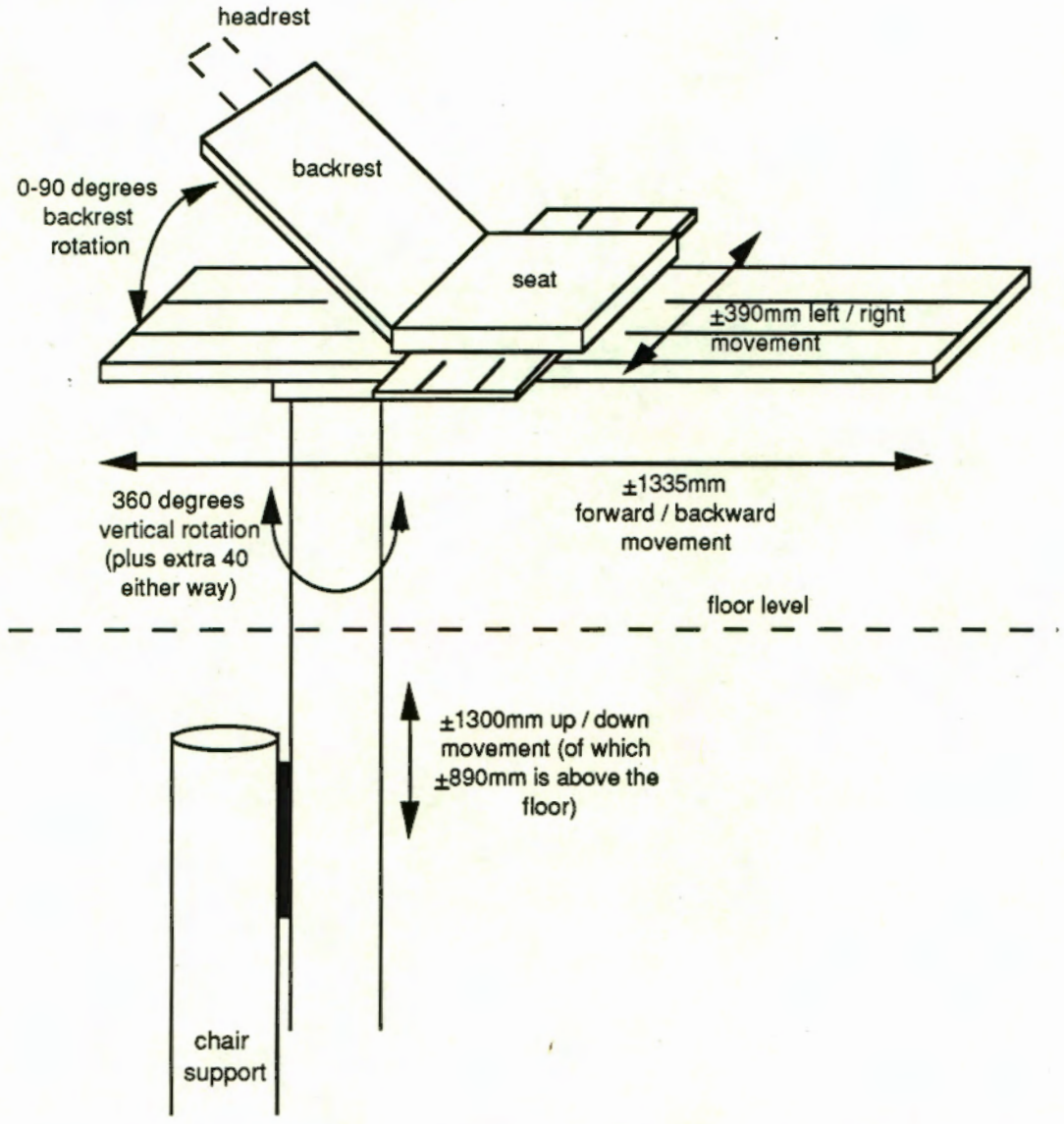

Figure 7.6. The possible translations and rotations of the chair

The extent of the vertical translation is such that the top of the seat will be approximately at beam level (±1250 millimetres above the floor) in its highest position and ±50 millimetres below the floor in its lowest position. The chair is able to lower itself below the floor when the backrest is horizontal. This capability was designed so that the SPG control frame could be positioned in its calibration position without hindrance from the chair, and so that the chair could be put back in its housing when not in use. The highest chair position will be required when the patient is being treated lying down, when the entry point is at the top of the head. It should be noted that the chair does not have the third rotation about the chair's forward/backward axis. However, the effect of this rotation on the patient's head can be simulated, in some cases, by applying a combination of the other translations and rotations. The orientation of the beam collimator (section 8.4.5) provides the extra degree of freedom. Sections 8.4.3 to 8.4.5 describe the alignment problems.

The resolution of the chair's translations is ±0.02 millimetres and of the rotations is ±0.01 degrees. However, due to slight deformations under load, the absolute accuracy of the chair's position is known to only ±0.5 millimetres (in translation) and ±0.5 degrees (in vertical rotation) when a person of approximately seventy kilograms is seated. Relative movements will be of a higher accuracy than the absolute figures given here (Private communication, A. Yates, Department of Mechanical Engineering, UCT).

8 THE PROPOSED PHOTOGRAMMETRIC SEQUENCE

Software, written in Microsoft C by the author, has been developed specifically for SPG. The proposed photogrammetric sequence outlined in this chapter is described with occasional reference to this software. The sequences have been devised with all the latest decisions and developments in mind. It is expected that minor adjustments to the proposed sequence will arise, as the project is currently still under completion and some final decisions still need to be made by the project management. However, no major revisions are foreseen.

The photogrammetric procedure can be divided into four different stages:

(i) Calibrating the cameras - the position and orientation of each camera is found using the control targets on the frame;
(ii) System check - this is a check on the camera calibrations and on the chair computer, to determine whether it has kept track of the chair position correctly;
(iii) Initial patient positioning - this stage comprises moving the patient into the beam line;
(iv) Monitoring the patient - this involves monitoring the patient to make sure all movements are recorded and properly dealt with.

Sections 8.1. - 8.5. deal with each of these SPG stages, as well as the location of the tumour, in detail.

8.1 CALIBRATING THE CAMERAS

A camera must be calibrated, when it has been repositioned or disturbed, or if a predefined period has lapsed since the previous calibration. It is proposed that the cameras be calibrated at the beginning of each day, but once the process becomes operational it may be adequate to calibrate every second day or every week if the cameras have undoubtedly not been touched. A long period between calibrations is not advisable but the compulsory procedure of checking the system (see section 8.3.) will ensure that, if the positions or orientations of any of the cameras have changed since their calibration, then the subsequent stages with the patient cannot be started before re-calibration.

8.1.1 Setting Up

The cameras must be securely fastened on their chosen mounts (stations) and their aperture setting properly adjusted if necessary. The cameras will have their focus and zoom (if the zoom lenses are used) taped down to ensure stability between calibrations. The control frame is then positioned in its calibration position. As mentioned in section 6.2, this position will be repeatable to a high accuracy due to special fittings on the floor, in which the proposed legs of the frame will sit. The control targets on the frame will be centred around the beam tumour point.

Room lighting must be dimmed or switched off and the camera lights switched on. No lights should be visible from any of the cameras. Before capturing any images, it is necessary to make sure that no large, unwanted reflections are appearing on the image. These might typically be caused by a person standing in view of one of the cameras.

8.1.2 Choosing the Camera Data

The operator chooses a camera for calibration, by choosing the MVP channel (0, 1 or 2) and by stating at which station (0 - 8) the camera sits. A live image from the chosen channel is displayed on the monitor. Expected image positions of the visible control targets are displayed as circles overlayed on the live camera image. These positions are calculated from the previously determined DLT transformation parameters for that camera station, and the known coordinates of the control targets. If these circles are not depicting the true positions of the targets then incorrect camera data (channel and station number) was chosen by the operator, or the camera has a different orientation since its last calibration. The operator must then decide whether to continue with the next stage or whether to correct the camera data.

8.1.3 Thresholding, Capturing and Searching the Image

The program enters the image processing routine in which thresholding, searching and target centering, as described in section 4.3.1, are performed. In the controlled environment of the treatment room, it is highly likely that the threshold value will remain fairly constant for a particular camera. These

threshold values could then be set as default values, thus shortening or perhaps eliminating the manual thresholding process. Once the targets have been detected and centered, their image coordinates are stored on file and displayed by circles on the video monitors.

8.1.4 Identification of Targets

Identification of targets is executed automatically, by comparing the observed image position of each target with a list of expected image positions of all the control targets visible from that camera station. The names of the targets are displayed and verified if correct, otherwise the operator manually enters the number of each target. It is possible at this stage to eliminate any non-targets which were detected.

8.1.5 Calibration

The camera calibration is solved using a least squares approach with the DLT model. Tests on target positioning accuracy (see section 9.3) have been carried out and results which are more than satisfactory for the treatment project have been obtained. The least squares routine reads in three data files:

(i) the parameter file which contains the previously calculated transformation parameters for each station;
(ii) the control target coordinate file which contains the X, Y and Z coordinates of all the control targets;
(iii) the observation file which contains the x and y image coordinates of all the visible targets.

Previously determined transformation parameters for the chosen station are used as provisional values for the current calibration. The least squares routine is iterated until an acceptable convergence is achieved. If:

(i) convergence does not occur;
(ii) a singular matrix is encountered;
(iii) a larger than acceptable (>0.010) *a posteriori* reference standard deviation of unit weight is calculated,

then the solution is stopped and the operator is advised to repeat the image capture and identification routines. Otherwise, the following are stored on disk in an output file for later reference:

(i) calculated transformation parameters;
(ii) the parameters' standard deviations;
(iii) the image coordinates and their residuals;
(iv) the *a posteriori* reference standard deviation of unit weight;
(v) a few other values such as aspect ratio, degrees of freedom, etc.

The parameter file is overwritten with the new transformation parameters if the solution was successful. All three cameras are calibrated in this way. These cameras have their calibrations checked (see section 9.1) by re-intersecting the control targets using their stored observations (image coordinates) and the calculated transformation parameters. If the discrepancies between the calculated and surveyed coordinates of the control targets are too large (i.e. larger than a preset value), a re-calibration of the cameras is needed. The full results of the calibration check are stored in an output file for possible later reference.

8.2 DETERMINING THE POSITION, SHAPE AND SIZE OF THE TUMOUR

The procedures described in this section are not part of SPG, but are part of the pre-treatment planning, undertaken by medical specialists at Groote Schuur and Tygerberg Hospitals. Central to the tumour location procedure is the debate over the use or non-use of a patient mask. However, the final decision on this aspect will not adversely affect SPG. The methods of determining three-dimensional coordinates of a tumour "pivot" point, reference targets and entry point(s) from CT scans have been investigated by Adams(1990), and some results are quoted. The collimator, used to determine the shape and size of the proton beam, is also briefly discussed.

8.2.1 Reference Targets

Reference targets are targets on the patient's head, which will be coordinated in both scan and SPG systems. These targets are used by SPG to determine the position of the tumour and entry point in the beam coordinate system.

If no mask is used, the reference targets on the head will be in positions which are least likely to move, even if the patients contract their facial muscles. If different targets are used for the scan and SPG stages, the target positions will need to be marked on the skin. The use of tiny tattoos, as skin markers, has been discussed as a possibility. The manual placing of targets on the marks brings up the question of "centering errors", although this could be checked when the scan coordinates are transformed into the beam coordinates.

The other alternative, that of using a patient mask, either with permanently attached reference targets suitable to both scan and SPG systems, or with physical clips (or other fittings) to force centre the two sets of targets, is also under consideration. This method does have certain conceivable advantages in that:

(i) the reference target positions can be optimised for use with both the scan and SPG systems;
(ii) the patient will not be able to move as easily if the mask is attached to the chair;
(iii) surface movements of the facial muscles will not alter the positions of the reference targets relative to the tumour;
(iv) there is no centering error in placing the targets;
(v) the mask could be designed to help cover any unwanted reflections from the patient's face (thus lowering the threshold value);
(vi) there would be no need for noticeable tattoo (or other) marks on the patient's skin.

On the other hand conceivable disadvantages are:

(i) possible patient discomfort with mask;
(ii) possible movements of the head inside the mask, albeit small;
(iii) the need to manufacture a personal mask for each patient.

It must be repeated again, that these decisions do not adversely affect SPG in any way as long as the chosen SPG targets are of a suitable size (± eight to ten millimetres), are circular and are easily visible on the SPG camera images.

Until now, small ball bearings have been used as reference targets in the CT scan. In the case of the MRI scan, small spherical plastic capsules filled with fish oil have been used.

8.2.2 Obtaining Three-Dimensional Coordinates from a CT Scan

Two types of images can be produced by the CT scan:

(i) a series of plane "slices" at known intervals through the head;
(ii) two mutually perpendicular plane images.

These images can be digitised directly off the screen or on a "hard copy" film negative. In (i), X and Y coordinates of relevant points can be digitised from the image "slices" and the Z coordinates are obtained from a knowledge of the position of the scanner. Three-dimensional coordinates can be obtained from (ii) by using central projection rules.

The reference targets, tumour pivot point and suitable entry point(s) are three-dimensionally coordinated using either of the two methods outlined above. According to Adams (1990), "it is possible to derive three dimensional co-ordinates of well defined targets to a vector precision of approx. 1.5mms." A data file containing point numbers and three-dimensional coordinates of all the necessary points (i.e. reference targets, tumour point and entry point(s)) is created on a floppy or stiffy disk for use with SPG.

8.2.3 The Collimator

For each entry point, a beam collimator, with the same shape and size of the tumour (as seen from the entry point), needs to be manufactured, (Figure 8.1).

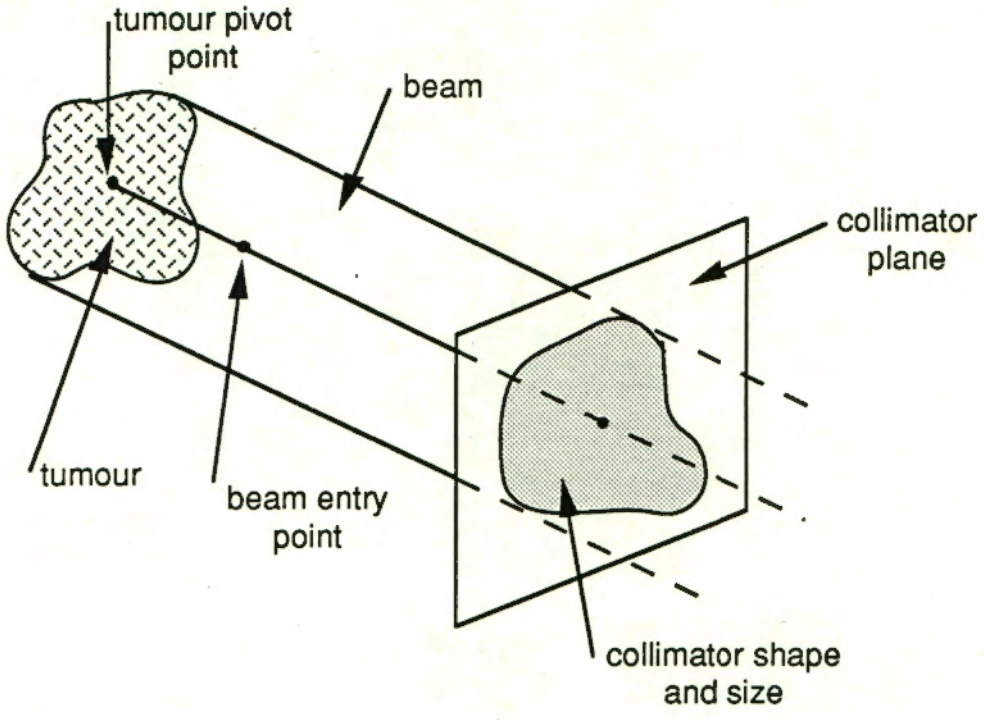

Figure 8.1. The shape and size of the collimator

The collimator plane is orthogonal to the proton beam. The shape and size of the collimator is determined from the CT or MRI images during the pre-treatment planning. In the treatment room, the required orientation of the collimator will be derived (see section 8.4.5) from the position of the patient in the chair, as determined by SPG using the reference targets.

8.3 CHECKING THE SYSTEM BEFORE USE

This stage was designed as a final pre-treatment check on the camera-chair system. The check is achieved by using SPG to coordinate a set of targets (probably six targets) attached to the backrest of the chair, when the chair is in its "zero" position. The "zero" position is any predefined chair position. The chair targets will have been initially coordinated in the beam system during the survey of the beam line.

The system check routine determines whether:

(i) the DLT transformation parameters are reflecting the true positions and orientations of the cameras;
(ii) the chair computer has correctly kept track of the chair position.

If the intersection of the chair targets results in coordinates different to that expected, either the chair is in the incorrect position or the cameras are not in the same position or orientation as reflected by the stored DLT transformation parameters. Such an outcome must result in a re-calibration of the cameras and the re-initialisation of the chair. The actual routine is now described:

(i) the chair is moved into its "zero" position;
(ii) the SPG operator chooses the three cameras to be used in the patient positioning and monitoring stages;
(iii) SPG displays expected target positions of the chair targets for each camera station;
(iv) if these are not correct then, assuming the chair and cameras are calibrated, incorrect camera data was chosen for one or more of the cameras, thus correct camera data must be re-entered;
(v) the three images are thresholded, captured and searched as in the calibration stage and targets are once again displayed by circles on the monitors;
(vi) the targets are then identified automatically or manually (if the automatic identification failed) and any non-targets eliminated;
(vii) the coordinates of the chair targets are calculated using a least squares intersection;
(viii) coordinate discrepancies are computed between the intersected coordinates and the surveyed chair target coordinates and if the discrepancies are too large (i.e. larger than preset values), the cameras need to be re-calibrated and the chair re-initialised.

Positioning and monitoring the patient can not be started until this check is passed. The full results of the system check are stored in an output file for possible later reference. This stage supplies a vital safety check on the entire chair-camera system. Tests on the chair's ability to resume a zero position and SPG's capacity to correctly record this, have been carried out and are discussed in section 9.2.

8.4 INITIAL PATIENT POSITIONING

This stage is concerned with aligning the patient's tumour and chosen entry point into the beam line. Basically it involves the following steps:

(i) coordinating the reference targets on the patient's head;
(ii) determining the position of the tumour point and entry point in the beam coordinate system;
(iii) calculating the movements necessary for alignment;
(iv) moving the patient with the chair;
(v) checking the patient's position.

It must be noted that the proton beam is only switched on at the completion of the positioning stages.

8.4.1 Determining the Coordinates of the Reference Targets in the Beam System

This stage starts with the seating of the patient in the chair. The patient is provisionally aligned in the pre-planned treatment position, by using the manual controller provided with the chair. During the manual alignment, the SPG operator enters the name of the file containing the CT (or MRI) scan coordinates of this particular patient's reference targets, tumour point and entry point(s). The patient is told to keep as still as possible during treatment. This will be made easier by the chair headrest and perhaps by a patient mask.

The same image processing routines of thresholding, searching and target centering on the three images are executed. The found targets need to be manually identified, as expected target positions cannot be assumed. At this stage, target identification involves naming the targets on the patient's head with the same numbers as used in the tumour location phase, in order that the subsequent transformation routine can correctly correlate targets. It is hoped that a standard target naming system will be introduced, so that the operators become familiar with identifying targets. This might entail always calling the target placed on the bridge of the nose as target 1 (for example) and similarly for the other reference target positions. After the target identifications, the reference targets' coordinates (in the beam system) are determined using the least squares intersection routine.

8.4.2 Determining the Position of the Tumour and Entry Points in the Beam Coordinate System

The coordinates of the tumour and entry point need to be transformed from the scan coordinate system into the beam coordinate system. The reference targets are used as the common points for calculating the transformation parameters. The transformation can be given by:

$$\begin{bmatrix} X_{beam} \\ Y_{beam} \\ Z_{beam} \end{bmatrix} = \begin{bmatrix} X_0 \\ Y_0 \\ Z_0 \end{bmatrix} + s\underline{R} \begin{bmatrix} X_{scan} \\ Y_{scan} \\ Z_{scan} \end{bmatrix} \qquad (8.1)$$

where X_{beam}, Y_{beam} and Z_{beam} are the coordinates of a reference target in the beam system and X_{scan}, Y_{scan} and Z_{scan} are its coordinates in the scan system. X_0, Y_0 and Z_0 are translation parameters, s is the scale factor between the two systems and $\underline{R}$ is the rotation matrix. If, however, the two systems are initially both reduced to their centres of gravity then the transformation can be formulated as:

$$\begin{bmatrix} X^0_{beam} \\ Y^0_{beam} \\ Z^0_{beam} \end{bmatrix} = s\underline{R} \begin{bmatrix} X^0_{scan} \\ Y^0_{scan} \\ Z^0_{scan} \end{bmatrix} \qquad (8.2)$$

where the superscript ^{0} refers to the coordinates reduced to the centre of gravity of the appropriate system. The Rodrigues parameters given in Thompson (1969) are used to solve for the rotation matrix, as they seem to converge more easily than the rotation angles themselves.

A least squares solution is used to calculate the Rodrigues parameters and scale factor. The scale factor is included, as the two sets of coordinates are determined by different techniques. Once the transformation parameters are known, the tumour and entry point scan coordinates can be transformed into the beam system. The positions of the tumour and entry point are now known relative to the beam line.

If an incorrect target identification occurred in either of the scan or SPG systems, the solution will either not converge or very poor residuals will result. The calculated residuals also give an indication of the relative positioning accuracies between the two systems. Any gross errors in the reference targets' coordinates will be picked up at this stage. However, there is no check on the correctness of the tumour and entry point scan coordinates at this stage.

8.4.3 Solution of the Alignment Problem

The recently determined coordinate vector (in the beam system) between tumour point and entry point must be aligned with the beam line, (Figure 8.2).

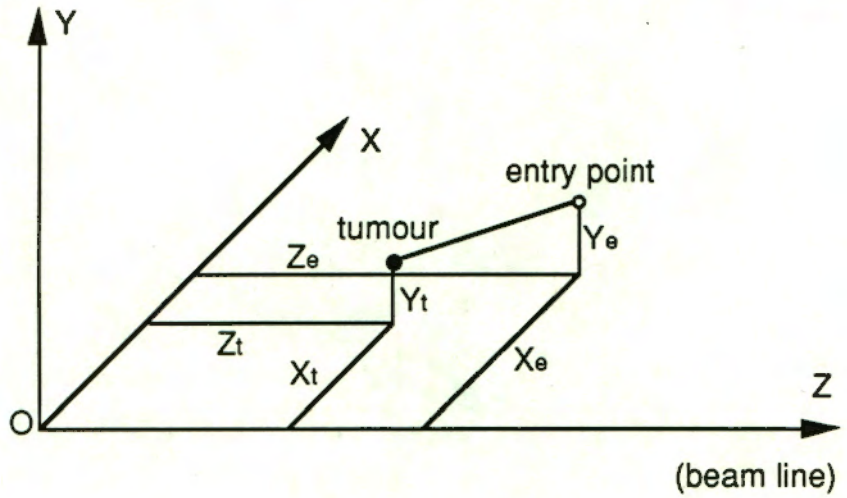

Figure 8.2. Arbitrary position of patient before alignment

In the figure, the tumour has coordinates X_t, Y_t and Z_t and the entry point is given by X_e, Y_e and Z_e. As the desired tumour point is the origin of the beam coordinate system, the necessary translations to position the tumour at this point are simply given by:

$$X \text{ translation} = - X_t \qquad (8.3)$$

$$Y \text{ translation} = - Y_t \qquad (8.4)$$

$$Z \text{ translation} = - Z_t \qquad (8.5)$$

After the translations, the tumour is in position and has coordinates (0,0,0). The entry point now has coordinates $(X_e - X_t, Y_e - Y_t, Z_e - Z_t)$. The remaining problem

is to rotate the patient's head, bringing the entry point into the beam line, (Figure 8.3).

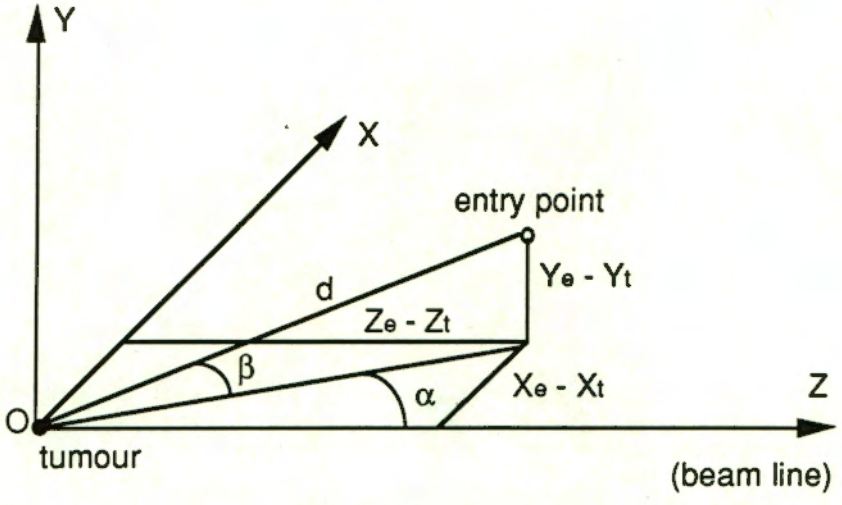

Figure 8.3. Rotating the head into the beam line

Two rotations, α and β, are used to align the entry point into the beam. α is the first rotation about the vertical axis (Y axis), which brings the entry point into the vertical plane intersecting the beam line, and β is the second rotation about the X axis, which brings the entry point into the beam line. The third rotation around the beam line (Z axis) is not required for the alignment of this vector; however it is necessary (see section 8.4.5) for orienting the collimator mentioned in section 8.2.3. The two rotations, α and β, can be directly computed from the figure:

$$\tan\alpha = \frac{X_e - X_t}{Z_e - Z_t} \quad \text{and} \tag{8.6}$$

$$\sin\beta = \frac{Y_e - Y_t}{d} \tag{8.7}$$

where d is the magnitude of the vector between tumour and entry point and is given by:

$$d = \sqrt{(X_e - X_t)^2 + (Y_e - Y_t)^2 + (Z_e - Z_t)^2} \tag{8.8}$$

These three translations and two rotations are relative to the beam system and need to be changed into the chair's mechanical translations and rotations.

8.4.4 Moving the Patient into the Beam Line

The three translations and two rotations determined by SPG using equations (8.3) to (8.7), are sent in a string through communication ports to the chair computer. The chair computer then calculates the necessary mechanical movements from a knowledge of:

(i) the three translations and two rotations received from SPG;
(ii) the current position of the chair.

SPG waits for the chair to complete its movements before continuing.

8.4.5 Checking the Patient's Position and Orienting the Collimator

Once the patient has been moved by the chair, SPG re-determines the position of the reference targets, tumour point and entry point. Threshold values from the last determination are used as starting values for the current thresholding, to ensure a more efficient procedure. If the tumour point and entry point are not sufficiently aligned with the beam, the chair will be sent new translations and rotations. The procedure is repeated until the patient is in the correct position.

As was mentioned in section 8.2.3, a collimator for each treatment position will have been manufactured. The collimator needs to be rotated around the beam line (Z axis), so that the proton beam is correctly oriented with the actual tumour orientation. This can be more clearly visualised from Figure 8.4.

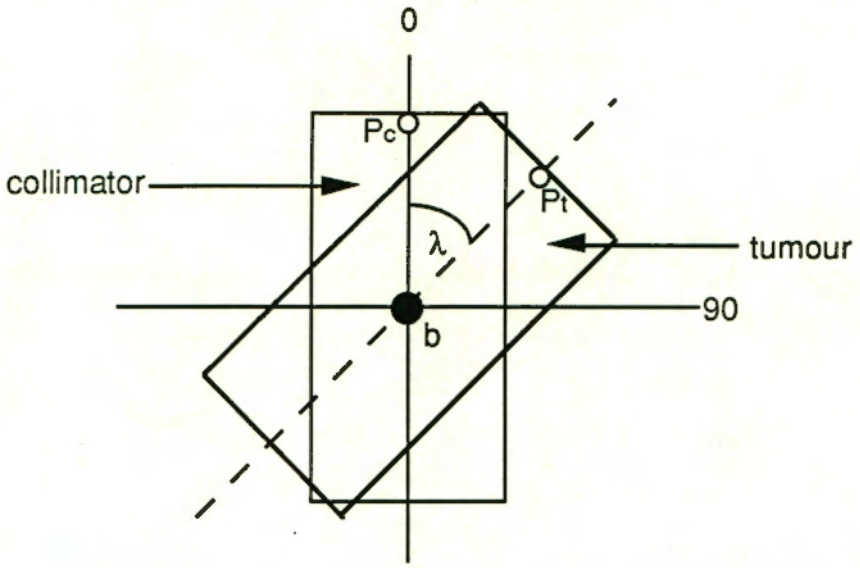

Figure 8.4. Simplified diagram showing the relationship between the collimator in its zero orientation and the tumour in its actual orientation, as seen from along the beam line

In order to determine the orientation correction to be applied to the collimator, a second tumour point is needed to define a tumour axis. In the diagram, this point is shown as P_c on the collimator and P_t on the tumour. This second point must have been coordinated in the initial scan system. When the collimator is manufactured, a mark is made at the intersection of the tumour axis and the edge of the collimator, so that the collimator can be placed into the beam line with the tumour axis vertically aligned. Another similar mark could be used to horizontally align the collimator. The collimator must be mounted in such a fashion that it rotates about the beam axis, shown as b in the diagram. The point P_t can be coordinated along with the tumour pivot point using SPG, therefore the angle, λ, of the vector from the vertical can be easily determined. SPG could output the angle, λ, and the collimator would then be manually (or possibly automatically) rotated through the correct amount. After orienting the collimator, the patient is ready for treatment. This information is relayed to the interlock system, which will activate the proton beam.

(Note, that the collimator concepts discussed in this section are only one of several possible solutions to the collimator problem, and like the mask, a final medical decision has still to be made.)

8.5 MONITORING THE PATIENT

In this final stage the patient, exposed to the active beam, is closely monitored for possible movements by SPG. It is at this stage that the highest requirement on computing speed is made and real-time capability is most essential. This determines the need for a different routine for searching and target centering on the three images, as the approach used for the previous stages would take three seconds, with assumed threshold values, just to determine image coordinates for about eight targets. This is unacceptable, as any time lapse in switching the beam off after a patient moves, could result in unnecessary exposure of healthy portions of the brain to the proton beam. In order to minimise the delay between a patient movement and the detection of such a movement, a modified approach to the previous stages was adopted.

The modified approach is characterised by:

(i) the manual thresholding as well as the target identification stages are eliminated as the relevant information can be assumed to be practically unchanged since the last patient positioning;

(ii) the full search routine is omitted and replaced by a target centering process which occurs in predetermined windows centered around the expected image coordinates of the reference targets;

(iii) in the initial patient positioning stage, the target centering routine is completed for all targets before the three-dimensional coordinates in the beam system are determined, while in this approach, the two routines are integrated so that the reference targets are sequentially processed;

(iv) if any of the reference targets do not appear in their predicted windows, the beam will be switched off without any further calculations.

From (iv) it can be appreciated that the window sizes must be carefully chosen. If the maximum tolerated movement of the patient's head, is say two millimetres from its expected position, then the size of the window is chosen to be big

enough to view an entire reference target when it is either at its expected position, at a distance two millimetres from its expected position or somewhere in between. However, the bigger the window size, the longer the centering takes; therefore the smallest possible window size which does not adversely affect the detection of target movements, is chosen. Figure 8.5 shows an approximate method of determining the image size of a target when it is directly facing the camera.

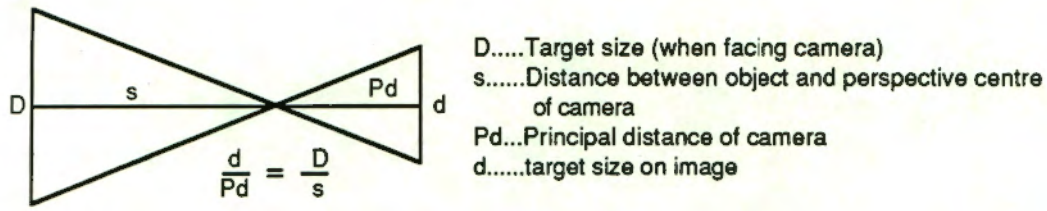

Figure 8.5. Approximate method of determining the image size of a target facing the camera

For possible figures of thirteen millimetres principal distance, three metres between targets and camera and eight millimetre diameter targets, the targets would cover thirty-five microns on the chip, which is equivalent to $\pm$4.5 vertical pixels or $\pm$3 horizontal pixels in the image, and the maximum movement, say two millimetres again, will correspond to nine microns on the chip or $\pm$1 vertical pixel or $\pm$0.8 horizontal pixels in the image. The window size would be chosen as approximately (1+4.5+1) by (0.8+3+0.8) image pixels or $\pm$7 by 5 image pixels. This allows for viewing a two millimetre movement. Due to flooding, the targets will appear larger on the image. For this reason a slightly larger window size will be chosen.

If it is found that the sum of all thresholded intensity values is zero in any of the target windows, a patient movement larger than the tolerance must have occurred (or the lights went off) and the beam is switched off immediately. Otherwise, if the sum is not zero, the three sets of image coordinates for the current target are calculated using the same weighted centre of gravity routine, and subsequently used in an intersection of that target. Each intersection evaluates the discrepancy with the desired position (which should be less than two millimetres). If this tolerance is not met, the beam is switched off. In addition, once all the reference targets have been coordinated, the positions of the tumour and entry points will be computed by a non-iterative least squares

transformation and their determined positions evaluated to see whether they have moved beyond the tolerance limit. If the patient is still in position, the process is repeated until:

(i) the patient receives the required treatment dose;
(ii) the operator chooses to end the treatment for some reason;
(iii) the patient moves more than allowed.

Any substantial movement is likely to affect the first reference target, so performing the processing sequentially provides a much faster check on any unwanted patient movements. It is also likely that if a smaller movement of the patient's head takes place, this movement would be detected before all the targets had been intersected and perhaps even after the first intersection. The update speed of the monitoring routine is given in section 9.4.

As a precautionary measure SPG allows the operator to stop the treatment manually if it is so decided.

9 EVALUATION OF THE SPG SYSTEM

A number of tests on SPG were carried out, including tests of positioning accuracy (i.e. accuracy of target coordinates) and preliminary tests with the mechanical chair. Extensive testing, on the achievable precision of aligning patients will only be carried out after the SPG and chair systems are installed at the NAC, a new control frame is built and an initial survey fixing frame and chair in the beam coordinate system is completed. The feasibility of the target detection and centering algorithm, as well as the target identification routine, is also discussed below.

The photogrammetry laboratory in the Department of Surveying and Geodetic Engineering, was used as the location for setting up the hardware of SPG, for developing the software routines and for testing these routines. A later test with the chair required setting up the system in a laboratory in the Department of Mechanical Engineering. Two camera / object configurations, one in the photogrammetry laboratory (Figure 9.1) and one in the mechanical engineering laboratory (Figure 9.2) have been employed in the tests.

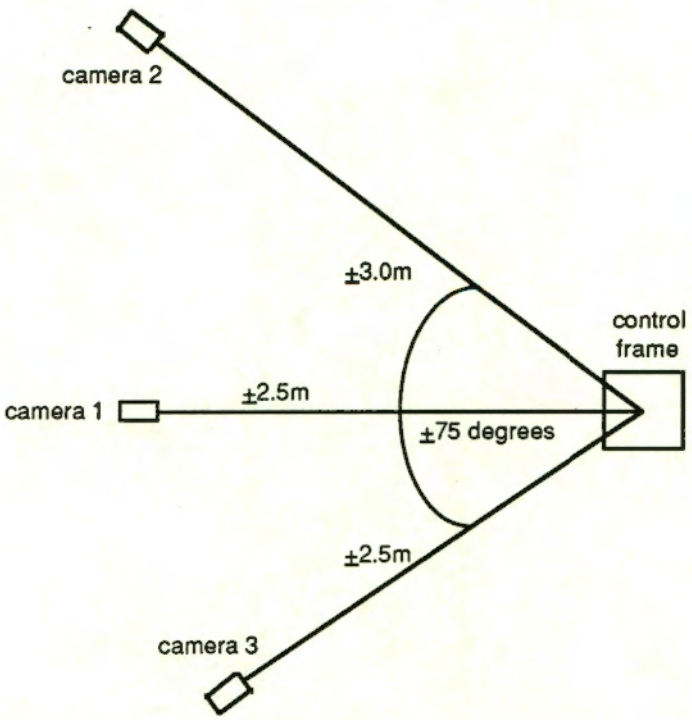

Figure 9.1. Configuration 1 - the camera positions used during the tests in the photogrammetry laboratory

(i) Configuration 1 (Figure 9.1) was utilised extensively in the development of SPG. The three cameras were all at approximately the level of the control frame (at the NAC, camera 1 will be at ±45 degrees above the horizontal), and a convergence angle of approximately 75 degrees separated the cameras (at the NAC, the angle will be 90 degrees). Due to this non-optimal configuration, twelve control targets were visible from cameras 2 and 3, and only eight from camera 1. The small number of visible control targets from camera 1, was found to be insufficient to adequately model for lens distortions , however satisfactory results without modelling lens distortions were achieved in the target positioning test (see section 9.2).

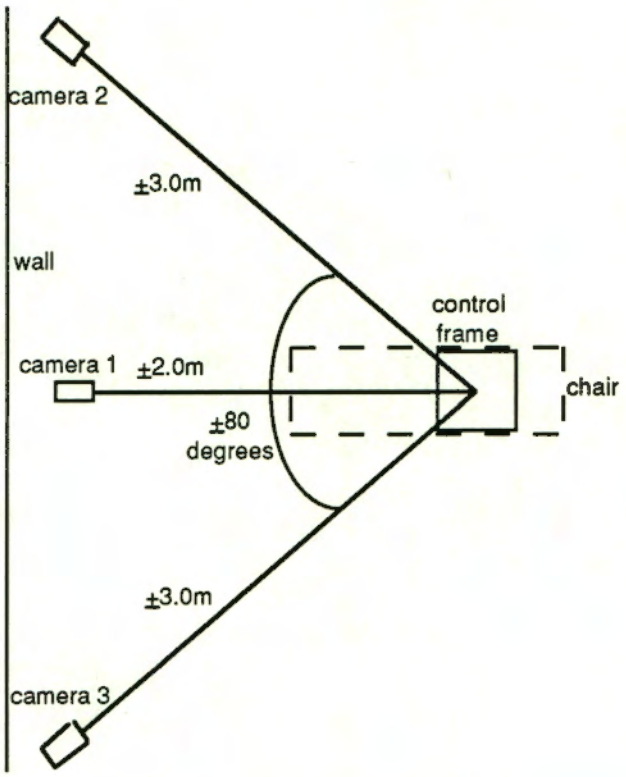

Figure 9.2. Configuration 2 - the camera positions used during the tests with the chair in the mechanical engineering laboratory

(ii) Configuration 2 (Figure 9.2) was employed in the mechanical engineering laboratory for the tests with the chair. Due to restrictions on space, camera 1 was only two metres away from the control frame, which necessitated exchanging the telephoto zoom lens with an eight millimetre lens of poorer

quality. However, an acceptable horizontal angle of convergence (80 degrees) between cameras 2 and 3 was achieved. Twelve control targets were visible from camera 2, eleven from camera 3 and again only eight from camera 1.

9.1 CALIBRATION RESULTS

During the development of SPG, numerous camera calibrations were carried out. The results were consistently similar, so a single example, obtained in the photogrammetry laboratory, is given here. Typical *a posteriori* standard deviations of unit weight, $\hat{\sigma}_0$, computed in the DLT least squares adjustment, are given in the table in Figure 9.3. Full results for this example appear in Appendix B.

	camera1	camera2	camera3
$\hat{\sigma}_0$	0.0013	0.0039	0.0035

Figure 9.3. $\hat{\sigma}_0$ values for each of the camera calibrations. Note that all observations were treated with equal weight in the adjustment.

The small $\hat{\sigma}_0$ of 0.0013 for the calibration of camera 1, is not as reliable as the other two, due to the fact that only eight control targets were visible from this position. No lens distortion parameters were included in the adjustment, due to the small number of targets visible from camera 1.

After each camera was calibrated, the common control targets were intersected using the original observations and the computed DLT transformation parameters. Discrepancies between the calculated and surveyed coordinates were determined for this same example, (Figure 9.4).

Target	dX (mm)	dY (mm)	dZ (mm)	vector (mm)
1	-0.25	0.10	-0.68	0.73
2	-0.23	-0.13	0.76	0.80
28	-0.32	-0.26	0.20	0.46
4	0.22	0.26	-0.04	0.34
3	0.02	-0.20	-0.17	0.26
26	0.00	-0.22	1.32	1.34
25	0.40	0.15	-1.55	1.61
RMSE	0.27	0.21	0.94	1.00

Figure 9.4. Discrepancies between calculated and surveyed control target coordinates

The poorer fix in the Z (depth) coordinate is to be expected in the given camera / object configuration (the frame was positioned in such a way as to approximately align the Z axis with the depth). These values do not provide a stringent test on the target positioning accuracy of the system, as the discrepancies are related to control targets which have been used in the determination of the DLT transformation parameters. However, the discrepancies still give a good indication of the quality of the camera calibrations.

9.2 TEST OF TARGET POSITIONING ACCURACY

In order to determine an estimate for the target positioning accuracy being obtained by SPG, sixteen retroreflective targets (five millimetre diameter) situated on a small wire frame (260 by 240 by 100 millimetres) were coordinated, once using a reflex metrograph and a number of times using SPG. The metrograph coordinates were transformed into the SPG coordinates, and

the "goodness of fit" indicated by the residuals, was used as a measure of the target positioning accuracy of SPG.

The reflex metrograph is a device which can directly measure three-dimensional coordinates of points on a small object, to an approximate precision of 0.5 millimetres. Four observations were made to each target on the small frame and the mean values were adopted as the final coordinates (see Appendix C).

The three SPG cameras were then calibrated. The calibrations were satisfactorily checked by re-intersecting the common control targets. The control frame was then removed and the small test frame placed in the middle of the control field. Coordinates for the sixteen test targets were determined, and are recorded in Appendix D for each of two tests. A three-dimensional transformation using the Rodrigues parameters was then executed (Appendix E), transforming the reflex metrograph coordinates into the SPG coordinates. The transformation was run with and without a scale factor, the better results being achieved in the first case, (Figure 9.5).

Test no.	mean discrepancy vector in target position	
	with scale factor	scale held fixed
1	0.79	0.92
2	0.81	0.97

Figure 9.5. Table of mean discrepancy vectors in target position, for each of the two transformations between reflex metrograph and SPG coordinates

The results show that the two systems agree with each other to under one millimetre, so one can conclude that the target positioning accuracy achievable with SPG, is superior to that achieved by the CT scan ($\pm$1.5 millimetres), even without modelling lens distortions.

9.3 TESTS WITH THE CHAIR

As mentioned before, SPG was set up with the chair in order to test the agreement between actual chair movements and SPG-detected movements. The tests were limited, as extensive testing was still to follow at the NAC. The configuration of cameras, chair and control frame has already been discussed at the beginning of chapter 9.

In order to photogrammetrically fix the chair's position, three retroreflective targets of eight millimetre diameter were attached to the chair's backrest. All three cameras were calibrated, and the chair targets coordinated at a "zero" chair position. The "zero" chair position values, displayed by the chair's own computer, were also recorded. The chair was then moved to a new position, using only its translations. The chair targets were again coordinated by SPG and the displacement vector for each target was determined. These were compared to the recorded chair movements and the differences were computed.

An example of a 40.1 millimetre (vector) chair movement is given here. The differences between the chair's movement (as displayed by the chair computer) and the computed SPG target movements are graphically depicted in Figure 9.6.

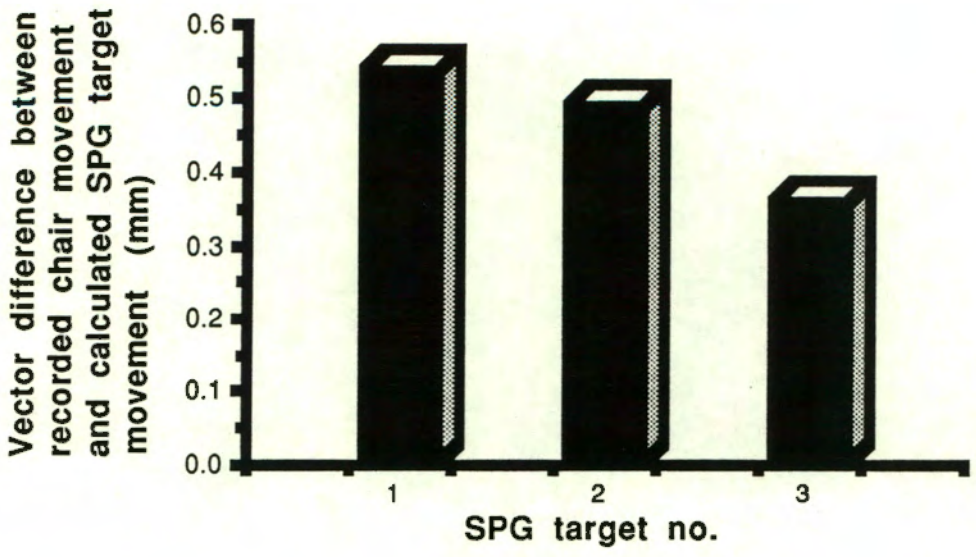

Figure 9.6. Graph showing vector differences between recorded chair movement and calculated SPG target movement.

The chair was then moved arbitrarily around, using all its translations and rotations. Using the chair computer's display, the chair was then brought back to its initial "zero" position. The targets on the backrest were once again coordinated, and the new values compared to the first set. Vector discrepancies are graphically depicted in Figure 9.7, for each target.

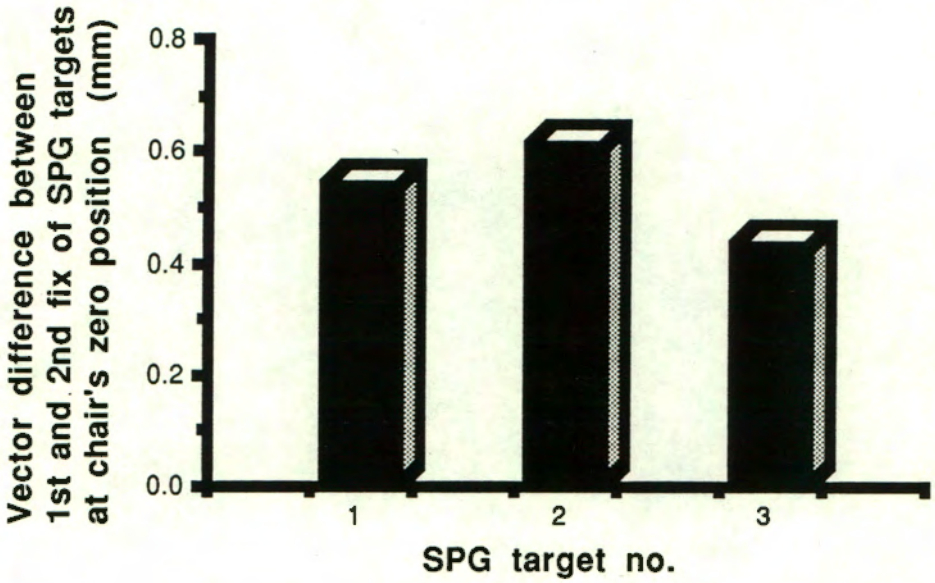

Figure 9.7. Vector differences between the initial and subsequent determination of the SPG targets at the "zero" chair position

The chair's rotations and the ability of the chair and SPG systems to accurately align a patient, will only be tested once the chair, control frame and beam are coordinated in the same system (beam coordinate system).

The preliminary tests with the chair, have shown a satisfactory agreement between chair translations and SPG detected movements (less than one millimetre). The chair's ability to return to the same position and the SPG's capacity to observe this, has also been demonstrated. One problem which did arise, was the occasional reflection off the varnished wood of the seat and backrest, a problem which if it should arise at the NAC, will be overcome by applying a different finish to the wood.

9.4 MONITORING RESULTS

As mentioned in section 8.5, the choice of dimensions for target windows in the monitoring routine is very important, as it affects the update speed and also the maximum target movement that can be detected. Tests were carried out on the update speed, using eight targets common to each camera and using a target window of nine by nine pixels. An update speed of $\pm$0.3 seconds, for determining the coordinates of the eight targets and for performing a non-iterative least squares transformation (refer to section 8.5), was measured. Therefore the maximum possible delay between a patient movement and the detection of such a movement will be $\pm$0.3 seconds (assuming eight targets are used).

If one remembers that a video cycle is 1/25th of a second (for the CCIR video standard used by the SPG cameras), then it can be seen that the SPG monitoring routine is $\pm$1/8th the frequency of the video cycle. According to Gruen and Beyer's (1987) definition expressed in section 1.1, the SPG monitoring routine is $\pm$1/8th the speed of a real-time system, if the process is considered as comprising the coordination of the eight reference targets and the tumour and entry point.

9.5 EFFICIENCY OF THE THRESHOLDING AND TARGET SEARCH ROUTINES

For clarity, the target search routine is defined here as including:

(i) the capturing of the grey image;
(ii) the creation of the thresholded image through a mapping function;
(iii) the location, edge determination and centering of all targets on the image;
(iv) the storing of image coordinates on the hard drive;
(v) the depiction of target positions on the video monitor.

This definition does not include the manual thresholding procedure. The processing time of the entire target search routine is approximately one second for an image containing twelve targets with an average of six by five pixel extent. The thresholding process, although manual, takes only five to ten

seconds, when starting with a threshold value of zero (black). It is expected that the lighting conditions will not vary at the NAC, therefore preset threshold values can be chosen, reducing the thresholding routine to a relatively quick confirmation by the operator.

The target search routine is reliant on the threshold value, which is chosen by the operator through inspection, and is therefore operator dependent. However, with an experienced operator, the routine will be totally reliable, assuming that no unwanted reflections exist. As has been pointed out before, unwanted non-targets can be eliminated in the target identification stage, but this would prove time-consuming and restrictive if more than a handful of such points were detected. Therefore, for an efficient thresholding routine, it is necessary to ensure that no large objects, with similar reflectance to the targets, are situated in the field of view. In all the preliminary tests, most objects could be eliminated from the binary image by thresholding. The one problem that did exist during the development stage, was that for practical reasons, the sunlight entering the windows could not be eliminated from the photogrammetry laboratory. Sunlight will not be a problem at the NAC, as there are no external windows and room lighting will be designed not to interfere with the SPG cameras, and will in any case be dimmed for most of the treatment.

By decreasing the aperture of the lens, it is possible to obtain greater contrast between the highly reflective targets and other bright objects, making the thresholding more reliable. The problem with decreasing the aperture of the lens too much, is that the darker objects, such as the control frame itself, become too dark to recognise, resulting in target identification difficulties. A possible solution to this problem is through the MVP commands, **offset** and **gain**, which can simulate the effect of changing the aperture, by adjusting the range over which the input signal to the anologue-to-digital converter is digitised. Using these commands, the incoming image could be digitised to simulate the effect of a small aperture, for the thresholding stage. Later, during the target identification stage, the commands would be re-employed to simulate the effect of a wider aperture, thus enabling the darker objects to be seen. A short program was written, for changing the **offset** and **gain** of the MVP, and the results showed that employing these two functions can be advantageous in certain lighting conditions. Up to this stage, their use has not been necessary, however at the NAC they could be easily implemented if the need arose.

9.6 THE TARGET IDENTIFICATION PROCESS

The evaluation of the target identification process needs to be divided into three parts, determining the efficiency of the routine in:

(i) the calibration stage;
(ii) the system check stage;
(iii) the patient positioning stage.

(i) In the case of the very first set of camera calibrations, or when a camera has been moved, the automatic identification of targets will not be possible, as their image positions are not known, thus manual identification will be needed. At least twelve targets will be visible, making the manual target identification the lengthiest process of a single camera calibration. The importance, in the calibration stage, is not the duration of the process, but the correct identification of each target. However, an incorrect identification will be picked up by the operator, either by the failure of the DLT solution or when the calibration check (re-intersection of the control targets) produces large discrepancies. Manual identification will also be necessary if any unwanted reflections appear on the image. Once the cameras have been initially calibrated, target identification during any further re-calibrations will be automatically executed, that is, if the cameras have remained in position and no unwanted reflections appear on the image. Automatic identification will increase the efficiency of the camera calibrations, although the operator will still have to confirm the resulting selection. Different sets of control targets are visible from each camera station, therefore the operator must be familiar with the control target numbering scheme, for an efficient target identification routine.

(ii) The system check stage is exactly the same from an operator's point of view, except that fewer targets need to be identified. The automatic identification should always succeed at this stage, assuming the cameras are still in the same position and orientation as reflected by their DLT transformation parameters, and if no undesired reflections appear on an image. If not, manual identification will be necessary. Because there will only be a few targets on the chair, the process will be fairly quick, even if a few unwanted reflections were detected.

(iii) Target identification is always manual during the patient positioning stage. The operator must correctly identify the targets with the same names as were used in the CT or MRI scan stage. A misidentification will result in the probable failure of the transformation solution, an unnecessary waste of time. The efficiency of the routine is all the more important at this stage, as the patient is now seated in the chair. The operator must therefore be familiar with all the target names for an efficient procedure. Any unwanted reflections detected by the target search routine, can also be eliminated at this stage.

Common to all the stages, especially in the patient positioning stage, is the need for an experienced operator to ensure maximum efficiency. As the operator will generally be the same person, it is likely that they will become efficient in a short period. A combination of automatic and manual target identification may not be the most elegant method, but it provides a reliable and fairly efficient solution, an important consideration for the treatment project.

10 CONCLUSIONS

The development of a real-time photogrammetric (RTP) system, known as the SPG system, for the positioning and monitoring of patients undergoing proton therapy, has been successfully investigated and the basic software completed, by the author. Conclusions, regarding a number of components of SPG, are drawn from these investigations.

10.1 HARDWARE

(i) The hardware components have been successfully integrated to form a powerful positioning system. Synchronisation of video signals caused initial problems, however a suitable solution was devised and implemented.

(ii) The MVP-AT proved a powerful frame-grabber and image processor, which meets the requirements of simultaneously grabbing and storing three images from three separate black and white video sources.

(iii) During the treatment operation at the NAC, only the patient is allowed to remain in the room. The SPG computer will therefore be housed in a separate control room, which is approximately thirty metres away from the CCD cameras. High quality video cabling will have to be used for sending the video signal to the MVP, so that attenuations are not introduced.

10.2 IMAGE PROCESSING ROUTINES

(i) The automatic target search routine relies on the manual thresholding process. Bright objects and direct light in the field of view pose problems for successful thresholding. Adjusting the aperture at the lens or at the analogue-to-digital converters through software, provides a method for reducing unwanted reflections appearing on the thresholded (binary) image. A manual thresholding software routine has been developed which allows easy choice of a suitable threshold value by viewing the binary image.

(ii) At the NAC, conditions will remain similar, so default threshold values will be pre-set to ensure an efficient thresholding routine.

(iii) A target search routine has been developed for specific use with the MVP. The routine is capable of searching an entire image, containing twelve targets, in only one second, using a 25MHz 386 PC with an 8087 maths co-processor. The reliability of the search depends entirely on the success of the thresholding routine.

(iv) Target correlation using a geometrical approach was investigated. The approach proved highly reliable for targets appearing on three images. Targets appearing on only two images were sometimes incorrectly matched. The routine was therefore not incorporated into the target identification routine, as its unreliability was not acceptable.

(v) Automatic target identification, using expected image positions, has been successfully implemented into SPG, for the initial stages. The operator will always confirm the automatic choice. In addition, an efficient software procedure for manually identifying detected targets on the image, has been developed. Detected non-targets are easily eliminated through manual identification. If the images are too dark (due to the aperture setting) manual identification becomes very difficult. It is therefore necessary for the aperture on the camera lens to be set at a compromise setting for both the thresholding and target identification routines. The aperture could also be easily adjusted through the MVP, using the **offset** and **gain** commands, to support both routines. Finally, it is very important that the operator is familiar with all the target numbers (in all stages), to ensure an efficient process.

10.3 CAMERA / OBJECT CONFIGURATION

(i) In a pre-analysis stage, the camera / object geometry was optimised. The camera mounts (stations) are presently being built to the specifications derived from this analysis.

(ii) If a mask is used on the patient, then it is conceivable that only camera stations 1, 2 and 3 need to be used, as the reference targets could be placed anywhere on the mask.

(iii) Due to environmental constraints the camera / object configurations used during the tests on SPG were not ideal. Slight improvements in the results are expected once the desired configuration is used at the NAC.

10.4 CONTROL TARGETS

(i) A provisional control frame was built for the development of SPG. Control targets were made from retroreflective tape and were attached directly onto the frame. The control frame itself is very stable, but the control targets would be susceptible to wear. Ideas of improvements for the new frame, are given in the recommendations (chapter 11).

(ii) A standard deviation (1σ level) of 0.1 millimetres in X, Y and Z, was achieved for the coordinates of the control frame targets. The standard deviations, obtained from the bundle adjustment, give an estimate of the theoretical accuracy that was achieved. They indicate that the observations were consistent and that the geometry used was sufficient for obtaining a high accuracy.

10.5 TARGETS AND LIGHTING

(i) Retroreflective tape has been successfully utilised for targets on the control frame. Strong directional lighting, emanating from the directions of the cameras, is very important when used in conjunction with this tape.

(ii) Conventional study lamps, with 100 watt bulbs, were used and were found to be adequate for the development stage. Recommendations regarding lighting, are made in chapter 11. Sunlight, although a problem in the photogrammetry laboratory at UCT, will not be a factor in the NAC vault, as there are no external windows.

10.6 THE MECHANICAL CHAIR

(i) Good agreement (under 1 millimetre) between the chair translations and SPG has been achieved in preliminary tests. Further tests will be executed once the chair is installed at the NAC.

(ii) The wooden seat and backrest produced patches of high reflectance, due to the glossy coat of varnish. A less reflective coat may be required when the systems become operational.

10.7 SOFTWARE DEVELOPMENT

(i) Software, written in Microsoft C, has been successfully implemented during the development of SPG. Minor changes, mostly aesthetic, still need to be completed.

(ii) C is a powerful programming language, ideally suited for all the tasks required by SPG. However, improvements in processing speed could be achieved by programming certain sub-routines (such as the target search routine) in assembly language, or by incorporating parallel processing techniques.

10.8 CAMERA CALIBRATION ROUTINE

(i) A single camera calibration takes approximately 45 seconds with manual target identification and only 15 to 20 seconds with automatic target identification. Both these times include manual thresholding.

(ii) The direct linear transformation (DLT) is used as the mathematical model for the camera calibrations and subsequent intersections. Provision for modelling radial lens distortion has been made in the calibration software routine, however sufficiently accurate results have been achieved without modelling the distortion.

(iii) For a reliable modelling of radial lens distortion, more control targets need to be visible from each camera station.

---

coordinates into SPG determined coordinates.

(iii) The computations for determining the rotations and translations, necessary to position and align the patient into the beam line, have been derived. Interfacing with the chair computer must still be completed.

(iv) The full procedure associated with the correct orientation of the beam collimator has still not been decided on by the medical specialists. The final decision will only cause minor changes to the transformation routine of SPG.

10.12 MONITORING

(i) SPG is capable of re-determining the three-dimensional coordinates of eight targets, the tumour point and entry point, approximately every 0.3 seconds using target windows of nine by nine pixels.

(ii) The target window size is affected by the size of the target on the image and by the maximum patient movement allowed in relation to the image. The update time given in (i) would increase if larger windows need to be used.

10.13 EFFICIENCY AND RELIABILITY OF THE SPG SYSTEM

(i) In a medical application such as this project, reliability plays a bigger factor than efficiency. However, the system must not be inefficient.

(ii) SPG has been developed as a combination of fully automatic and computer-aided manual routines. The system's efficiency depends on the operator familiarity with the various routines. It is felt that the system design is sufficiently user friendly to allow an inexperienced operator to soon become efficient.

(iii) Once the cameras are mounted in their planned positions, and all lighting problems have been eliminated, the SPG routines will be highly efficient and completely reliable.

(iv) The SPG routines are capable of forming a suitable platform from which to continue research in the field of real-time photogrammetry.

11 RECOMMENDATIONS

Recommended system parameters which are mostly concerned with the practical implementation of SPG are listed below.

(i) The final control frame, to be used at the NAC, must be of equivalent dimensions to the old frame, if the same camera lenses are to be used. The retroreflective control targets should be housed in a thin metal disk, so that their edges are protected from wear, Figure 11.1.

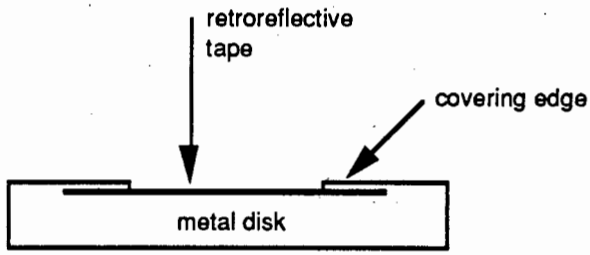

Figure 11.1. Recommended control target disk for protecting the retroreflective tape

The covering edges of the disk must be finely machined, to ensure a highly symmetrical target, and must be very thin, so that the target is not partially hidden, and subsequently asymmetrical, when viewed from an angle. More control targets could be added to the frame, thus strengthening the camera calibrations and allowing for a reliable modelling of radial lens distortions.

(ii) The reference targets should be circular, highly reflective (preferably retroreflective tape) and approximately eight to ten millimetres in diameter. A black outer ring would help define the edges of the target more clearly.

(iii) Fluorescent ringlights, arranged around the camera lens, are recommended for illuminating the targets. The use of fluorescent light would ensure that the cameras are not subjected to high temperatures which could affect their performance. The possibility of using near infra-red lights deserves attention, as the near infra-red portion of the spectrum, while detectable to the CCD cameras, is invisible to the patient.

(iv) In the unlikely event of thresholding difficulties at the NAC, an interactive target detection routine integrated with the target identification process, could easily be incorporated.

(v) The effects of radiation on the cameras and power supply units could not be evaluated. These should be assessed to determine their impact (if any) on the lifetime of the equipment and on the geometrical and electronic stability of the cameras.

(vi) A standard numbering system, for reference targets on the patient's head, must be used, so that the operator becomes familiar with the target numbers.

(vii) An investigation of the stability of the cameras over long periods should be carried out, so that a suitable time span between camera calibrations can be determined.

(viii) Further investigations into automatic target correlation could benefit the target identification stage, if a reliable solution is found.

12 CLOSING REMARKS

The practical use of real-time photogrammetry, in a major medical project, has been described in the preceding pages. Research, in the field of real-time photogrammetry is continuing in the Department of Surveying and Geodetic Engineering, at the University of Cape Town. Some specific areas of future interest are:

(i) software development for use with parallel processors, transducers and neural networks;
(ii) development of suitable additional parameter sets for use with CCD cameras;
(iii) dynamic modelling of moving objects;
(iv) investigations of automatic target correlation algorithms;
(v) continuing software development for real-time applications.

As real time photogrammetric techniques become more advanced, a wide range of applications can be expected to emerge.

REFERENCES

Adams, L. P., 1981. *X-ray Stereophotogrammetry locating the precise, three-dimensional position of image points*, Medical and Biological Engineering and Computing, 19, pp. 569-578.

Adams, L. P., 1989. *Report on Patient Support System for Proton Therapy Stereophotogrammetric Positioning System*, University of Cape Town Report, 5 pages.

Adams, L. P., 1990. *Report on obtaining 3 dimensional Coordinates from CT Scans*, NAC project report, 13 pages.

Adams, L. P. and R. F. Hurly, 1983. *Maclear's Grand Parade Baseline and St George's Cathedral*, SA Survey Journal, pp. 4-17.

Adams, L. P. and H. Ruther, 1989. *A Stereophotogrammetric System Using Multiple Digital Cameras fot the Accurate Placement of a Proton Beam*, OPTICAL 3-D MEASUREMENT TECHNIQUES, Editors: A. Gruen / H. Kahmen, Wichmann, Karlsruhe, pp. 164-172.

Beyer, Horst A., 1991. *Automated Dimensional Inspection of Cars in Crash Tests with Digital Photogrammetry*, SPIE, Vol. 1526, Industrial Vision Metrology, Winnipeg, 1991, 8 pages.

Beyer, H. A., H. P. Fassler and J. Wen, 1989. *Real-Time Photogrammetry in High-Speed Robotics*, OPTICAL 3-D MEASUREMENT TECHNIQUES, Editors: Gruen and Kahmen, pp. 271-280.

Brown, D. C., 1958. *A solution to the general problem of multiple station analytical stereotriangulation*, RCA Data Reduction Technical Report No. 43.

Brown, D. C., 1980. *Application of close-range photogrammetry to measurements of structures in orbit*, Volume 1, GSI Technical Report No 80-012.

Brown, D. C., 1982. *STARS, A Turnkey System for Close Range Photogrammetry*, Proceedings International Archives of Photogrammetry, Vol. 24, V/I. PRECISION AND SPEED IN CLOSE RANGE PHOTOGRAMMETRY, York, England.

Brown, D. C., 1985. *Adaptation of the Bundle Method for Triangulation of Observations Made by Digital Theodolites*, Proceedings Conference of Southern African Surveyors, Part 1, No. 43.

El-Hakim, S. F., 1986a. *Real-Time Image Metrology with CCD Cameras*, Photogrammetric Engineering and Remote Sensing, Vol. 52, No. 11, pp. 1757-1766.

El-Hakim, S. F., 1986b. *A Real-Time System for Object Measurement with CCD Cameras,* International Archives of Photogrammetry and Remote Sensing, 26(5), pp. 363-373.

El-Hakim, Sabry F., 1989. *A Hierarchical Approach to Stereo Vision*, Photogrammetric Engineering and Remote Sensing, Vol 55, No. 4, pp. 443-448.

Fraser, Clive S., 1991. *Photogrammetric Measurement to One Part in a Million*, submitted to Photogrammetric Engineering and Remote Sensing, April 1991, 15 pages.

Fritsch, D, 1991. *Reconstruction of a Sub-Reflector by Digital Photogrammetric Methods*, presented at EDIS/SAGIS, official workshop of ISPRS working group V-4, Pretoria, July 1991.

Fryer, John G., 1989. *Camera Calibration in Non-Topographic Photogrammetry*, NON-TOPOGRAPHIC PHOTOGRAMMETRY, Second Edition, Editor: H. M. Karara, American Society for Photogrammetry and Remote Sensing.

Gonzalez, Rafael C. and Paul Wintz, 1977. DIGITAL IMAGE PROCESSING, Addison-Wesley Publishing Company.

Gruen, A. W., 1985. *Adaptive Least Squares Correlation: A Powerful Image Matching Technique*, South African Journal of Photogrammetry, Remote Sensing and Cartography, 14(3), pp. 175-187.

Gruen, Armin, 1988. *Towards Real-Time Photogrammetry*, Photogrammetria, 42, pp. 209-244.

Gruen, Armin W., 1989. *Digital Photogrammetric Processing Systems: Current Status and Prospects*, Photogrammetric Engineering and Remote Sensing, Vol. 55, No. 5, pp. 581-586.

Gruen, Armin W. and Horst A. Beyer, 1987. *Real-Time Photogrammetry at the Digital Photogrammetric Station (DIPS) of ETH Zurich*, The Canadian Surveyor, Vol. 41, No. 2, pp. 181-199.

Gruen, Armin and Emmanuel Baltsavias, 1988. *Automatic 3-D Measurement of Human Faces with CCD-cameras*, SPIE Proceedings, Vol. 1030, Biostereometrics '88, Basel, pp. 106-116.

Gruen, A. and H. A. Beyer, 1991. *DIPS II - Turning a Standard Computer Workstation into a Digital Photogrammetric Station*, Zeitschrift fur Photogrammetrie und Fernerkundung, No. 1, pp 2 - 10.

Haggren, Henrik, 1987. *Real-Time Photogrammetry as used for Machine Vision Applications*, The Canadian Surveyor, Vol. 41, No. 2, pp. 201-208.

Haggren, H. and E. Leikas, 1987. *Mapvision: The Photogrammetric Machine Vision System*, Photogrammetric Engineering and Remote Sensing, 53(8), pp. 1103-1108

Karara, H. M. and Y. I. Abdel-Aziz, 1974. *Accuracy aspects of non-metric imageries,* Photogram. Eng., 40(11), pp. 1107-1117.

Kratky, V., 1979. *Real-Time Photogrammetric Support of Dynamic Three-Dimensional Control*, Photogrammetric Engineering and Remote Sensing, Vol. 45, No. 9, pp. 1231-1242.

Lenz, Reimar and Dieter Fritsch, 1990. *Accuracy of Videometry with CCD Sensors*, ISPRS Journal of Photogrammetry and Remote Sensing, 45, pp. 90-110

Matrox, 1989. Matrox MVP-AT installation and reference manuals, Matrox Electronic Systems, Ltd., Quebec, Canada.

McGlone, J. C., 1989. *Analytical Data-Reduction Schemes in Non-Topographic Photogrammetry*, NON-TOPOGRAPHIC PHOTOGRAMMETRY, Second Edition, Editor: H. M. Karara, American Society for Photogrammetry and Remote Sensing.

Real, R. R. and Y. Fujimoto, 1986. *Digital Video Stereoscopy: Real-Time Instrumentation Issues*, International Archives of Photogrammetry and Remote Sensing, 26(2), pp. 85-99.

Rosenfeld, Azriel, 1984. *Image Analysis*, DIGITAL IMAGE PROCESSING TECHNIQUES, Volume 2 in COMPUTATIONAL TECHNIQUES, Academic Press Inc.

Ruther, H., 1989. *Near-Real-Time Photogrammetry on a Personal Computer PHOENICS*, Consas proceedings, Vol. 1, 11 pages.

Ruther, H. and N. Parkyn, 1990. *Near real time photogrammetry on a personal computer*, Photogrammetric Record, 13(75), pp. 415-422.

Ruther, H. and R. Wildschek, 1989. *Digital Photogrammetry for the Acquisition of Surface Data for Automatic Milling Processes*, OPTICAL 3-D MEASUREMENT TECHNIQUES, Editors: Gruen and Kahmen, pp. 360-369.

Thompson, E. H., 1969. AN INTRODUCTION TO THE ALGEBRA OF MATRICES WITH SOME APPLICATIONS, Adam Hilger LTD London.

Torlegard, K., 1981. *Accuracy improvement in Close Range Photogrammetry*, Schriftenreihe, HSBw, Studiengang Vermessungswesen, Hochschule der Bundeswehr Munchen.

Wong, Kam W., 1987. *Real-Time Machine Vision Systems*, The Canadian Surveyor, Vol. 41, No. 2, pp. 173-180.

Wong, Kam W. and Wei-Hsin Ho, 1986. *Close-Range Mapping with a Solid State Camera*, Photogrammetric Engineering and Remote Sensing, Vol. 52, No. 1, pp. 67-74.

APPENDICES

A : DETERMINATION OF CONTROL TARGET COORDINATES

The bundle adjustment results for the determination of the control target co-ordinates are given below. In the tables below, STA6 refers to station 4 in the text and likewise STA7 refers to station 5, STA10 to station 6, STA5 to station 3, STA2 to station 2 and STA1 to station 1.

BUNDLE ADJUSTMENT

PROJECT : CONT TIME : 09 50 41 DATE : 28 01 1991

ITERATIONS : 2

PARAMETERS FOR IMAGE 1 (STA6)
units: mm and degrees

PARAMETER	LAST CORRECTION	FINAL VALUE	σ
Xp	- .0000	- .0000	.0000
Yp	.0000	.0000	.0000
Pd	- .0000	- 206.2650	.0000
phi(z)	- .0000000	.0108783	.0052057
omega(x)	.0000000	198.1540072	.0045075
kappa(y)	.0000000	53.5348544	.0013743
Xc	- .00	- 10.70	.0000
Yc	- .00	1471.00	.0000
Zc	- .00	4707.70	.0000

CORRELATIONS IMAGE 1

	Xp	Yp	Pd	phi	omega	kappa	Xc	Yc	Zc
Xp	1.00	.00	.00	.00	- .00	- .00	- .00	.00	- .00
Yp		1.00	- .00	.00	- .00	- .00	.00	- .00	- .00
Pd			1.00	.00	- .00	- .00	.00	- .00	- .00
phi				1.00	- .94	.45	.00	.00	.00
omega					1.00	- .43	.00	.00	- .00
kappa						1.00	- .00	- .00	- .00
Xc							1.00	.00	.00
Yc								1.00	- .00
Zc									1.00

PARAMETERS FOR IMAGE 2 (STA7)
units: mm and degrees

PARAMETER	LAST CORRECTION	FINAL VALUE	σ
Xp	.0000	.0000	.0000
Yp	.0000	.0000	.0000
Pd	.0000	- 206.2650	.0000
phi(z)	- .0000000	.0072453	.0035123
omega(x)	.0000000	204.4344870	.0028142
kappa(y)	.0000000	34.1640421	.0017701
Xc	.00	1531.30	.0000
Yc	.00	1463.50	.0000
Zc	- .00	4707.20	.0000

CORRELATIONS IMAGE 2

	Xp	Yp	Pd	phi	omega	kappa	Xc	Yc	Zc
Xp	1.00	- .00	.00	.00	- .00	- .00	- .00	- .00	- .00
Yp		1.00	- .00	- .00	- .00	.00	.00	- .00	- .00
Pd			1.00	- .00	.00	.00	.00	- .00	- .00
phi				1.00	- .71	.35	.00	- .00	.00
omega					1.00	- .25	- .00	.00	- .00
kappa						1.00	- .00	- .00	- .00
Xc							1.00	.00	.00
Yc								1.00	- .00
Zc									1.00

PARAMETERS FOR IMAGE 3 (STA10)
units: mm and degrees

PARAMETER	LAST CORRECTION	FINAL VALUE	σ
Xp	.0000	.0000	.0000
Yp	- .0000	- .0000	.0000
Pd	- .0000	- 206.2650	.0000
phi(z)	.0000000	- .0123899	.0046238
omega(x)	.0000000	198.2101144	.0040087
kappa(y)	- .0000000	- 52.8708282	.0013852
Xc	.00	6109.20	.0000
Yc	- .00	1459.50	.0000
Zc	- .00	4714.00	.0000

CORRELATIONS IMAGE 3

	Xp	Yp	Pd	phi	omega	kappa	Xc	Yc	Zc
Xp	1.00	.00	- .00	.00	.00	- .00	- .00	- .00	.00
Yp		1.00	- .00	- .00	- .00	.00	- .00	- .00	- .00
Pd			1.00	.00	.00	.00	- .00	- .00	- .00
phi				1.00	.92	.45	.00	.00	- .00
omega					1.00	.42	.00	.00	- .00
kappa						1.00	- .00	- .00	.00
Xc							1.00	- .00	- .00
Yc								1.00	- .00
Zc									1.00

PARAMETERS FOR IMAGE 4 (STA3)
units: mm and degrees

PARAMETER	LAST CORRECTION	FINAL VALUE	σ
Xp	- .0000	- .0000	.0000
Yp	- .0000	- .0000	.0000
Pd	.0000	- 206.2650	.0000
phi(z)	.0000000	179.9823821	.0046149
omega(x)	- .0000000	17.8967420	.0039365
kappa(y)	- .0000000	51.8101261	.0013688
Xc	- .00	- .00	.0000
Yc	- .00	1471.50	.0000
Zc	- .00	- .00	.0000

CORRELATIONS IMAGE 4

	Xp	Yp	Pd	phi	omega	kappa	Xc	Yc	Zc
Xp	1.00	.00	.00	- .00	.00	.00	.00	.00	- .00
Yp		1.00	- .00	.00	- .00	.00	.00	- .00	.00
Pd			1.00	.00	.00	.00	.00	- .00	.00
phi				1.00	- .92	.47	.00	.00	- .00
omega					1.00	- .43	- .00	.00	.00
kappa						1.00	- .00	.00	.00
Xc							1.00	.00	- .00
Yc								1.00	.00
Zc									1.00

PARAMETERS FOR IMAGE 5 (STA2)
units: mm and degrees

PARAMETER	LAST CORRECTION	FINAL VALUE	σ
Xp	- .0000	- .0000	.0000
Yp	- .0000	- .0000	.0000
Pd	- .0000	- 206.2650	.0000
phi(z)	- .0000000	180.0053942	.0034081
omega(x)	.0000000	24.0383289	.0026096
kappa(y)	.0000000	- 31.8709288	.0017146
Xc	- .00	4588.80	.0000
Yc	- .00	1481.00	.0000
Zc	.00	2.80	.0000

CORRELATIONS IMAGE 5

	Xp	Yp	Pd	phi	omega	kappa	Xc	Yc	Zc
Xp	1.00	- .00	- .00	- .00	- .00	.00	.00	- .00	.00
Yp		1.00	- .00	.00	- .00	- .00	- .00	- .00	.00
Pd			1.00	.00	.00	- .00	- .00	- .00	.00
phi				1.00	.67	.36	.00	.00	.00
omega					1.00	.24	.00	.00	.00
kappa						1.00	- .00	- .00	- .00
Xc							1.00	- .00	.00
Yc								1.00	.00
Zc									1.00

PARAMETERS FOR IMAGE 6 (STA1)
units: mm and degrees

PARAMETER	LAST CORRECTION	FINAL VALUE	σ
Xp	.0000	.0000	.0000
Yp	.0000	.0000	.0000
Pd	.0000	- 206.2650	.0000
phi(z)	- .0000000	180.0004990	.0049775
omega(x)	- .0000000	17.9756111	.0041912
kappa(y)	.0000000	- 51.3629969	.0013649
Xc	.00	6113.33	.0000
Yc	.00	1466.00	.0000
Zc	- .00	- .00	.0000

CORRELATIONS IMAGE 6

	Xp	Yp	Pd	phi	omega	kappa	Xc	Yc	Zc
Xp	1.00	.00	- .00	- .00	- .00	.00	.00	.00	.00
Yp		1.00	- .00	- .00	- .00	.00	- .00	- .00	.00
Pd			1.00	- .00	.00	.00	- .00	- .00	.00
phi				1.00	.93	.46	.00	- .00	.00
omega					1.00	.43	- .00	.00	.00
kappa						1.00	- .00	.00	- .00
Xc							1.00	- .00	.00
Yc								1.00	.00
Zc									1.00

OBJECT POINT COORDINATES

POINT NAME	FINAL VALUES (mm) X	Y	Z	STANDARD DEVIATIONS (mm) σx	σy	σz
F1	2882.24	589.01	2723.77	.09	.10	.08
F2	3282.26	585.47	2717.58	.09	.10	.08
F3	2885.02	8.62	2728.53	.10	.11	.09
F4	3278.66	9.75	2728.08	.10	.11	.09
F9	2966.53	20.66	2713.87	.09	.12	.09
F10	3193.37	20.09	2713.25	.09	.12	.09
L1	2780.53	585.77	2226.94	.08	.10	.09
L2	2784.12	586.67	2618.81	.08	.10	.09
L3	2777.32	9.21	2230.60	.09	.12	.10
L4	2779.05	9.69	2625.19	.09	.11	.09
L9	2791.64	21.49	2301.93	.10	.12	.09
L10	2792.49	21.69	2548.43	.09	.12	.09
B5	3281.95	583.96	2142.19	.09	.11	.10
B6	2883.48	583.24	2146.39	.09	.11	.10
B7	3278.01	9.88	2151.65	.10	.13	.11
B8	2880.84	9.27	2153.10	.10	.12	.11
B9	3197.71	21.06	2140.60	.09	.12	.09
B10	2966.59	20.43	2141.21	.09	.12	.09
R5	3362.30	583.46	2616.13	.10	.11	.09
R6	3358.62	584.02	2223.63	.10	.12	.09
R7	3359.57	7.53	2623.73	.11	.12	.10
R8	3356.73	9.31	2228.16	.11	.13	.10
R9	3370.91	19.46	2547.98	.09	.12	.09
R10	3368.57	20.61	2305.06	.09	.12	.09
L5	2805.64	583.97	2226.21	.10	.11	.09
L6	2809.26	586.40	2618.12	.10	.12	.09
L7	2802.71	9.03	2230.16	.11	.12	.10
L8	2804.48	9.46	2623.51	.11	.13	.10
R1	3388.12	584.18	2616.63	.08	.10	.09
R2	3384.53	586.18	2221.85	.08	.10	.09
R3	3384.70	8.35	2623.44	.09	.12	.10
R4	3381.69	8.35	2227.07	.09	.11	.09
F5	2882.04	586.72	2698.06	.09	.11	.10
F6	3281.25	583.98	2691.86	.09	.11	.10
F7	2883.29	9.85	2702.83	.10	.13	.11
F8	3276.18	8.07	2702.40	.10	.12	.11
B1	3280.35	584.48	2116.44	.09	.10	.09

B2	2882.41	583.32	2120.65	.09	.10	.08
B3	3278.72	7.64	2125.93	.10	.11	.09
B4	2879.53	8.19	2127.39	.10	.12	.09

OBSERVATIONS FROM IMAGE 1 (STA6)

POINT NAME	PLATE COORDINATES (mm) x	y	RESIDUALS (mm) Vx	Vy	LENS CORR. (mm) Dx	Dy	WEIGHTS Px	Py	CHECK	
F1	- 7.0921	14.5730	.0015	- .0012	.0000	.0000	1.0000	1.0000	- .0000	- .0000
F2	- 18.7880	18.5835	- .0007	.0005	.0000	.0000	1.0000	1.0000	- .0000	- .0000
F3	- 7.0546	- 16.1747	- .0001	- .0001	.0000	.0000	1.0000	1.0000	- .0000	- .0000
F4	- 18.3275	- 9.9429	.0025	- .0018	.0000	.0000	1.0000	1.0000	- .0000	- .0000
F9	- 8.8930	- 14.0416	- .0018	- .0007	.0000	.0000	1.0000	1.0000	- .0000	- .0000
F10	- 15.3884	- 10.5426	- .0022	- .0020	.0000	.0000	1.0000	1.0000	- .0000	- .0000
L1	18.1903	17.2299	.0038	- .0041	.0000	.0000	1.0000	1.0000	- .0000	- .0000
L2	1.0761	14.2110	.0019	- .0029	.0000	.0000	1.0000	1.0000	- .0000	- .0000
L3	17.3357	- 11.9672	.0013	.0031	.0000	.0000	1.0000	1.0000	- .0000	- .0000
L4	.9079	- 16.6255	.0012	.0005	.0000	.0000	1.0000	1.0000	- .0000	- .0000
L9	14.0432	- 11.9568	.0012	- .0009	.0000	.0000	1.0000	1.0000	- .0000	- .0000
L10	3.8030	- 14.8386	.0013	- .0010	.0000	.0000	1.0000	1.0000	- .0000	- .0000
B5	5.1677	22.2656	- .0031	.0014	.0000	.0000	1.0000	1.0000	- .0000	- .0000
B6	17.8053	18.6865	- .0005	.0013	.0000	.0000	1.0000	1.0000	- .0000	- .0000
B7	4.7158	- 4.2262	- .0004	.0026	.0000	.0000	1.0000	1.0000	- .0000	- .0000
B8	16.8614	- 9.5807	- .0027	.0011	.0000	.0000	1.0000	1.0000	- .0000	- .0000
B9	7.4640	- 4.6341	- .0025	- .0002	.0000	.0000	1.0000	1.0000	- .0000	- .0000
B10	14.5404	- 7.7289	- .0037	.0013	.0000	.0000	1.0000	1.0000	- .0000	- .0000
R5	- 16.4957	19.9241	.0004	- .0004	.0000	.0000	1.0000	1.0000	- .0000	- .0000
R6	- .2397	22.4017	.0039	.0032	.0000	.0000	1.0000	1.0000	- .0000	- .0000
R7	- 16.0409	- 7.8201	.0009	.0005	.0000	.0000	1.0000	1.0000	- .0000	- .0000
R8	- .3462	- 3.9763	- .0006	.0031	.0000	.0000	1.0000	1.0000	- .0000	- .0000
R9	- 13.2329	- 6.3619	- .0014	- .0033	.0000	.0000	1.0000	1.0000	- .0000	- .0000

OBSERVATIONS FROM IMAGE 2 (STA7)

POINT NAME	PLATE COORDINATES (mm) x	y	RESIDUALS (mm) Vx	Vy	LENS CORR. (mm) Dx	Dy	WEIGHTS Px	Py	CHECK	
F1	- .3300	15.9293	- .0007	.0023	.0000	.0000	1.0000	1.0000	- .0000	- .0000
F2	- 24.8078	21.5846	.0012	.0028	.0000	.0000	1.0000	1.0000	- .0000	- .0000
F3	- .6752	- 24.6442	.0004	.0010	.0000	.0000	1.0000	1.0000	- .0000	- .0000
F4	- 23.1120	- 16.5818	- .0021	.0005	.0000	.0000	1.0000	1.0000	- .0000	- .0000
F9	- 4.9773	- 21.6855	.0014	.0009	.0000	.0000	1.0000	1.0000	- .0000	- .0000
F10	- 17.8811	- 17.1622	- .0018	.0014	.0000	.0000	1.0000	1.0000	- .0000	- .0000
L1	25.8079	24.4436	- .0029	.0018	.0000	.0000	1.0000	1.0000	- .0000	- .0000
L2	10.8932	16.6248	- .0015	.0020	.0000	.0000	1.0000	1.0000	- .0000	- .0000
L3	23.8959	- 12.4070	- .0014	- .0009	.0000	.0000	1.0000	1.0000	- .0000	- .0000

L4	10.0367	- 23.5795	- .0015	.0011	.0000	.0000	1.0000	1.0000	- .0000	- .0000
L10	12.1252	- 20.1868	.0015	- .0001	.0000	.0000	1.0000	1.0000	- .0000	- .0000
B5	- .5335	31.2894	.0023	- .0019	.0000	.0000	1.0000	1.0000	- .0000	- .0000
B6	22.0546	26.9073	.0008	.0010	.0000	.0000	1.0000	1.0000	- .0000	- .0000
B7	- .6239	- 2.5758	.0004	- .0027	.0000	.0000	1.0000	1.0000	- .0000	- .0000
B8	20.3627	- 8.7287	.0020	- .0017	.0000	.0000	1.0000	1.0000	- .0000	- .0000
B9	3.7995	- 2.8929	.0010	- .0009	.0000	.0000	1.0000	1.0000	- .0000	- .0000
B10	16.0008	- 6.4383	.0014	- .0045	.0000	.0000	1.0000	1.0000	- .0000	- .0000
R5	- 24.4507	24.3934	- .0002	.0002	.0000	.0000	1.0000	1.0000	- .0000	- .0000
R6	- 7.6382	30.8565	- .0029	- .0009	.0000	.0000	1.0000	1.0000	- .0000	- .0000
R7	- 22.7692	- 12.4477	.0001	- .0025	.0000	.0000	1.0000	1.0000	- .0000	- .0000
R8	- 7.1800	- 3.1005	.0002	- .0010	.0000	.0000	1.0000	1.0000	- .0000	- .0000
R9	- 20.1963	- 9.6537	.0054	.0008	.0000	.0000	1.0000	1.0000	- .0000	- .0000
R10	- 10.5642	- 3.9737	- .0033	.0013	.0000	.0000	1.0000	1.0000	- .0000	- .0000

OBSERVATIONS FROM IMAGE 3 (STA10)

POINT NAME	PLATE COORDINATES (mm) x	y	RESIDUALS (mm) Vx	Vy	LENS CORR. (mm) Dx	Dy	WEIGHTS Px	Py	CHECK	
F1	19.3137	18.8920	.0014	- .0021	.0000	.0000	1.0000	1.0000	.0000	- .0000
F2	6.6523	14.5690	.0011	- .0039	.0000	.0000	1.0000	1.0000	.0000	- .0000
F3	18.5811	- 10.2078	.0006	- .0012	.0000	.0000	1.0000	1.0000	.0000	- .0000
F4	6.9250	- 16.3810	.0004	.0011	.0000	.0000	1.0000	1.0000	.0000	- .0000
F9	15.6919	- 10.6744	- .0015	.0013	.0000	.0000	1.0000	1.0000	.0000	- .0000
F10	8.9468	- 14.2434	.0009	.0009	.0000	.0000	1.0000	1.0000	.0000	- .0000
L10	13.5239	- 6.3929	.0036	.0039	.0000	.0000	1.0000	1.0000	.0000	- .0000
B5	- 18.2292	19.0097	- .0012	.0010	.0000	.0000	1.0000	1.0000	.0000	- .0000
B6	- 4.9192	22.4738	.0004	- .0028	.0000	.0000	1.0000	1.0000	.0000	- .0000
B7	- 16.9290	- 9.5177	- .0007	.0007	.0000	.0000	1.0000	1.0000	.0000	- .0000
B8	- 4.3855	- 4.2262	- .0017	.0011	.0000	.0000	1.0000	1.0000	.0000	- .0000
B9	- 14.6866	- 7.7359	- .0016	- .0001	.0000	.0000	1.0000	1.0000	.0000	- .0000
B10	- 7.3840	- 4.6959	- .0003	.0012	.0000	.0000	1.0000	1.0000	.0000	- .0000
R9	- 4.0434	- 15.1436	- .0018	.0016	.0000	.0000	1.0000	1.0000	.0000	- .0000
R10	- 14.0503	- 12.0869	- .0011	- .0016	.0000	.0000	1.0000	1.0000	.0000	- .0000
L5	.5262	22.6510	.0006	- .0016	.0000	.0000	1.0000	1.0000	.0000	- .0000
L6	16.6613	20.1833	.0015	.0025	.0000	.0000	1.0000	1.0000	.0000	- .0000
L7	.7387	- 3.9922	.0015	.0040	.0000	.0000	1.0000	1.0000	.0000	- .0000
L8	16.2953	- 7.8951	.0022	.0034	.0000	.0000	1.0000	1.0000	.0000	- .0000
R1	- 1.7236	14.1591	- .0019	- .0043	.0000	.0000	1.0000	1.0000	.0000	- .0000
R2	- 18.7447	17.5293	.0009	- .0012	.0000	.0000	1.0000	1.0000	.0000	- .0000
R3	- 1.2195	- 16.9105	- .0031	- .0031	.0000	.0000	1.0000	1.0000	.0000	- .0000
R4	- 17.5781	- 11.9807	- .0003	- .0003	.0000	.0000	1.0000	1.0000	.0000	- .0000

OBSERVATIONS FROM IMAGE 4 (STA5)

POINT NAME	PLATE COORDINATES (mm) x	y	RESIDUALS (mm) Vx	Vy	LENS CORR. (mm) Dx	Dy	WEIGHTS Px	Py	CHECK	
F9	- 14.4800	- 7.2361	- .0015	.0005	.0000	.0000	1.0000	1.0000	- .0000	- .0000
F10	- 7.3783	- 4.4405	.0025	- .0018	.0000	.0000	1.0000	1.0000	- .0000	- .0000
L1	- 1.7646	14.1320	- .0011	.0018	.0000	.0000	1.0000	1.0000	- .0000	- .0000
L2	- 17.8517	17.3222	- .0011	.0002	.0000	.0000	1.0000	1.0000	- .0000	- .0000
L3	- 1.9506	- 16.0010	- .0011	- .0019	.0000	.0000	1.0000	1.0000	- .0000	- .0000

L4	- 17.4930	- 11.2426	- .0016	- .0019	.0000	.0000	1.0000	1.0000	- .0000	- .0000
L9	- 4.4327	- 14.2790	.0013	- .0006	.0000	.0000	1.0000	1.0000	- .0000	- .0000
L10	- 14.1555	- 11.3491	.0032	.0004	.0000	.0000	1.0000	1.0000	- .0000	- .0000
B9	14.8185	- 10.1833	.0004	.0002	.0000	.0000	1.0000	1.0000	- .0000	- .0000
B10	7.9326	- 13.5880	.0018	.0019	.0000	.0000	1.0000	1.0000	- .0000	- .0000
R5	1.0702	22.0719	- .0001	.0002	.0000	.0000	1.0000	1.0000	- .0000	- .0000
R6	16.5640	19.5592	- .0014	- .0019	.0000	.0000	1.0000	1.0000	- .0000	- .0000
R7	.6707	- 3.8610	.0011	.0028	.0000	.0000	1.0000	1.0000	- .0000	- .0000
R8	15.6398	- 7.6503	- .0002	- .0018	.0000	.0000	1.0000	1.0000	- .0000	- .0000
R10	12.9234	- 6.2177	- .0023	.0026	.0000	.0000	1.0000	1.0000	- .0000	- .0000
F5	- 17.4090	18.7947	- .0006	.0002	.0000	.0000	1.0000	1.0000	- .0000	- .0000
F6	- 4.1713	21.9302	- .0003	.0018	.0000	.0000	1.0000	1.0000	- .0000	- .0000
F7	- 16.8088	- 8.9472	- .0016	.0025	.0000	.0000	1.0000	1.0000	- .0000	- .0000
F8	- 4.5343	- 4.0879	- .0004	.0019	.0000	.0000	1.0000	1.0000	- .0000	- .0000
B1	18.9319	18.1420	.0006	- .0008	.0000	.0000	1.0000	1.0000	- .0000	- .0000
B2	6.4620	14.1952	- .0002	- .0018	.0000	.0000	1.0000	1.0000	- .0000	- .0000
B3	17.6774	- 9.8442	.0015	- .0035	.0000	.0000	1.0000	1.0000	- .0000	- .0000
B4	5.7770	- 15.7174	.0011	- .0010	.0000	.0000	1.0000	1.0000	- .0000	- .0000

OBSERVATIONS FROM IMAGE 5 (STA2)

POINT NAME	PLATE COORDINATES (mm) x	y	RESIDUALS (mm) Vx	Vy	LENS CORR. (mm) Dx	Dy	WEIGHTS Px	Py	CHECK	
F9	3.1949	- 2.7902	- .0009	- .0001	.0000	.0000	1.0000	1.0000	.0000	- .0000
F10	15.0702	- 5.9134	- .0022	.0021	.0000	.0000	1.0000	1.0000	.0000	- .0000
L9	- 19.8447	- 9.6150	- .0006	.0004	.0000	.0000	1.0000	1.0000	.0000	- .0000
L10	- 10.8862	- 3.9594	.0015	- .0008	.0000	.0000	1.0000	1.0000	.0000	- .0000
B9	- 3.7018	- 20.7965	- .0007	.0023	.0000	.0000	1.0000	1.0000	.0000	- .0000
B10	- 16.8801	- 16.6726	.0004	- .0020	.0000	.0000	1.0000	1.0000	.0000	- .0000
R9	20.2370	- 12.5784	.0003	- .0005	.0000	.0000	1.0000	1.0000	.0000	- .0000
R10	12.4714	- 19.1053	- .0033	.0006	.0000	.0000	1.0000	1.0000	.0000	- .0000
L5	- 23.7967	23.3047	.0018	.0000	.0000	.0000	1.0000	1.0000	.0000	- .0000
L6	- 8.2681	29.8392	.0028	- .0004	.0000	.0000	1.0000	1.0000	.0000	- .0000
L7	- 22.0365	- 12.2763	.0001	- .0030	.0000	.0000	1.0000	1.0000	.0000	- .0000
L8	- 7.7666	- 3.1736	.0036	.0004	.0000	.0000	1.0000	1.0000	.0000	- .0000
R1	25.0271	23.8262	- .0018	.0035	.0000	.0000	1.0000	1.0000	.0000	- .0000
R2	11.5274	16.1963	.0016	- .0027	.0000	.0000	1.0000	1.0000	.0000	- .0000
R3	23.1959	- 11.5277	- .0040	.0035	.0000	.0000	1.0000	1.0000	.0000	- .0000
R4	10.6023	- 22.4199	- .0003	.0002	.0000	.0000	1.0000	1.0000	.0000	- .0000
F5	- 1.6538	30.3713	.0012	- .0020	.0000	.0000	1.0000	1.0000	.0000	- .0000
F6	20.7163	26.2475	- .0005	- .0005	.0000	.0000	1.0000	1.0000	.0000	- .0000
F7	- 1.3291	- 2.5147	.0014	- .0010	.0000	.0000	1.0000	1.0000	.0000	- .0000
F8	19.2705	- 8.0067	- .0004	.0011	.0000	.0000	1.0000	1.0000	.0000	- .0000
B1	.3847	15.1635	- .0013	- .0031	.0000	.0000	1.0000	1.0000	.0000	- .0000
B2	- 24.1043	20.3766	.0014	- .0012	.0000	.0000	1.0000	1.0000	.0000	- .0000
B3	.6136	- 23.6105	.0009	.0014	.0000	.0000	1.0000	1.0000	.0000	- .0000
B4	- 22.1341	- 16.2943	- .0008	.0021	.0000	.0000	1.0000	1.0000	.0000	- .0000

OBSERVATIONS FROM IMAGE 6 (STA1)

POINT NAME	PLATE COORDINATES (mm) x	y	RESIDUALS (mm) Vx	Vy	LENS CORR. (mm) Dx	Dy	WEIGHTS Px	Py	CHECK	
F9	7.2732	- 4.3754	.0020	- .0023	.0000	.0000	1.0000	1.0000	.0000	- .0000
F10	14.4542	- 7.2515	- .0013	- .0016	.0000	.0000	1.0000	1.0000	.0000	- .0000
L9	- 13.2973	- 6.2520	.0025	.0011	.0000	.0000	1.0000	1.0000	.0000	- .0000
L10	- 3.8630	- 3.8301	.0026	- .0023	.0000	.0000	1.0000	1.0000	.0000	- .0000
B9	- 7.8814	- 13.7604	- .0005	- .0018	.0000	.0000	1.0000	1.0000	.0000	- .0000
B10	- 14.8592	- 10.3725	- .0027	.0033	.0000	.0000	1.0000	1.0000	.0000	- .0000
R9	14.3365	- 11.5540	.0063	.0011	.0000	.0000	1.0000	1.0000	.0000	- .0000
R10	4.6434	- 14.3945	- .0013	- .0028	.0000	.0000	1.0000	1.0000	.0000	- .0000
L5	- 16.6093	19.7152	- .0029	.0016	.0000	.0000	1.0000	1.0000	.0000	- .0000
L6	- .8609	22.3705	- .0034	- .0021	.0000	.0000	1.0000	1.0000	.0000	- .0000
L7	- 15.8380	- 7.7011	.0014	- .0001	.0000	.0000	1.0000	1.0000	.0000	- .0000
L8	- .7680	- 3.7971	- .0040	- .0041	.0000	.0000	1.0000	1.0000	.0000	- .0000
R1	18.3342	17.2655	.0011	.0003	.0000	.0000	1.0000	1.0000	.0000	- .0000
R2	1.8095	14.1912	- .0020	.0047	.0000	.0000	1.0000	1.0000	.0000	- .0000
R3	17.6573	- 11.4105	.0034	- .0006	.0000	.0000	1.0000	1.0000	.0000	- .0000
R4	1.8453	- 16.2149	.0002	.0002	.0000	.0000	1.0000	1.0000	.0000	- .0000
F5	4.3414	22.3128	- .0014	.0023	.0000	.0000	1.0000	1.0000	.0000	- .0000
F6	17.3490	18.8066	.0002	- .0010	.0000	.0000	1.0000	1.0000	.0000	- .0000
F7	4.3761	- 3.9647	- .0026	- .0014	.0000	.0000	1.0000	1.0000	.0000	- .0000
F8	16.8184	- 9.0212	- .0003	- .0030	.0000	.0000	1.0000	1.0000	.0000	- .0000
B1	- 6.5687	14.3118	.0026	.0049	.0000	.0000	1.0000	1.0000	.0000	- .0000
B2	- 18.9267	18.2428	- .0013	.0036	.0000	.0000	1.0000	1.0000	.0000	- .0000
B3	- 5.9024	- 15.8941	.0001	.0015	.0000	.0000	1.0000	1.0000	.0000	- .0000
B4	- 17.9108	- 9.8805	.0013	- .0016	.0000	.0000	1.0000	1.0000	.0000	- .0000

A POSTERIORI STANDARD DEVIATION OF UNIT WEIGHT = .0027654

No. of stations: 6

Reduced no. of observations: 280
No. of control points used: 0
No. of targets observed: 40
No. of object points fixed: 40
Degrees of freedom: 142

Iteration threshold: .00000010
Maximum no. of iterations: 1
Lens distortion model: 0
Gross error detection: N
Digital camera: N

Note that the target names used in appendix A were subsequently renumbered (see p A9). The relationships are:

F1 - F10 became 1 - 10
L1 - L10 " 11 - 20
B1 - B10 " 21 - 30
R1 - R10 " 31 - 40

Coordinates of control points

Target	X	Y	Z
1	2882.2	589.0	2723.7
2	3282.3	585.5	2717.6
3	2885.0	8.6	2728.5
4	3278.7	9.8	2728.1
5	2882.0	586.7	2698.1
6	3281.3	584.0	2691.9
7	2883.3	9.9	2702.8
8	3276.2	8.1	2702.4
9	2966.5	20.7	2713.9
10	3193.4	20.1	2713.3
11	2780.5	585.8	2226.9
12	2784.1	586.7	2618.8
13	2777.3	9.2	2230.6
14	2779.1	9.7	2625.2
15	2805.6	584.0	2226.2
16	2809.3	586.4	2618.1
17	2802.7	9.0	2230.2
18	2804.5	9.5	2623.5
19	2791.6	21.5	2301.9
20	2792.5	21.7	2548.4
21	3280.4	584.5	2116.4
22	2882.4	583.3	2120.7
23	3278.7	7.6	2125.9
24	2879.5	8.2	2127.4
25	3282.0	584.0	2142.2
26	2883.5	583.2	2146.4
27	3278.0	9.9	2151.7
28	2880.8	9.3	2153.1
29	3197.7	21.1	2140.6
30	2966.6	20.4	2141.2
31	3388.1	584.2	2616.6
32	3384.5	586.2	2221.9
33	3384.7	8.4	2623.4
34	3381.7	8.4	2227.1
35	3362.3	583.5	2616.1
36	3358.6	584.0	2223.6
37	3359.6	7.5	2623.7
38	3356.7	9.3	2228.2
39	3370.9	19.5	2548.0
40	3368.6	20.6	2305.1

B : CALIBRATION EXAMPLE

An example of a set of camera calibrations is tabled below:

Observations from camera 1

1	203.22	21.36
2	405.45	38.62
26	177.54	56.08
25	341.30	66.38
28	169.27	403.71
27	332.46	406.94
3	195.34	458.95
4	394.43	460.49

Observations from camera 2

1	300.23	20.50
12	227.62	26.80
2	438.53	34.02
11	116.25	51.14
36	313.07	61.76
38	321.02	399.89
37	438.84	411.98
28	143.54	420.08
4	448.26	420.32
13	124.35	429.45
3	311.06	445.78
14	236.18	447.00

Observations from camera 3

2	255.35	14.48
31	336.50	21.29
1	86.35	42.31
16	95.75	61.55
25	413.13	84.97
15	212.59	101.24
26	260.87	105.17
17	205.10	466.11
28	253.40	466.75
3	77.11	475.26
4	243.36	488.56
33	327.94	490.90

Calibration of Camera 1

No. of iterations: 3
No. of points: 8
Degrees of freedom: 5

Horizontal translaton: 256
Vertical translaton: 256
Horizontal scale: 0.01096
Vertical scale: 0.00760

DLT-parameters

Param.	Calculated	std. dev.
b11	2.892e-003	9.067e-006
b12	9.582e-005	1.019e-006
b13	4.376e-004	1.703e-006
b14	-9.879e+000	3.096e-002
b21	-8.035e-005	1.377e-006
b22	2.923e-003	8.860e-006
b23	-1.254e-004	1.036e-006
b24	-2.406e-001	5.002e-003
b31	3.454e-005	9.874e-007
b32	-6.414e-006	8.953e-007
b33	-2.153e-004	6.652e-007

Observations & corrections (mm)

Pt	Image Coords.		Residuals		Lens Corrns.	
	x	y	Vx	Vy	Dx	Dy
1	-0.5785	1.7833	-0.0008	-0.0004	0.0000	0.0000
2	1.6330	1.6521	0.0000	-0.0001	0.0000	0.0000
26	-0.8599	1.5194	0.0008	0.0008	0.0000	0.0000
25	0.9349	1.4411	0.0002	-0.0002	0.0000	0.0000
28	-0.9506	-1.1226	0.0002	-0.0016	0.0000	0.0000
27	0.8380	-1.1471	-0.0011	0.0010	0.0000	0.0000
3	-0.6648	-1.5424	0.0000	0.0010	0.0000	0.0000
4	1.5172	-1.5541	0.0007	-0.0006	0.0000	0.0000

a posteriori standard deviation of unit weight = 0.0013

Calibration of Camera 2

No. of iterations: 3
No. of points: 12
Degrees of freedom: 13

Horizontal translaton: 256
Vertical translaton: 256
Horizontal scale: 0.01096
Vertical scale: 0.00760

DLT-parameters

Param.	Calculated	std. dev.
b11	3.927e-003	4.210e-005
b12	-1.505e-004	4.445e-006
b13	3.191e-003	3.299e-005
b14	-1.949e+001	2.042e-001
b21	1.767e-004	4.863e-006
b22	5.058e-003	5.254e-005
b23	1.974e-005	4.971e-006
b24	-1.920e+000	2.515e-002
b31	2.093e-004	4.776e-006
b32	-7.225e-006	3.320e-006
b33	-2.540e-004	2.760e-006

Observations & corrections (mm)

Pt	Image Coords.		Residuals		Lens Corrns.	
	x	y	Vx	Vy	Dx	Dy
1	0.4848	1.7898	-0.0048	-0.0015	0.0000	0.0000
12	-0.3110	1.7419	-0.0000	0.0004	0.0000	0.0000
2	2.0005	1.6870	0.0021	0.0007	0.0000	0.0000
11	-1.5317	1.5569	0.0017	0.0026	0.0000	0.0000
36	0.6255	1.4762	0.0018	-0.0023	0.0000	0.0000
38	0.7126	-1.0936	-0.0043	0.0065	0.0000	0.0000
37	2.0039	-1.1854	0.0010	-0.0070	0.0000	0.0000
28	-1.2326	-1.2470	-0.0017	-0.0039	0.0000	0.0000
4	2.1072	-1.2488	0.0007	0.0036	0.0000	0.0000
13	-1.4429	-1.3182	0.0015	-0.0007	0.0000	0.0000
3	0.6035	-1.4423	-0.0006	0.0013	0.0000	0.0000
14	-0.2172	-1.4516	0.0024	0.0004	0.0000	0.0000

a posteriori standard deviation of unit weight = 0.0039

Calibration Check for Cameras 1, 2 & 3

Pt.	CALCULATED CONTROL VALUES (mm)			DISCREPANCIES (mm)		
	X	Y	Z	dX	dY	dZ
1	2882.45	588.90	2724.38	-0.25	0.10	-0.68
2	3282.53	585.63	2716.84	-0.23	-0.13	0.76
28	2881.12	9.56	2152.90	-0.32	-0.26	0.20
4	3278.48	9.54	2728.14	0.22	0.26	-0.04
3	2884.98	8.80	2728.67	0.02	-0.20	-0.17
26	2883.50	583.42	2145.08	0.00	-0.22	1.32
25	3281.60	583.85	2143.75	0.40	0.15	-1.55

C : REFLEX METROGRAPH COORDINATES OF THE TEST TARGETS

Direct observations of the coordinates of the points on the small frame, using the reflex metrograph.

Point	X	Y	Z
1	-164.250	-176.170	27.400
	-164.400	-176.100	27.595
	-164.535	-176.410	27.215
	-164.745	-176.585	27.250
	-164.483	-176.316	27.365
2	- 29.215	-178.115	24.640
	- 28.955	-177.550	24.845
	- 28.820	-177.425	24.925
	- 29.090	-177.645	24.835
	- 29.020	-177.684	24.811
3	59.535	-177.760	25.025
	59.720	-177.635	24.940
	59.710	-177.875	24.690
	59.715	-177.565	24.900
	59.670	-177.709	24.889
4	73.270	- 79.885	27.140
	73.465	- 79.865	27.280
	73.330	- 79.595	27.555
	73.570	- 79.950	27.150
	73.409	- 79.824	27.281
5	59.905	54.125	27.265
	59.995	54.270	27.345
	59.985	54.150	27.295
	59.820	53.955	27.230
	59.926	54.125	27.284
6	- 35.860	54.445	27.715
	- 35.615	54.325	27.835
	- 35.465	54.315	27.665
	- 35.660	54.300	27.670
	- 35.650	54.346	27.721

7	-166.130	52.480	30.130
	-166.190	52.610	30.410
	-166.160	52.820	30.350
	-166.215	52.490	30.095
	-166.174	52.600	30.246
8	-178.940	- 87.690	30.275
	-179.045	- 88.200	30.015
	-179.050	- 88.130	30.205
	-179.030	- 87.900	30.095
	-179.016	- 87.980	30.147
9	-136.350	-145.065	127.025
	-136.525	-145.230	126.950
	-136.645	-145.375	126.975
	-136.570	-145.235	127.020
	-136.522	-145.226	126.993
10	- 34.095	-151.360	123.850
	- 34.165	-151.075	124.130
	- 34.085	-151.480	123.855
	- 34.150	-151.480	124.005
	- 34.124	-151.349	123.960
11	29.980	-148.445	124.010
	29.915	-148.525	123.960
	29.900	-148.520	124.055
	29.685	-148.255	124.080
	29.870	-148.436	124.026
12	42.980	- 81.925	124.115
	43.155	- 81.420	124.235
	43.085	- 81.350	124.345
	42.985	- 81.820	124.005
	43.051	- 81.629	124.175

13	23.695	21.435	124.610
	23.560	21.240	124.560
	23.725	21.355	124.690
	23.845	21.410	124.685
	23.706	21.360	124.636
14	- 32.435	22.070	125.805
	- 32.610	21.905	125.865
	- 32.565	22.000	125.820
	- 32.495	21.920	125.780
	- 32.526	21.974	125.818
15	-139.190	22.885	129.140
	-139.095	23.040	129.240
	-139.180	22.815	129.130
	-139.095	22.780	129.330
	-139.140	22.880	129.210
16	-147.540	- 84.350	129.325
	-147.290	- 83.855	129.490
	-147.530	- 83.735	129.485
	-147.390	- 84.050	129.475
	-147.437	- 83.998	129.444

Final coordinates of points on the small frame, determined using the reflex metrograph

1	-164.483	-176.316	27.365
2	-29.020	-177.684	24.811
3	59.670	-177.709	24.889
4	73.409	-79.824	27.281
5	59.926	54.125	27.284
6	-35.650	54.346	27.721
7	-166.174	52.600	30.246
8	-179.016	-87.980	30.147
9	-136.522	-145.226	126.993
10	-34.124	-151.349	123.960
11	29.870	-148.436	124.026
12	43.051	-81.629	124.175
13	23.706	21.360	124.636
14	-32.526	21.974	125.818
15	-139.140	22.880	129.210
16	-147.437	-83.998	129.444

D : SPG COORDINATES OF THE TEST TARGETS

Coordinates of points on the small frame, determined by the SPG system

Fix 1

1	2998.65	198.18	2428.48
2	3134.92	195.53	2428.46
3	3223.78	193.96	2430.24
4	3237.62	292.21	2426.19
5	3227.55	426.61	2415.72
6	3131.42	427.71	2414.43
7	3000.59	427.97	2415.34
8	2984.04	287.29	2424.78
9	3024.99	236.48	2525.23
10	3128.17	229.20	2524.67
11	3192.32	231.11	2525.69
12	3205.51	297.83	2522.22
13	3189.10	401.64	2514.71
14	3132.27	402.86	2514.92
15	3025.28	405.75	2516.44
16	3014.05	298.73	2524.21

Coordinates of points on the small frame, determined by the SPG system

FIX 2

1	2969.21	198.86	2435.05
2	3105.56	195.07	2433.17
3	3194.72	192.46	2434.14
4	3209.29	290.63	2433.63
5	3200.66	425.45	2428.21
6	3104.33	427.73	2427.88
7	2973.63	429.26	2429.63
8	2955.66	288.40	2434.56
9	2996.98	233.61	2532.70
10	3100.07	225.26	2530.84
11	3164.31	226.65	2531.13
12	3178.10	293.18	2530.02
13	3162.59	397.41	2526.71
14	3105.72	399.13	2527.47
15	2998.84	403.16	2530.23
16	2986.55	295.88	2534.01

E : TRANSFORMATION RESULTS

The reflex metrograph coordinates (old system) are transformed into the SPG determined coordinates (new system).

Transformation 1: "Metrograph" coordinates into SPG Fix 1 coordinates - scale factor included.

No. of iterations = 9

Old System Translations
X-translation = 48.403750 + -0.000000 +/- 0.128774
Y-translation = 67.679125 + 0.000000 +/- 0.128774
Z-translation = -76.750375 + -0.000000 +/- 0.128774

Rodrigues Rotation Parameters
lambda = -0.071529 +/- 0.001274
mu = -0.017910 +/- 0.001257
nu = -0.014322 +/- 0.001023

Scale unfixed
Scale = 1.003859 +/- 0.000955

New System Translations
X-translation = 3115.641250
Y-translation = 309.566250
Z-translation = 2471.983125

Original coordinates of new system

Point	X	Y	Z	vX	vY	vZ
1	2998.6500	198.1800	2428.4800	-0.2735	0.6644	-0.3061
2	3134.9200	195.5300	2428.4600	-0.5694	-0.0965	-0.2435
3	3223.7800	193.9600	2430.2400	-0.4223	0.2377	-0.3058
4	3237.6200	292.2100	2426.1900	0.9526	-0.0273	-0.6135
5	3227.5500	426.6100	2415.7200	-0.4999	-0.1335	0.0230
6	3131.4200	427.7100	2414.4300	-0.2938	0.3300	-0.0304
7	3000.5900	427.9700	2415.3400	-0.5273	0.2934	-0.6979
8	2984.0400	287.2900	2424.7800	1.0277	0.3948	-0.4121
9	3024.9900	236.4800	2525.2300	0.1768	0.2646	0.9759
10	3128.1700	229.2000	2524.6700	-0.2760	-0.2080	0.8287
11	3192.3200	231.1100	2525.6900	-0.1593	-0.0744	0.8481
12	3205.5100	297.8300	2522.2200	0.8785	-0.0779	-0.0711
13	3189.1000	401.6400	2514.7100	-0.5894	-0.4777	0.1717
14	3132.2700	402.8600	2514.9200	-0.2050	-0.2269	0.0626
15	3025.2800	405.7500	2516.4400	-0.2578	-0.5039	-0.0953
16	3014.0500	298.7300	2524.2100	1.0382	-0.3587	-0.1343

Transformed coordinates

Point	X	Y	Z
1	2998.3765	198.8444	2428.1739
2	3134.3506	195.4335	2428.2165
3	3223.3577	194.1977	2429.9342
4	3238.5726	292.1827	2425.5765
5	3227.0501	426.4765	2415.7430
6	3131.1262	428.0400	2414.3996
7	3000.0627	428.2634	2414.6421
8	2985.0677	287.6848	2424.3679
9	3025.1668	236.7446	2526.2059
10	3127.8940	228.9920	2525.4987
11	3192.1607	231.0356	2526.5381
12	3206.3885	297.7521	2522.1489
13	3188.5106	401.1623	2514.8817
14	3132.0650	402.6331	2514.9826
15	3025.0222	405.2461	2516.3447
16	3015.0882	298.3713	2524.0757

$\hat{\sigma}_o$ = 0.5171

Transformation 2 : "Metrograph" coordinates into SPG Fix 1 coordinates
- scale held fixed.

No. of iterations = 7

Old System Translations
X-translation = 48.403750 + -0.000000 +/- 0.151017
Y-translation = 67.679125 + 0.000000 +/- 0.151017
Z-translation = -76.750375 + -0.000000 +/- 0.151017

Rodrigues Rotation Parameters
lambda = -0.071529 +/- 0.001495
mu = -0.017910 +/- 0.001474
nu = -0.014322 +/- 0.001199

Scale held fixed
Scale = 1.000000

New System Translations
X-translation = 3115.641250
Y-translation = 309.566250
Z-translation = 2471.983125

Original coordinates of new system

Point	X	Y	Z	vX	vY	vZ
1	2998.6500	198.1800	2428.4800	0.1773	1.0901	-0.1377
2	3134.9200	195.5300	2428.4600	-0.6414	0.3422	-0.0752
3	3223.7800	193.9600	2430.2400	-0.8364	0.6812	-0.1441
4	3237.6200	292.2100	2426.1900	0.4800	0.0396	-0.4351
5	3227.5500	426.6100	2415.7200	-0.9281	-0.5829	0.2392
6	3131.4200	427.7100	2414.4300	-0.3533	-0.1255	0.1910
7	3000.5900	427.9700	2415.3400	-0.0830	-0.1629	-0.4775
8	2984.0400	287.2900	2424.7800	1.5296	0.4790	-0.2290
9	3024.9900	236.4800	2525.2300	0.5246	0.5445	0.7675
10	3128.1700	229.2000	2524.6700	-0.3231	0.1018	0.6230
11	3192.3200	231.1100	2525.6900	-0.4535	0.2275	0.6384
12	3205.5100	297.8300	2522.2200	0.5296	-0.0325	-0.2639
13	3189.1000	401.6400	2514.7100	-0.8695	-0.8298	0.0068
14	3132.2700	402.8600	2514.9200	-0.2681	-0.5846	-0.1027
15	3025.2800	405.7500	2516.4400	0.0905	-0.8718	-0.2658
16	3014.0500	298.7300	2524.2100	1.4247	-0.3157	-0.3346

Transformed coordinates

Point	X	Y	Z
1	2998.8273	199.2701	2428.3423
2	3134.2786	195.8722	2428.3848
3	3222.9436	194.6412	2430.0959
4	3238.1000	292.2496	2425.7549
5	3226.6219	426.0271	2415.9592
6	3131.0667	427.5845	2414.6210
7	3000.5070	427.8071	2414.8625
8	2985.5696	287.7690	2424.5510
9	3025.5146	237.0245	2525.9975
10	3127.8469	229.3018	2525.2930
11	3191.8665	231.3375	2526.3284
12	3206.0396	297.7975	2521.9561
13	3188.2305	400.8102	2514.7168
14	3132.0019	402.2754	2514.8173
15	3025.3705	404.8782	2516.1742
16	3015.4747	298.4143	2523.8754

$\hat{\sigma}_o$ = 0.6041

Transformation 3 : "Metrograph" coordinates into SPG Fix 2 coordinates - scale factor included.

No. of iterations = 7

Old System Translations
X-translation = 48.403750 + -0.000000 +/- 0.133715
Y-translation = 67.679125 + -0.000000 +/- 0.133715
Z-translation = -76.750375 + -0.000000 +/- 0.133715

Rodrigues Rotation Parameters
lambda = -0.035262 +/- 0.001322
mu = -0.007854 +/- 0.001305
nu = -0.024413 +/- 0.001061

Scale unfixed
Scale = 1.004428 +/- 0.000992

New System Translations
X-translation = 3087.888750
Y-translation = 307.633750
Z-translation = 2481.211250

Original coordinates of new system

Point	X	Y	Z	vX	vY	vZ
1	2969.2100	198.8600	2435.0500	-0.1859	0.8320	-0.5405
2	3105.5600	195.0700	2433.1700	-0.5324	-0.1428	-0.0492
3	3194.7200	192.4600	2434.1400	-0.6402	0.2835	-0.2024
4	3209.2900	290.6300	2433.6300	0.9800	0.0916	-0.6329
5	3200.6600	425.4500	2428.2100	-0.6266	0.0188	-0.0510
6	3104.3300	427.7300	2427.8800	-0.2621	0.3053	-0.0851
7	2973.6300	429.2600	2429.6300	-0.6828	0.2938	-0.3245
8	2955.6600	288.4000	2434.5600	0.9282	0.3905	-0.4976
9	2996.9800	233.6100	2532.7000	0.1435	0.1361	0.9483
10	3100.0700	225.2600	2530.8400	-0.2572	-0.2616	0.8317
11	3164.3100	226.6500	2531.1300	-0.1696	-0.2856	1.0374
12	3178.1000	293.1800	2530.0200	0.9210	-0.0904	0.0479
13	3162.5900	397.4100	2526.7100	-0.4582	-0.4826	0.0238
14	3105.7200	399.1300	2527.4700	-0.0443	-0.1741	-0.0391
15	2998.8400	403.1600	2530.2300	-0.2182	-0.5763	-0.3130
16	2986.5500	295.8800	2534.0100	1.1047	-0.3383	-0.1539

Transformed coordinates

Point	X	Y	Z
1	2969.0241	199.6920	2434.5095
2	3105.0276	194.9272	2433.1208
3	3194.0798	192.7435	2433.9376
4	3210.2700	290.7216	2432.9971
5	3200.0334	425.4688	2428.1590
6	3104.0679	428.0353	2427.7949
7	2972.9472	429.5538	2429.3055
8	2956.5882	288.7905	2434.0624
9	2997.1235	233.7461	2533.6483
10	3099.8128	224.9984	2531.6717
11	3164.1404	226.3644	2532.1674
12	3179.0210	293.0896	2530.0679
13	3162.1318	396.9274	2526.7338
14	3105.6757	398.9559	2527.4309
15	2998.6218	402.5837	2529.9170
16	2987.6547	295.5417	2533.8561

$\hat{\sigma}_0 =$ 0.5372

Transformation 4 : "Metrograph" coordinates into SPG Fix 2 coordinates - scale held fixed.

No. of iterations = 6

Old System Translations
X-translation = 48.403750 + -0.000000 +/- 0.161735
Y-translation = 67.679125 + -0.000000 +/- 0.161735
Z-translation = -76.750375 + -0.000000 +/- 0.161735

Rodrigues Rotation Parameters
lambda = -0.035262 +/- 0.001599
mu = -0.007854 +/- 0.001579
nu = -0.024413 +/- 0.001284

Scale held fixed
Scale = 1.000000

New System Translations
X-translation = 3087.888750
Y-translation = 307.633750
Z-translation = 2481.211250

Original coordinates of new system

Point	X	Y	Z	vX	vY	vZ
1	2969.2100	198.8600	2435.0500	0.3382	1.3079	-0.3346
2	3105.5600	195.0700	2433.1700	-0.6080	0.3541	0.1628
3	3194.7200	192.4600	2434.1400	-1.1083	0.7900	0.0060
4	3209.2900	290.6300	2433.6300	0.4405	0.1662	-0.4203
5	3200.6600	425.4500	2428.2100	-1.1210	-0.5007	0.1829
6	3104.3300	427.7300	2427.8800	-0.3334	-0.2255	0.1504
7	2973.6300	429.2600	2429.6300	-0.1761	-0.2437	-0.0957
8	2955.6600	288.4000	2434.5600	1.5070	0.4736	-0.2897
9	2996.9800	233.6100	2532.7000	0.5437	0.4618	0.7171
10	3100.0700	225.2600	2530.8400	-0.3097	0.1027	0.6092
11	3164.3100	226.6500	2531.1300	-0.5058	0.0727	0.8127
12	3178.1000	293.1800	2530.0200	0.5192	-0.0263	-0.1674
13	3162.5900	397.4100	2526.7100	-0.7855	-0.8763	-0.1769
14	3105.7200	399.1300	2527.4700	-0.1227	-0.5767	-0.2429
15	2998.8400	403.1600	2530.2300	0.1754	-0.9949	-0.5277
16	2986.5500	295.8800	2534.0100	1.5466	-0.2850	-0.3859

Transformed coordinates

Point	X	Y	Z
1	2969.5482	200.1679	2434.7154
2	3104.9520	195.4241	2433.3328
3	3193.6117	193.2500	2434.1460
4	3209.7305	290.7962	2433.2097
5	3199.5390	424.9493	2428.3929
6	3103.9966	427.5045	2428.0304
7	2973.4539	429.0163	2429.5343
8	2957.1670	288.8736	2434.2703
9	2997.5237	234.0718	2533.4171
10	3099.7603	225.3627	2531.4492
11	3163.8042	226.7227	2531.9427
12	3178.6192	293.1537	2529.8526
13	3161.8045	396.5337	2526.5331
14	3105.5973	398.5533	2527.2271
15	2999.0154	402.1651	2529.7023
16	2988.0966	295.5950	2533.6241

$\hat{\sigma}_o$ = 0.6469